NASA CR-135385

NASA

PLUG CLUSTER MODULE DEMONSTRATION

by

D. C. Rousar

AEROJET LIQUID ROCKET COMPANY

Sacramento, California

prepared for

NATIONAL AERONAUTICS AND SPACE ADMINISTRATION

July 1978

CONTRACT NAS 3-20107

NASA Lewis Research Center
Cleveland, Ohio
C. A. Aukerman, Project Manager

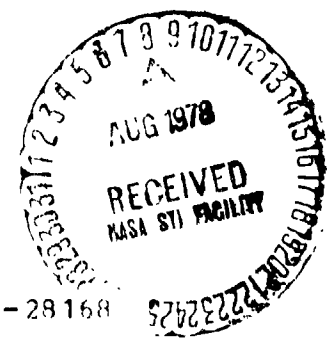

(NASA-CR-135385) PLUG CLUSTER MODULE DEMONSTRATION Final Report, 6 Jun. 1976 - 11 Jun. 1977 (Aerojet Liquid Rocket Co.) 151 p HC A08/MF A01 CSCL 21H

N78-28168

G3/20

Unclas
25876

1. Report No.	2. Government Accession No.	3. Recipient's Catalog No.
NASA CR-135385		

4. Title and Subtitle	5. Report Date
Plug Cluster Module Demonstration	July 1978
	6. Performing Organization Code

7. Author(s)	8. Performing Organization Report No.
D. C. Rousar	
	10. Work Unit No.

9. Performing Organization Name and Address	11. Contract or Grant No.
Aerojet Liquid Rocket Company Sacramento, California	NAS 3-20107
	13. Type of Report and Period Covered Final Report 6 June 1976-11 June 1977

12. Sponsoring Agency Name and Address	14. Sponsoring Agency Code
National Aeronautics and Space Administration Washington, D.C. 20546	

15. Supplementary Notes

Project Manager, C. A. Aukerman, NASA Lewis Research Center, Cleveland, Ohio

16. Abstract

The low pressure, film cooled rocket engine design concept developed during two previous ALRC programs was re-evaluated for application as a module for a plug cluster engine capable of performing space shuttle OTV missions. The nominal engine mixture ratio was 5.5 and the engine life requirements were; 1200 thermal cycles, 10 hours total operating life. The program consisted of pretest analysis; engine tests, performed using residual components; and post-test analysis. The pretest analysis indicated that operation of the film cooled engine at O/F = 5.5 was feasible. During the engine tests, steady state wall temperature and performance measurements were obtained over a range of film cooling flow rates, and the durability of the engine was demonstrated by firing the test engine 1220 times at a nominal performance ranging from 430 - 432 seconds (based on 40/1 nozzle and ambient temperature propellants). The performance of the test engine was limited by film coolant sleeve damage which had occurred during previous testing. The post-test analyses indicated that the nominal performance level can be increased to 436 seconds.

17. Key Words (Suggested by Author(s))	18. Distribution Statement
Plug Cluster Module Film Cooling Performance Loss Cycle Life	Unclassified - Unlimited

19. Security Classif. (of this report)	20. Security Classif. (of this page)	21. No. of Pages	22. Price*
Unclassified	Unclassified		

FOREWORD

The Plug Cluster Module Demonstration Program (Contract NAS 3-20107) was conducted by the Technology Engineering Department of the Aerojet Liquid Rocket Company for the NASA-Lewis Research Center. C. A. Aukerman was the NASA-Lewis Project Manager. At ALRC, the Program Manager was L. B. Bassham, the Operations Project Manager was R. J. LaBotz, and the Project Engineer was D. C. Rousar. Significant contributions to this program were also made by the following ALRC Personnel:

J. D. Duey
R. S. Gross
R. K. Ishikawa
J. I. Ito
E. Lueders
S. L. Munger
P. M. Loyd
D. E. Robertson
L. Schoenman
R. E. Walker

TABLE OF CONTENTS

LIST OF TABLES

LIST OF FIGURES

LIST OF FIGURES (cont.)

LIST OF FIGURES (cont.)

I. SUMMARY

During the Plug Cluster Module Demonstration Program, the low pressure, film cooled oxygen-hydrogen rocket engine design concept developed during two previous ALRC programs, the APS and ITA programs described in References 1 and 2, was reevaluated for application as a module for a plug cluster engine which is capable of performing Space Shuttle OTV missions. The performance of the plug cluster engine was evaluated in a parallel study program (Contract NAS 3-20109). For the plug cluster application, the nominal engine mixture ratio was increased from 4.0 to 5.5 and the engine cycle life requirement was reduced from 50,000 to 1200 cycles. The total required engine life was considered to be 10 hours.

The program was designed so that it was not necessary to fabricate new test components. The injector, igniter, and film cooled chamber tested were all residual from previous ALRC and NASA Lewis programs.

There were basically three phases of this program: (1) pretest analysis and test system preparation, (2) testing, and (3) post-test analysis. During the pretest analysis, a preliminary evaluation of the APS/ITA engine concept for the plug cluster application was obtained and the testing conditions were finalized. The pretest analysis included performance, structural and thermal analyses. This pretest evaluation indicated that operation of an APS/ITA type engine at O/F = 5.5 was feasible and that a specific impulse performance of about 430 seconds[1] could be obtained.

During the initial tests, performance verification tests were performed in which steady state wall temperature and performance measurements were obtained over a range of film cooling flowrates. The extrapolated performance vs film coolant flow characteristic was about the same as expected. Some "streaking" occurred in these tests as a result of film coolant sleeve damage which had occurred during the 16,310 previous test firings conducted with the thrust chamber that was tested. Disregarding these streaks, it was found that the chamber wall temperatures at the film cooling rates of interest (~20% of the total fuel) were lower than predicted.

Test conditions for the life verification test series were chosen using the data from the initial performance verification tests. Subsequently a life verification/test series was conducted in which the durability of the APS/ITA design concept was proven by firing the test engine 1220 times. Each firing consisted of a thermal strain cycle of the throat region. The 40/1 extrapolated performance level for these tests ranged from 430-432 seconds. It was necessary to increase film coolant flow and

[1] All specific impulse performance values stated in this Section are based on a 40/1 area ratio nozzle and ambient temperature oxygen-hydrogen propellants.

reduce firing duration during the life verification tests because the previously damaged areas of the film coolant sleeve deteriorated further. However, this did not detract from the chamber durability demonstration.

During post-test analyses, the performance and film cooling heat transfer data were correlated and revised predictions were made based on these correlations. A slightly modified version of the ITA engine design was found to be suitable for plug cluster module applications and is recommended. The required design modifications consist of incorporating the APS injection sleeve design and increasing the chamber wall thickness. This modified design is predicted to satisfy the desired engine life requirements (1200 firings, 10 hr total engine life) and operate at a specific impulse performance of 436 seconds.

It was found that no injector redesign is required for the ITA injector operating at 5.5 mixture ratio with ambient temperature (300°K) propellants. The film cooled chamber wall temperature data was correlated in terms of the entrainment film cooling model described in Reference 3. The ratio of film coolant and core gas mass velocities provided a good correlation of the entrainment fractions calculated from the wall temperature data. A velocity ratio correlation was also adequate for the subsonic region. Core gas acceleration was found to decrease entrainment more than expected.

II. INTRODUCTION

The purpose of the Plug Cluster Module Demonstration Program was to evaluate the feasibility of using a small H_2-O_2 thruster as a module for an advanced high performance space engine such as an orbit transfer vehicle (OTV) engine. The particular advanced engine concept being considered consists of small low pressure engines clustered around the outer diameter or base of a plug nozzle. This engine design approach offers more flexibility than an annular throat thrust chamber, and it also presents the opportunity to use small thrusters as building blocks for low cost advanced engines.

The film-cooled Auxiliary Propulsion System Thruster developed under NAS 3-14354 (APS program, Ref. 1) and carried to an Integrated Thruster Assembly under NAS 3-15850 (ITA program, Ref. 2) has three distinct advantages for clustered plug engine applications: (1) performance and life have been demonstrated in flight weight hardware, (2) the thin, film cooled wall at the throat is relatively compliant to thermal strain, and (3) the engine operates with high performance at low chamber pressure. As a result of these advantages, the clustered ITA engine design approach offers an attractive alternative to a high pressure conventional engine and could result in a low cost, low risk advanced space engine.

II, Introduction (cont.)

The ITA thruster is shown in Figure 1. It was developed to operate primarily at a 4.0 O_2/H_2 mixture ratio (O/F). Higher O/F values, in the range of 5-6, are required for an OTV main engine and this poses a potential design problem for a hydrogen film cooled engine since less fuel is available for cooling. For the OTV application, the high O/F cooling problem is alleviated by the significantly lower engine life requirement. The cyclic life of an OTV main engine is 1200 cycles compared to the 50,000 cycle life of the ITA thruster.

The specific objectives of this program were: (1) to re-evaluate the original ITA design concept of a low pressure, hydrogen film cooled thruster for operation at a mixture ratio of 5.5, and (2) to determine the maximum vacuum specific impulse that can be obtained consistent with an engine life of 1200 cycles.

The program consisted of 4 technical tasks: Task I - Assessment of Module Feasibility, Task II - Preparation for Testing, Task III - Experimental Test Program, and Task IV - Experimental Assessment of Module Feasibility. The work accomplished during these tasks consists of: (1) a pre-test analytical assessment of the thruster cycle life and performance characteristics at the revised operating condition, (2) preparation of a test system, (3) eight performance verification test firings with fuel film coolant flow percentages ranging from 35% to 18%, (4) 1220 life verification test firings at a nominal performance level of 430 - 432 sec (based on ambient temperature propellants and 40/1 nozzle ara ratio), and (5) a post-test analytical re-assessment of the thruster based on the experimental results which were obtained.

The thrust chamber assembly tested was residual from the Reference 1 program. All tests were performed with sea level back pressure and a 4.43/1 area ratio truncated nozzle.

III. TEST APPARATUS

A. THRUST CHAMBER ASSEMBLY

The test assembly consisted of the following components:

(1) A regen/film cooled thrust chamber,
(2) a 72 element premix type injector,
(3) an O_2/H_2 spark igniter assembly, and
(4) an injector/chamber adapter

A post-test photograph of these components is shown as Figure 2.

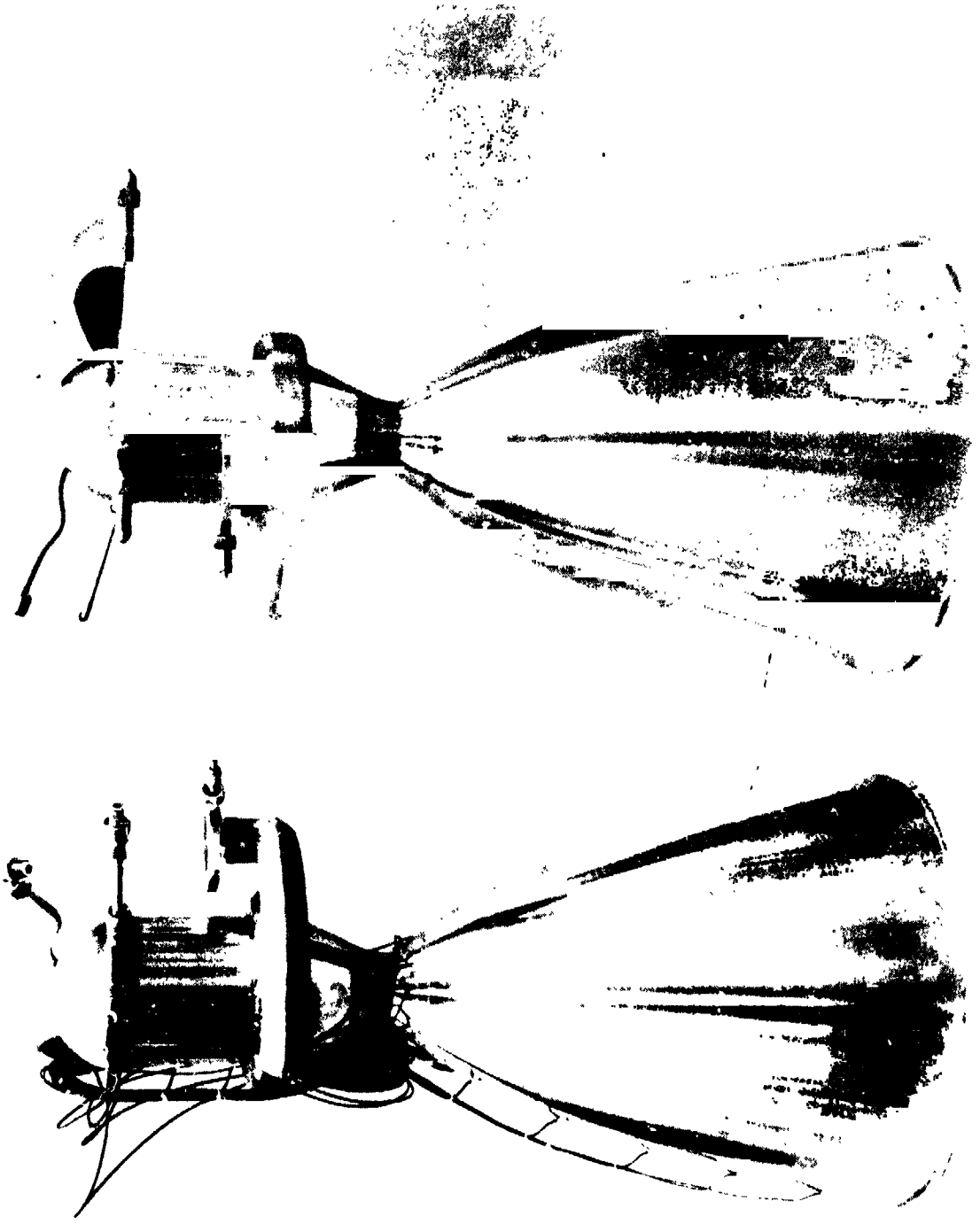

Figure 1. ITA Engines

Figure 2. Test Components Utilized for the Plug Cluster Module Demonstration Program (Post-Test)

III, A, Thrust Chamber Assembly (cont.)

1. Thrust Chamber

The regen/film cooled thrust chamber was designed and fabricated on the Reference 1 Program. This unit is designated P/N 1160334, S/N 2, and was provided by the NASA-Lewis Research Center at the onset of the program. The nozzle had been truncated to an area ratio of 4.43/1 (originally a 40/1 nozzle). The measured throat diameter is 4.841 cm and the measured exit diameter is 10.190 cm. Prior to testing on this program, thermocouples were installed on the backside of the chamber wall as shown on Figure 3. Cold flow tests with water and gaseous nitrogen were performed on both the regeneratively cooled circuit and the film coolant sleeve prior to the test firings. The water flow tests showed that none of the cooling passages were plugged and the nitrogen flow tests yielded ΔP measurements consistent with results obtained on the same chamber in 1971 before it was test fired. The ΔP data are shown on Figure 4.

This chamber had been fired 16,310 times during test programs at ALRC and NASA-LeRC prior to this program. The film coolant injection sleeve was damaged during this previous testing and this caused "streaking" to occur on the film cooled nozzle. At the onset of testing on this program, the damage consisted of: (1) 6 small longitudinal cracks at the tip of the copper injection sleeve, (2) a slight "pulling away" of the sleeve from the chamber wall in the area where the cracks exist, (3) corrosion of the sleeve upstream of the injection point and (4) several circumferential cracks in the downstream half of the injection sleeve. A pre-test photograph of the damaged area is shown on Figure 5.

2. Premix Injector

The "Modified I" premix injector used (P/N 1161401, S/N 6) was also residual from the Reference 1 Program. During APS related testing, this injector was fired 3685 times, after which a new injector face was installed. It was subsequently fired 29 times during the Combustion Effects on Film Cooling Test Program (Ref. 3).

Cold flow tests of this injector were performed with gaseous nitrogen prior to the test firings to insure that the unit was in satisfactory operating condition. The tests were performed by flowing gaseous N_2 through the oxidizer and fuel circuits. The oxidizer and fuel circuits were flowed separately and the flow from each element in the outer row was measured using a plastic tube/rotameter assembly.

The test flow rates were chosen so that the oxygen and hydrogen Mach numbers were simulated for operating conditions of 300 psia chamber pressure and injector mixture ratios (O/F) of 4 and 7. The O/F = 4 cold flow test duplicated a pre-fire cold flow test performed on this

	cm	(in.)
Δz	3.18	(1.25)
d_t	4.84	(1.906)
d_e	10.19	(4.012)
a	.13	(.05)
b	1.65	(.65)
c	.51	(.2)
d	1.91	(.75)
e	2.41	(.95)
f	.51	(.2)

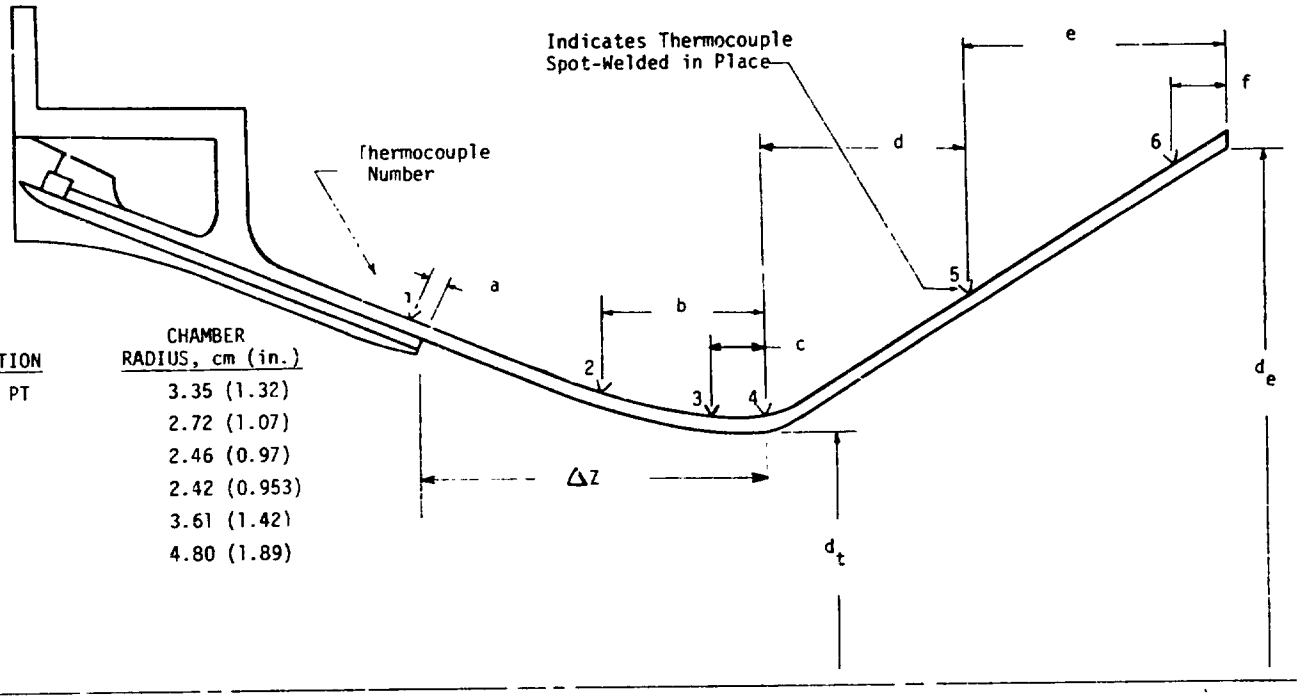

LOCATION	CHAMBER RADIUS, cm (in.)
INJ. PT	3.35 (1.32)
2	2.72 (1.07)
3	2.46 (0.97)
4	2.42 (0.953)
5	3.61 (1.42)
6	4.80 (1.89)

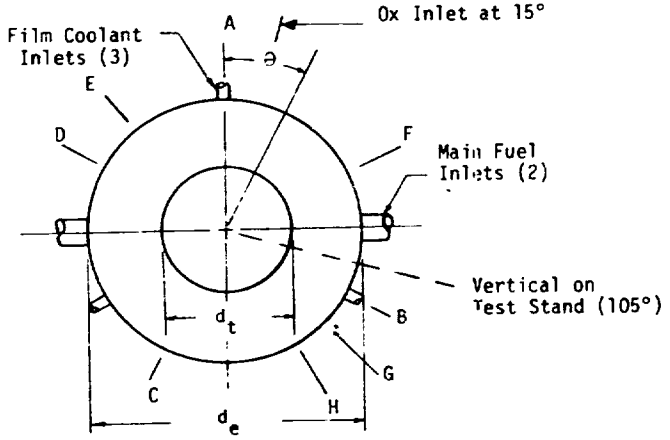

Thermocouple Row	θ	Thermocouple Axial Position
A	0°	1,2,3,4,5,6
B	120°	1,2,3,4,5,6 (Max. Gap)
C	210°	1,2,3,4,5,6
D	300°	1,2,3,4,5,6
E	320°	1,2,4,6
F	65°	1,2,4,6
G	135°	6
H	150°	6

Figure 3. Chamber Geometry and Thermocouple Locations

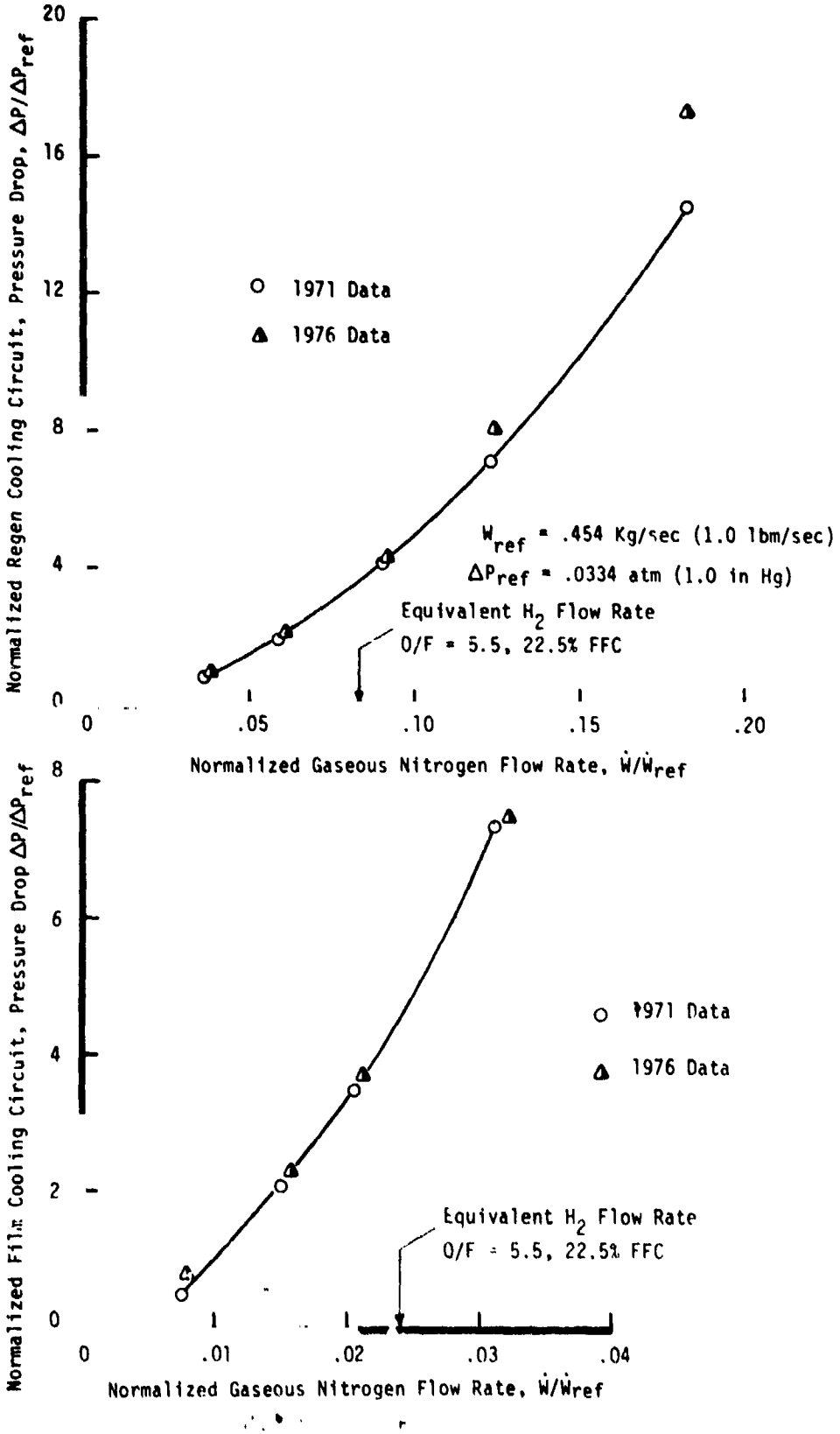

Figure 4. Cold Flow ΔP Data

Figure 5. Pre-Test View of Film Coolant Sleeve

injector during the Reference 3 program. The core O/F = 7 test represented a typical test condition for the Plug Module program (O/F = 5.5, 21.4% FFC).

Mixture ratios calculated for the outer element row from the cold flow data are plotted on Figure 6. These data indicated that the mixture ratio in the individual elements were within + 7% of the nominal values which is consistent with the Reference 3 cold flow results. It was concluded that the injector was in satisfactory operating condition.

3. O_2/H_2 Spark Igniter

The spark igniter assembly used was previously utilized during the Combustion Effects Program and the Gas O_2-Gas H_2 Combustion Program (Reference 4).

4. Adapter

The injector-chamber adapter, P/N 1161420, is residual from Contract NAS 3-14354 and was supplied by NASA-Lewis. This adapter is necessary when assembling the APS injector with a film cooled APS chamber.

B. TEST SYSTEM

All tests were conducted in Bay 6 of the ALRC Research Physics Laboratory. A sea-level type test facility was used to conduct an experimental evaluation of the film cooled thruster. The test facility contained a thrust stand, a sequencer, gaseous hydrogen feed system and gaseous oxygen feed system. The engine was mounted horizontally as shown on Figure 7. The test facility is shown schematically in Figure 8.

The force measuring system consisted of a thrust carriage, on which the test engine and propellant feed lines are secured, a force measuring transducer, and a hydraulic calibration system. The thrust carriage assembly was supported in a plane normal to the thrust axis by flexure plates which produce a parallelogram type support structure. Force in the thrust axis was transmitted through the carriage assembly to two strain gage load cells. Thrust axis bias was measured before each performance verification test with a standard cell which is hydraulic actuated against the carriage assembly. During the performance verification tests, the measured thrust bias factors ranged from 2.05 to 2.79%. For each individual test, the thruat bias of the two strain gage load cells always agreed within .03%.

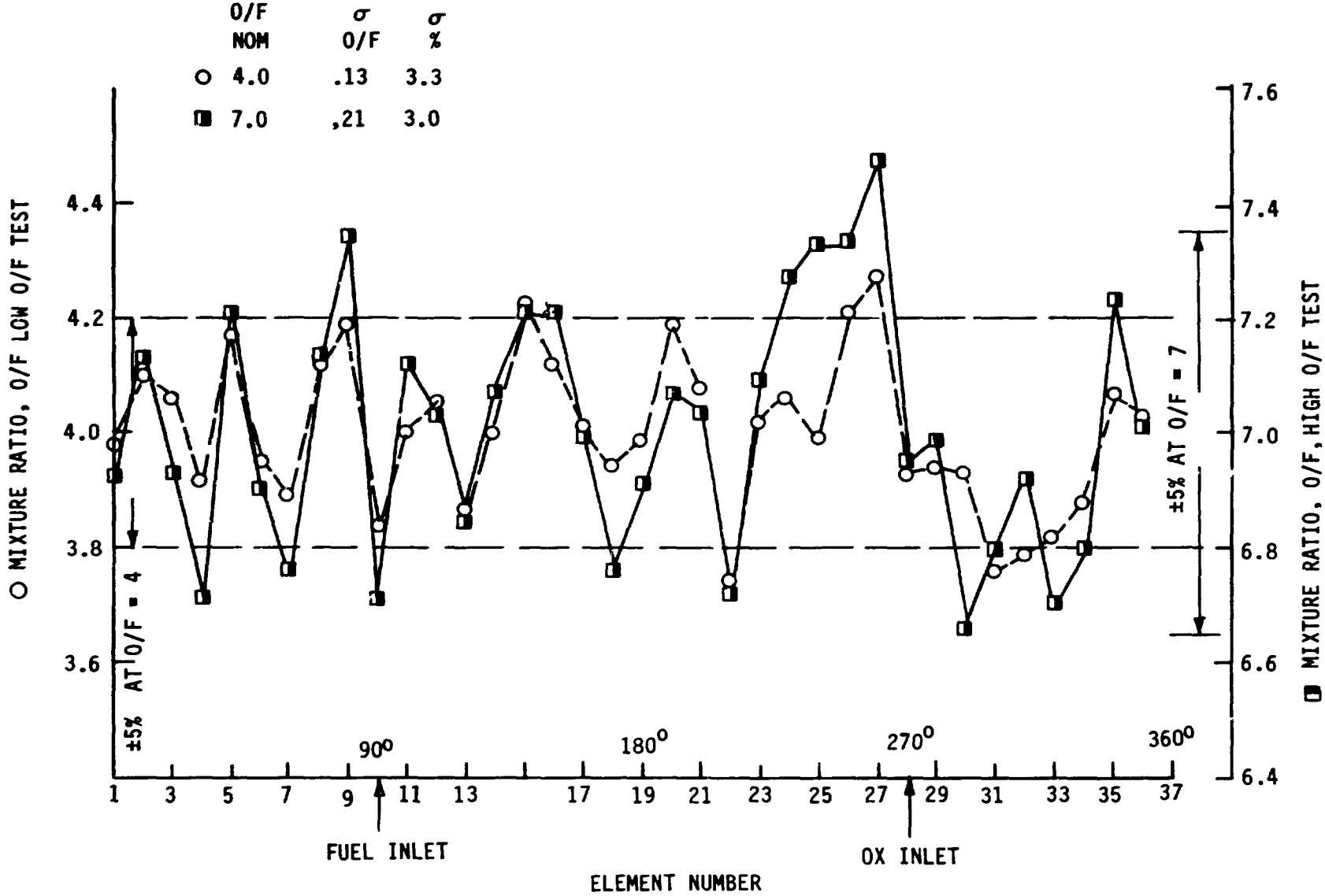

Figure 6. Outer Row Mixture Ratio Distribution, APS Modified I Premix Injector (S/N 6)

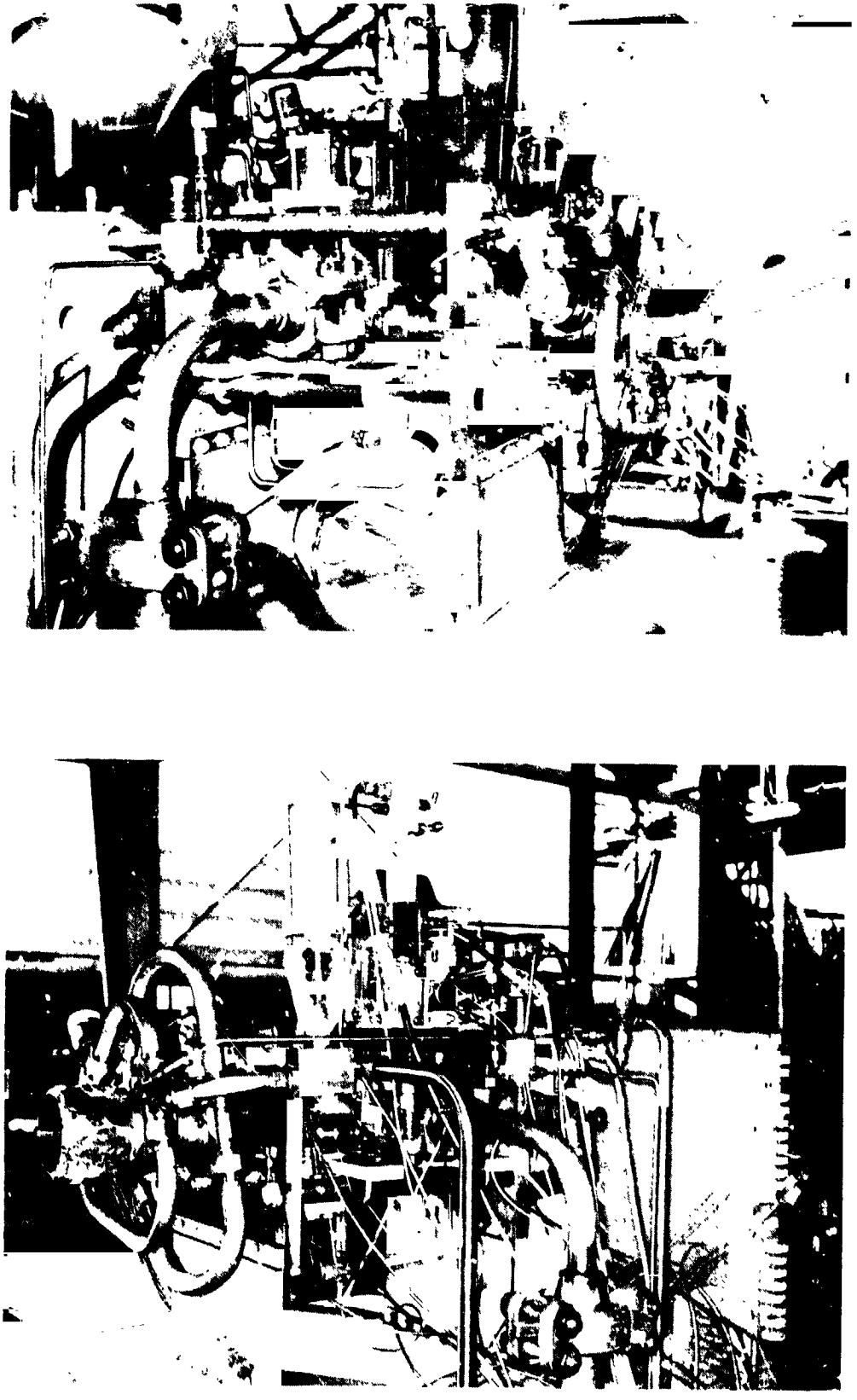

Figure 7. Test System Photographs

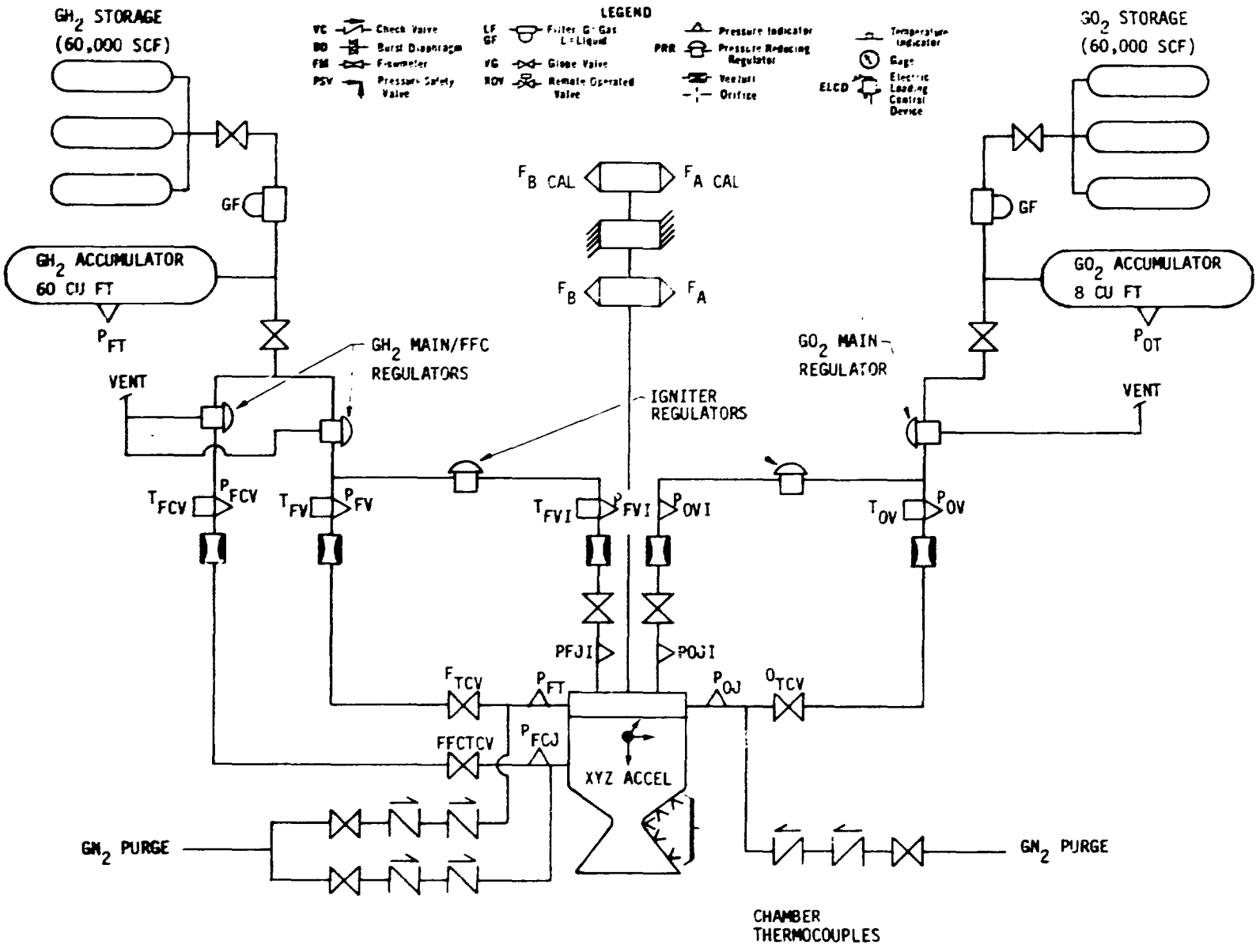

Figure 8. Test System Schematic

III, B, Test System (cont.)

The gaseous hydrogen and gaseous oxygen feed systems consisted of a 60,000 SCF propellant storage trailer, accumulator, pressure regulator, flowmeter section, and thrust chamber valve. The accumulators were located adjacent to the thrust stand and contained sufficient quantities of propellant for approximately 15 seconds continuous test duration. Propellant flow to the engine was measured and controlled by sonic venturis located between the pressure regulators and thrust chamber valves. The thrust chamber valves were hydraulically actuated fast-response valves.

During the 8 performance verification tests, the following parameters were measured: thrust, propellant flow rates, propellant temperatures, chamber wall temperatures, system pressures, and accelerometer output. All of these data except thrust and accelerometer output were also recorded during the life verification tests.

IV. PRE-TEST ANALYSES

The pre-test analyses were performed to provide a preliminary assessment of the thrust chamber performance and cycle life characteristics. These analyses provided the basis for establishing testing conditions for the performance verification and life verification tests.

A. PRE-TEST HEAT TRANSFER ANALYSIS

The pre-test heat transfer analysis was performed for the dump-regen and film cooled regions of the APS and ITA thrust chamber designs. These designs are shown on Figures 9 and 10. The analytical modeling of each thrust chamber was done using the HOCOOL computer program prepared for NASA-Lewis by ALRC on a previous program (Ref. 3). Pertinent design details for the APS and ITA chamber designs are listed on Table I. The pre-test heat transfer analysis details are given in Appendix B.

The heat transfer analysis consisted of three distinct steps: (1) setting up an analytical model using the HOCOOL computer program, (2) correlating the model with APS and ITA test data, and (3) generating the pre-test predictions. The predictions consisted of injection sleeve wall temperature, adiabatic wall temperature in the film cooled chamber, nozzle wall temperature, and performance loss due to film cooling effects. Three basic cases were analyzed and they are summarized in the following tabulation. A 5.5 overall O_2/H_2 mixture ratio and 300 psia chamber pressure were assumed for all three cases.

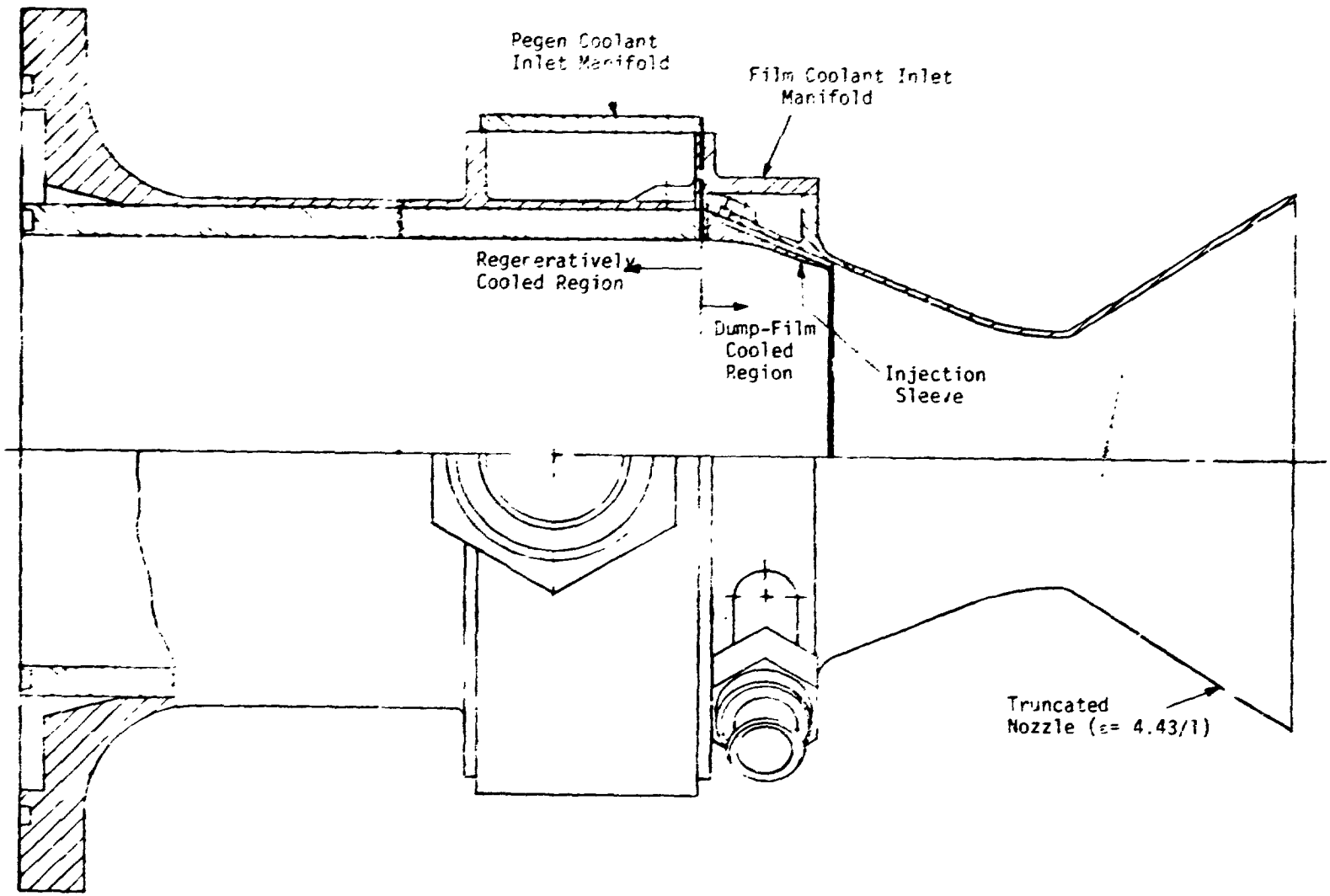

Figure 9. APS Thrust Chamber Design

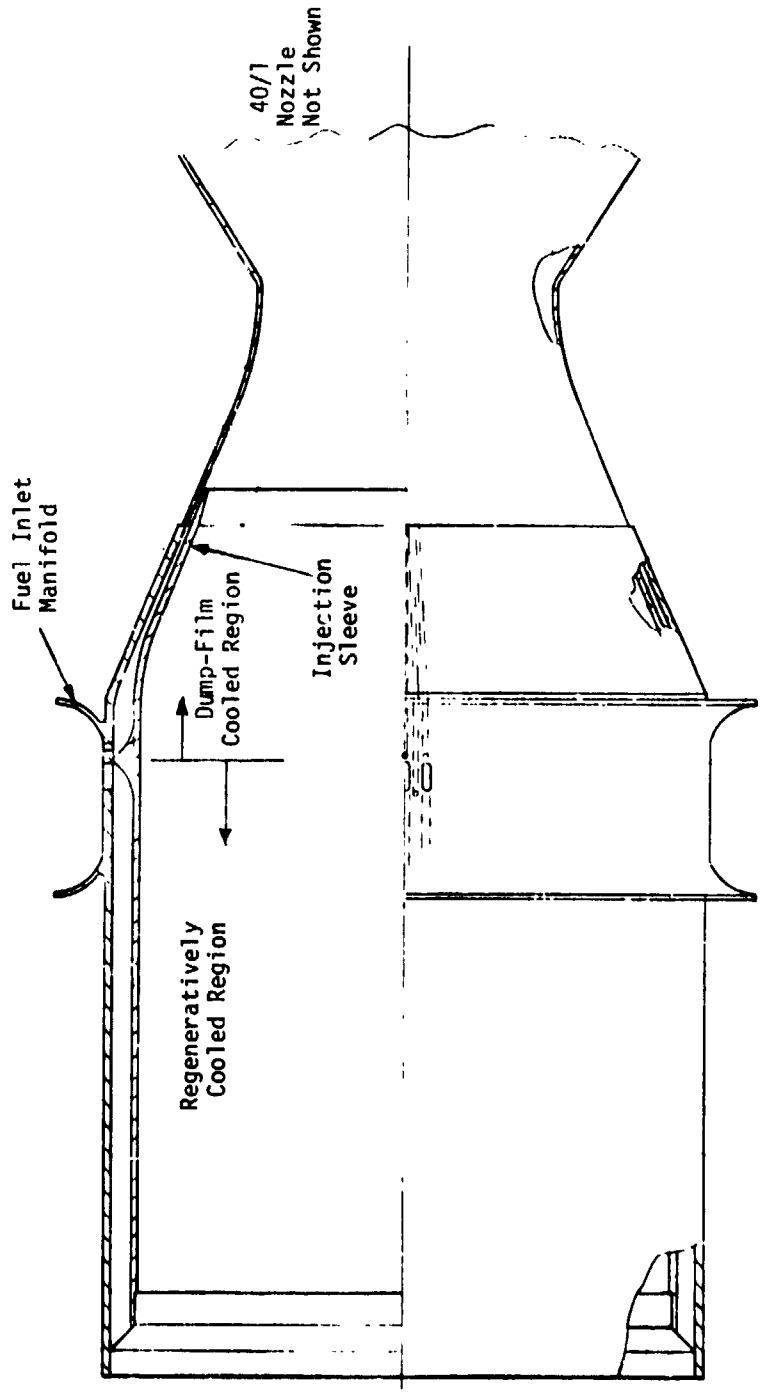

Figure 10. ITA Thrust Chamber Design

TABLE I

DESIGN DATA FOR THE DUMP-FILM COOLED REGION

	APS Chamber	ITA Chamber
Number of Injection Channels	120	160
Channel Size at Injection Point, cm	.10 x .10	.076 x .076
Total Flow Area at Injection Point, cm^2	1.24	.93
Land Width at Injection Point, cm	.069	.053
Lip Thickness at Injection Point, cm	.064	.044
Channel Width Within Sleeve, cm	.10, Const.	.076, Const.
Channel Depth Within Sleeve, cm	.10, Const.	.10 - .076 (Tapers over 1.9cm length)
Sleeve Material	OFHC Cu	Zr-Cu
Sleeve Gas-Side Wall Thickness, cm (Downstream of Inlet Region)	.10 - 0.64	.10 - 0.44
Film Coolant Circuit	Separate from Regen Circuit	Parallel with Regen Circuit
Film Cooled Chamber Material	Haynes 188	Haynes 188
Film Cooled Chamber Wall Thickness, cm	.127/.102	.081/.071

IV, A, Pre-Test Heat Transfer Analysis (cont.)

Case	Chamber	H_2 Inlet Temperature	O_2 Inlet Temperature	Percent FFC
1	APS	294°K	294°K	10,15,20,25,30
2	ITA	294°K	294°K	10,15,20,25,30
3	ITA	138°K	208°K	10,15,20,25,30

1. Dump Cooled Injection Sleeve

The dump cooled sleeve is defined as the thrust chamber region which is convectively cooled by the film coolant before it is injected onto the chamber wall (see Figures 9 and 10). In this region, the hydrogen flows in rectangular coolant slots which have been machined into a copper liner. The copper liner is brazed to the ID of a Haynes 188 outer shell.

Wall temperatures calculated for the tip of the coolant injection sleeve are plotted as a function of the fuel film cooling percentage on Figure 11. Axial wall temperature distributions for the ITA chamber design are shown on Figure 12. The injection sleeve wall temperature decreases with increasing % FFC and increases along the length of the cooling channel. Sleeve temperature is a potential operating limit for high performance designs where low film cooling flow rates and injection points close to the throat are desired.

2. Film Cooled Chamber

Axial profiles of the adiabatic wall temperature, T_{aw}, calculated for the three cases considered are shown on Figure 13. The predictions for the APS and ITA chamber are different because the Reference 1 and 2 wall temperature data show that the ITA coolant injection sleeve design promoted mixing of the film coolant and core gases upstream of the throat. This is discussed further in Appendix B. In the subsonic and throat regions, the steady state chamber wall temperature is approximately equal to the adiabatic wall temperature. However, thermal radiation effects cause the nozzle wall temperature to be significantly less than T_{aw}. An estimate of the radiation effects for the APS and ITA chambers was made and the ITA results are shown on Figure 14. The predictions obtained for the adiabatic temperature at the throat and the nozzle exit are shown on Figure 15. The throat wall temperature and the maximum nozzle temperature both increase with decreased film cooling flow rate. The throat temperature is most critical at low film coolant flow rates (~10%) but the maximum wall temperature exists in the nozzle at the higher coolant flows (~15%). The throat temperature and nozzle temperature represent operating limits for a high performance design.

B. PRE-TEST PERFORMANCE ANALYSIS

The delivered performance of the test engine operating at O/F = 5.5 and for a range of film cooling flow rates was estimated prior to the

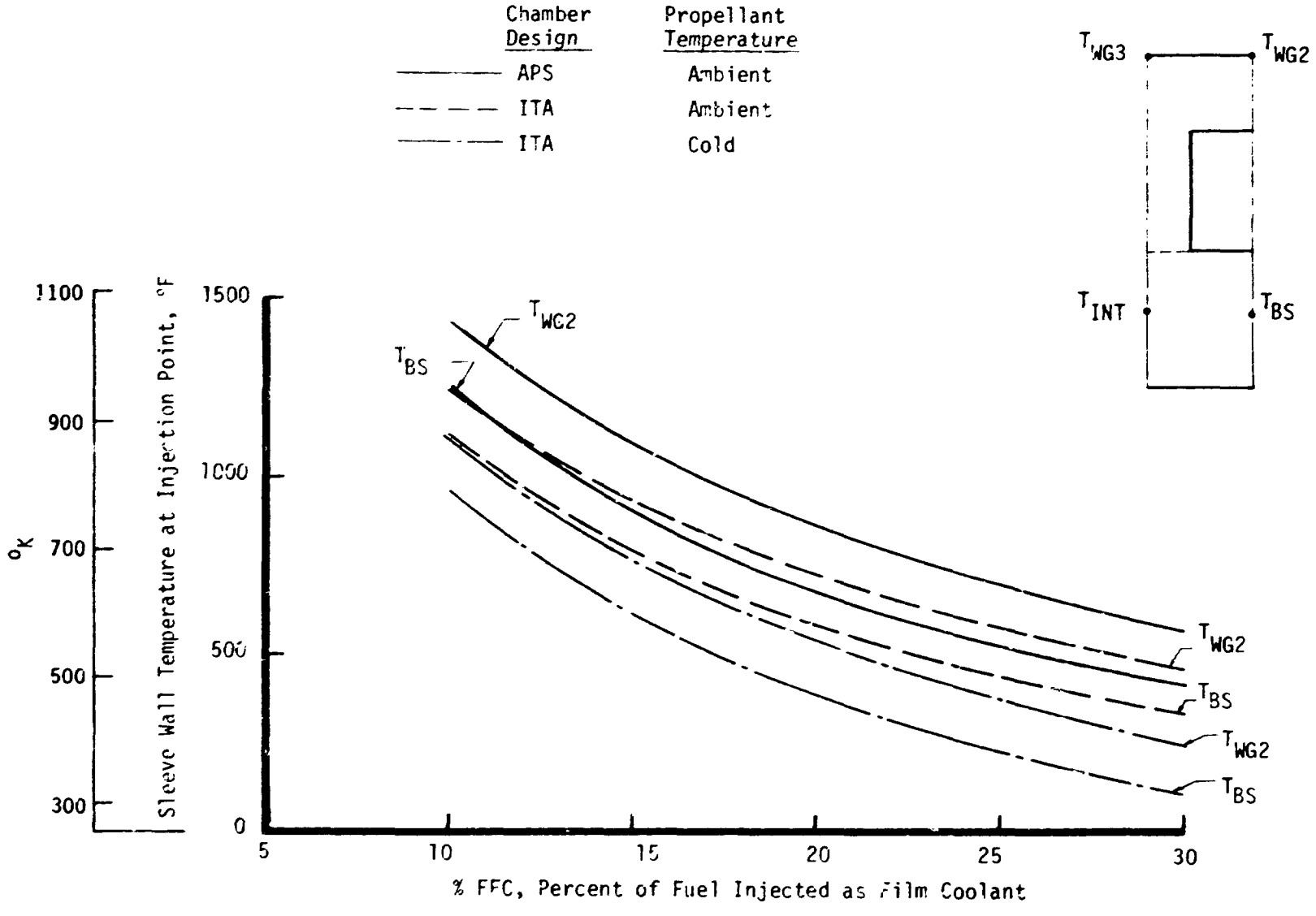

Figure 11. Effect of Film Coolant Flow Rate on Sleeve Temperature

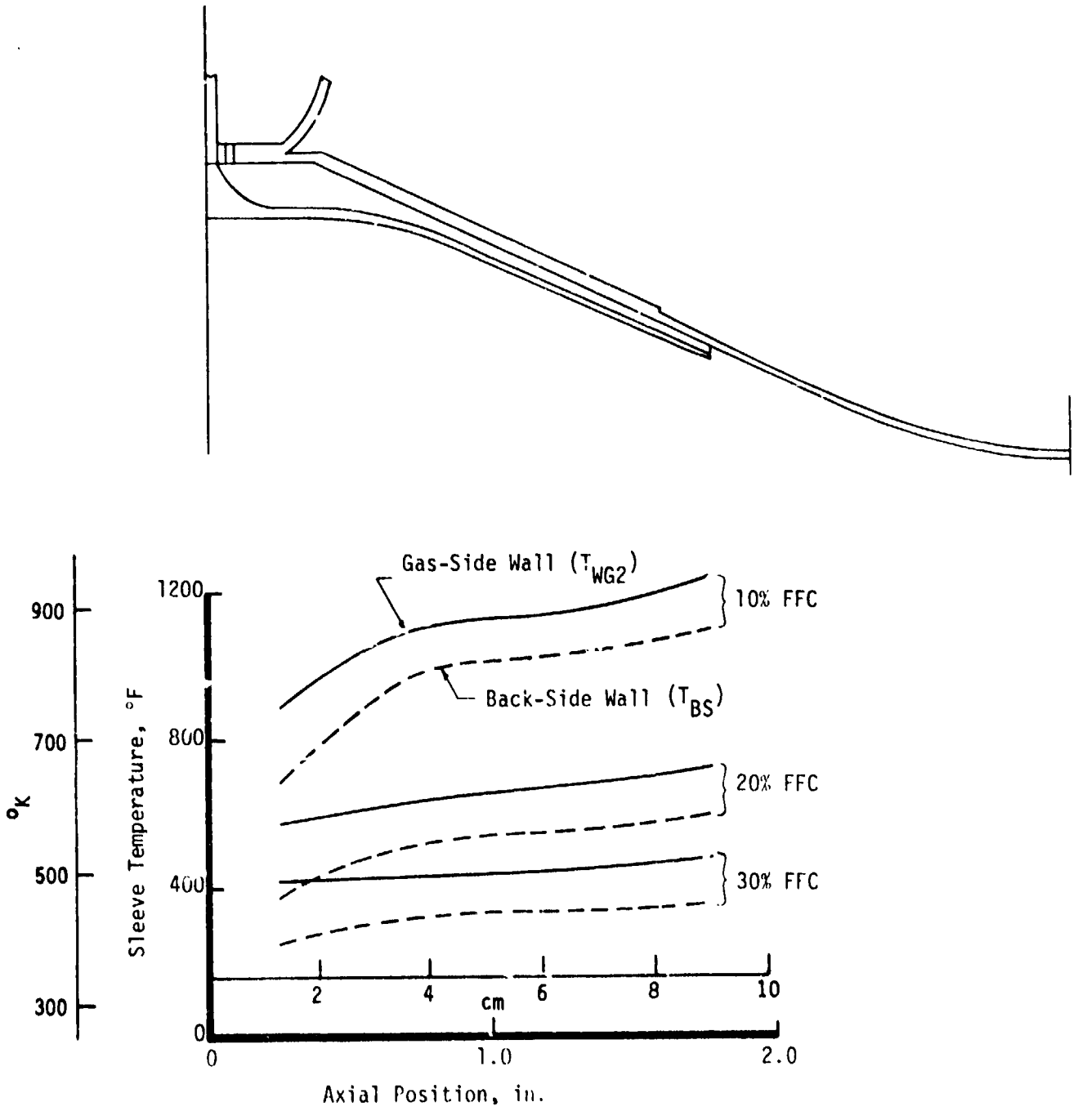

Figure 12. Axial Sleeve Wall Temperature Distribution

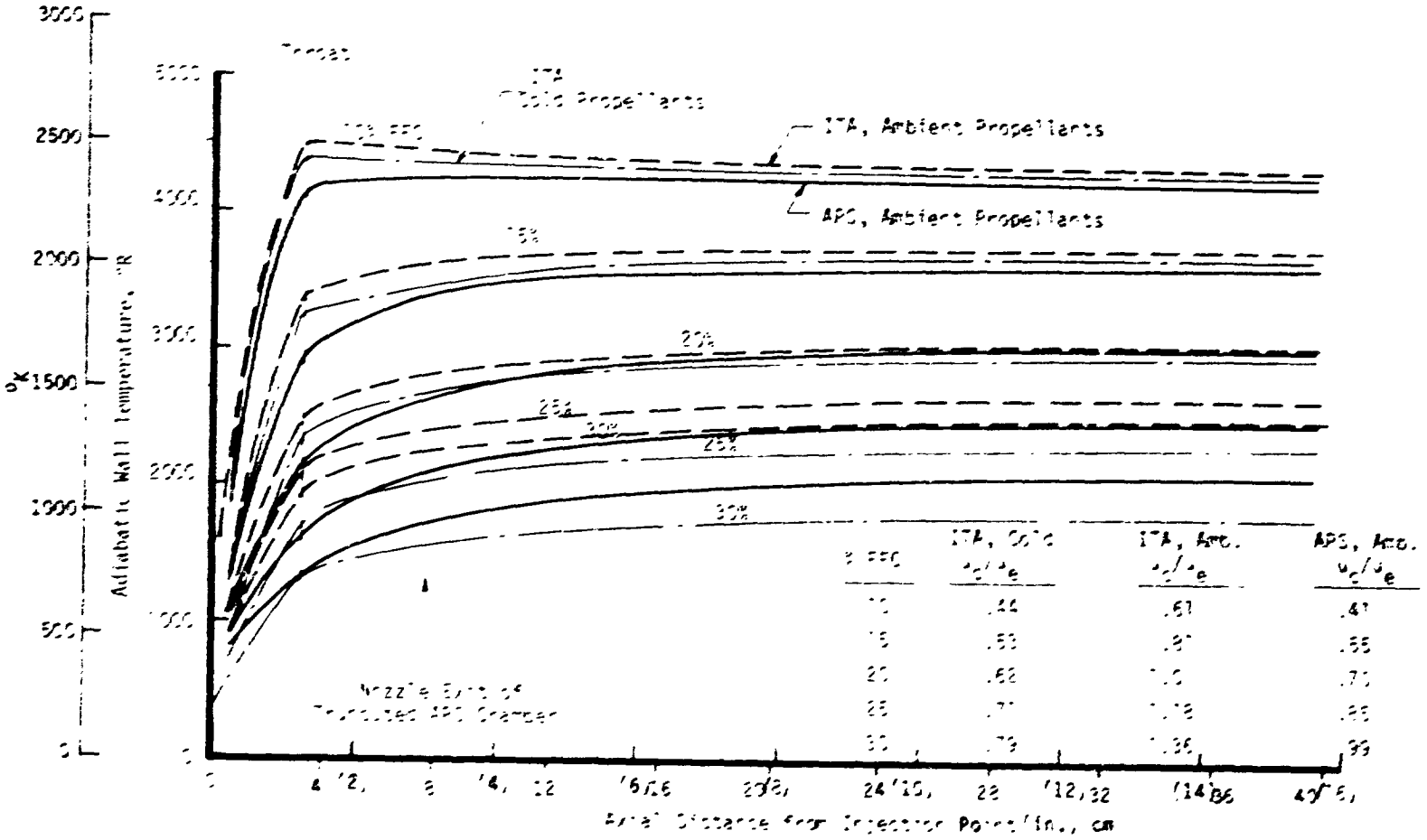

% FEC	ITA, Cold u_c/u_e	ITA, Amb. u_c/u_e	APS, Amb. u_c/u_e
10	.44	.61	.47
15	.53	.81	.55
20	.62	1.0	.71
25	.71	1.18	.85
30	.79	1.36	.99

Figure 13. Pretest Adiabatic Wall Temperature Predictions

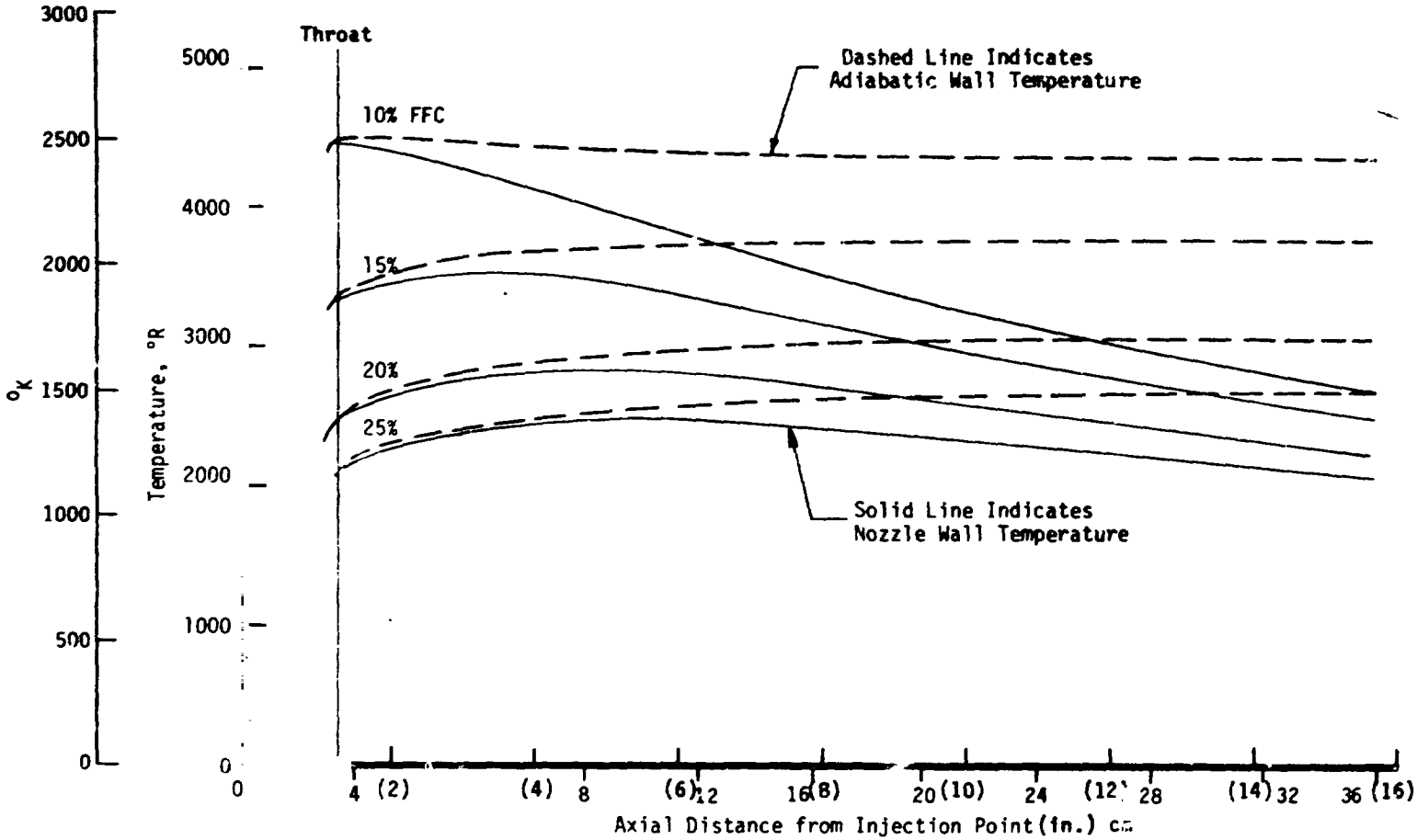

Figure 14. Pretest Prediction of ITA Nozzle Wall Temperature

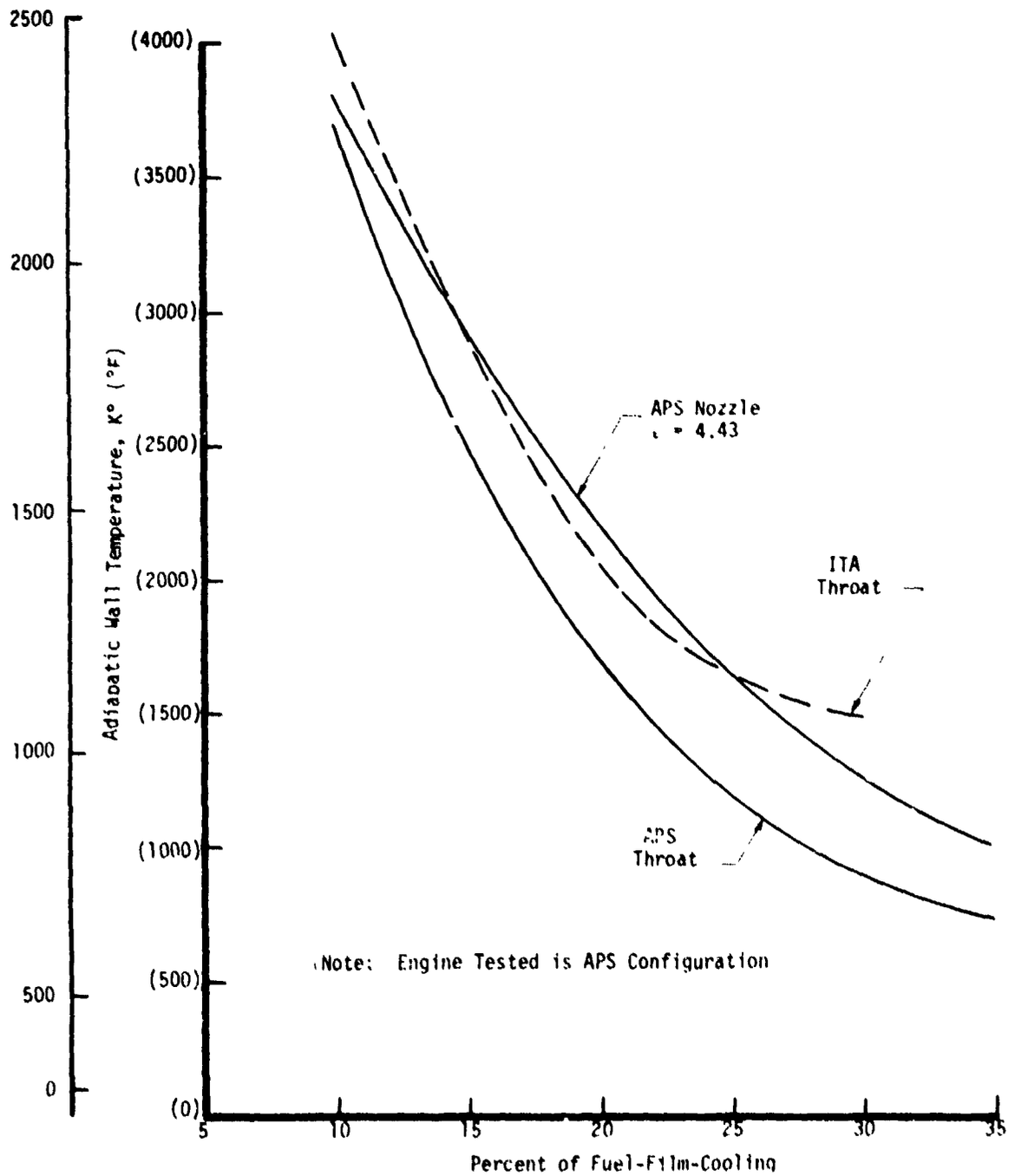

Figure 15. Predicted Effect of Film Coolant Flow Rate on Throat Temperature

start of testing. The estimates were based on the data of References 1 and 2 and the film-cooling-performance loss predictions obtained during the course of the pretest heat transfer analysis.

The performance was calculated by subtracting losses due to kinetics (KL), nozzle divergence (DL), boundary layer effects (BLL), imperfect energy release (ERL), and film cooling (FCL) from the theoretical ODE performance at the overall oxygen/hydrogen mixture ratio of 5.5. The pretest performance analysis details are given in Appendix C. Predicted effects of film coolant flow rate and temperature on performance are shown on Figures 16 and 17.

The injector utilized on this program is the Modified I Premix-Triplet type design developed on the Reference 1 and 2 programs. The operation of a typical Modified I injector element is shown schematically on Figure 18. The oxidizer flows axially as in a co-axial element design but the fuel is injected radially inward so as to promote mixing but yet provide adequate face cooling and chamber wall heat transfer characteristics. The performance of the Modified I design was experimentally evaluated in both the APS and ITA programs.

C. PRE-TEST STRUCTURES ANALYSIS

The pre-test structures analysis consisted of determining cycle life for the nozzle throat, creep limit for the throat region, and creep limit for the nozzle region. The analysis was performed by applying the analytical techniques reported in Reference 2 to the ITA and APS thrust chamber designs.

1. Cycle Life Limits

A review of the previous cycle life analyses performed for the APS chamber (Table IV-3, Ref. 1) and the ITA chamber (Table XVI, Ref. 2) indicated that the most critical location for cycle life is the nozzle throat.

In evaluating throat cyclic life, thermal stresses were determined from Equation 7.32 of References 5 which is for the case of thermal shock in a ductile flat plate. For low values of Biot number, the following relationship is obtained:

$$\sigma_T = \frac{E\alpha(T_{aw} - T_o)}{(1-\nu)\left[1.50 + \frac{3.25}{\beta}\right]} \qquad (1)$$

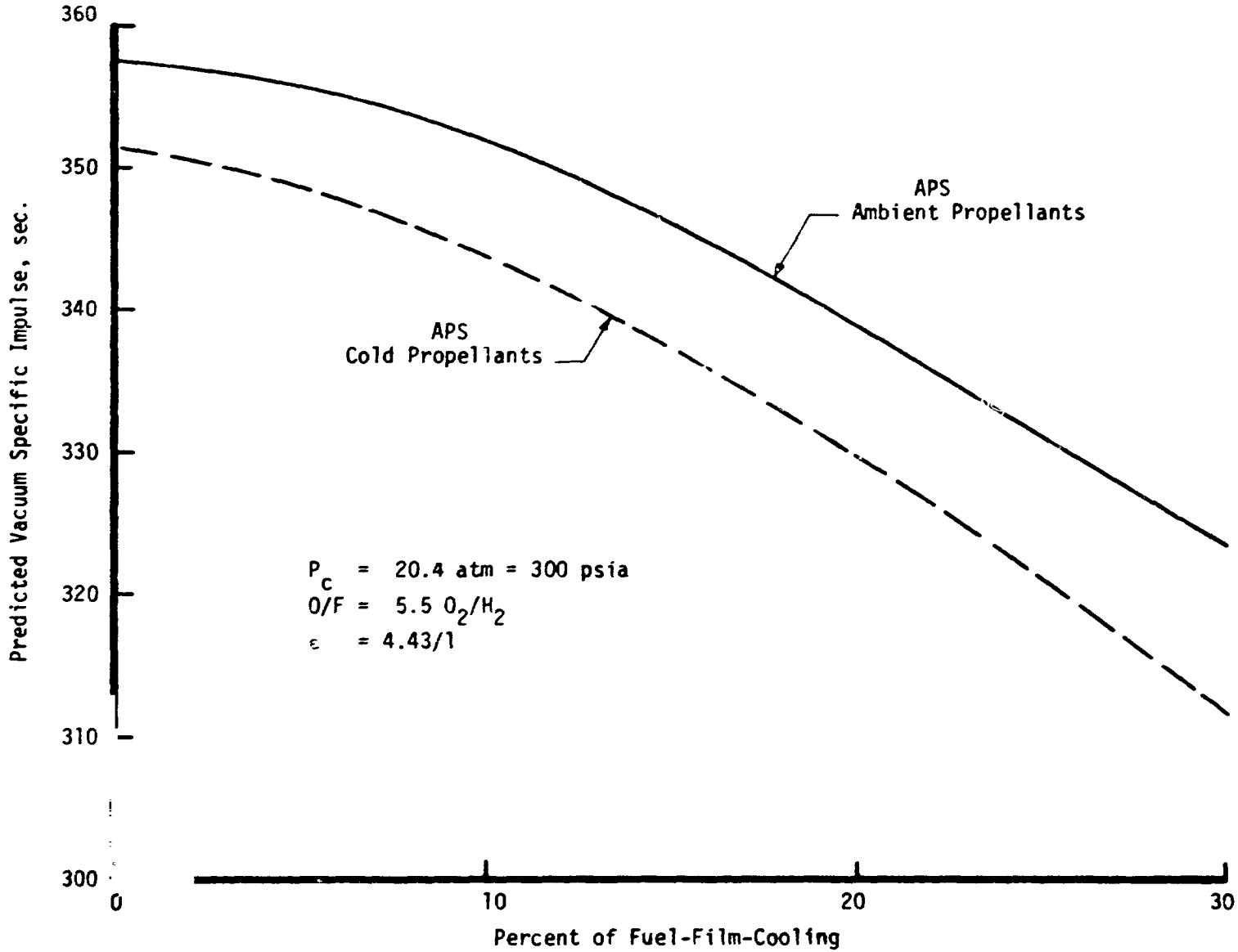

Figure 16. Pretest Performance Prediction, 4.43/1 Nozzle

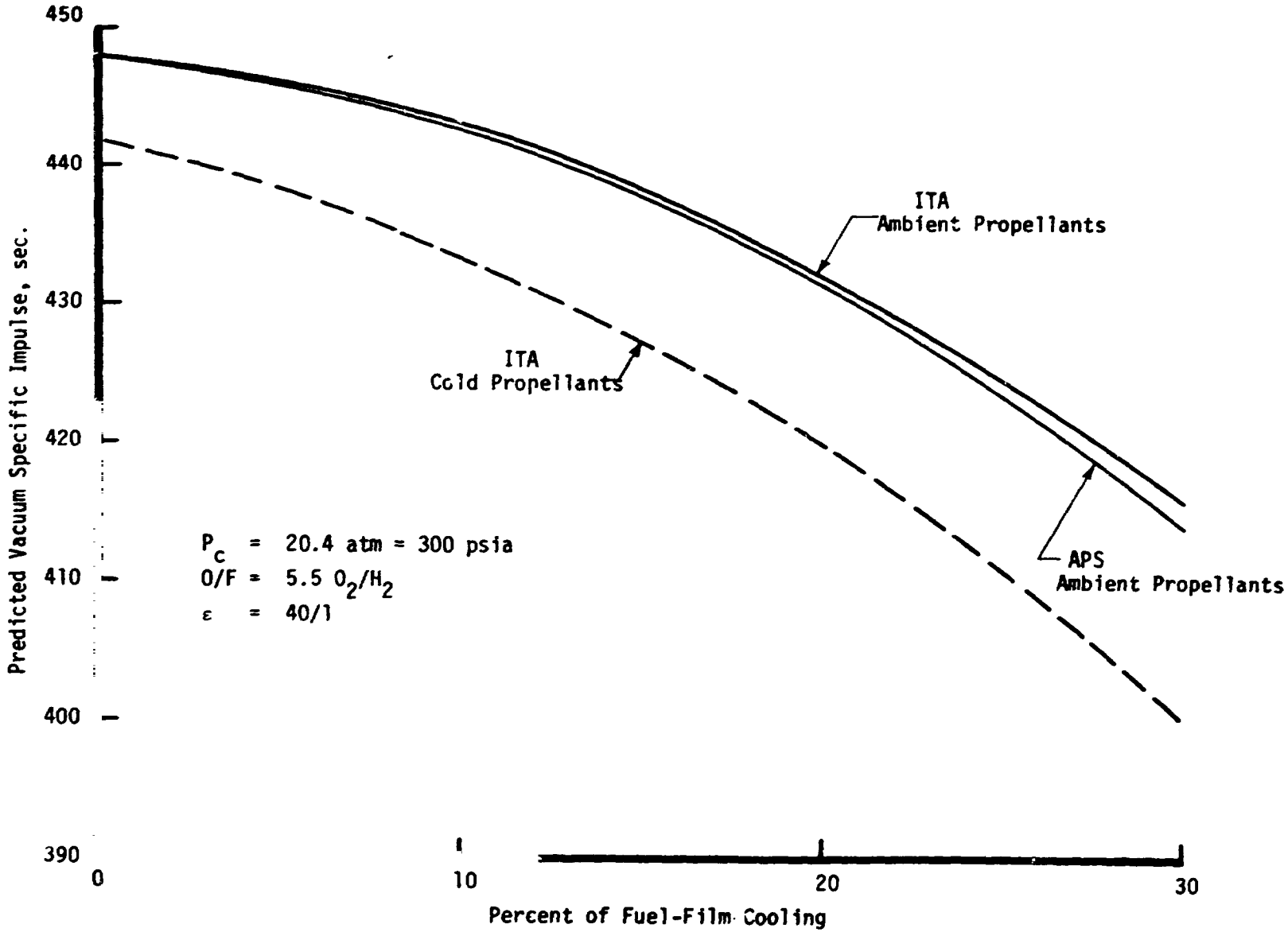

Figure 17. Pretest Performance Prediction, 40/1 Nozzle

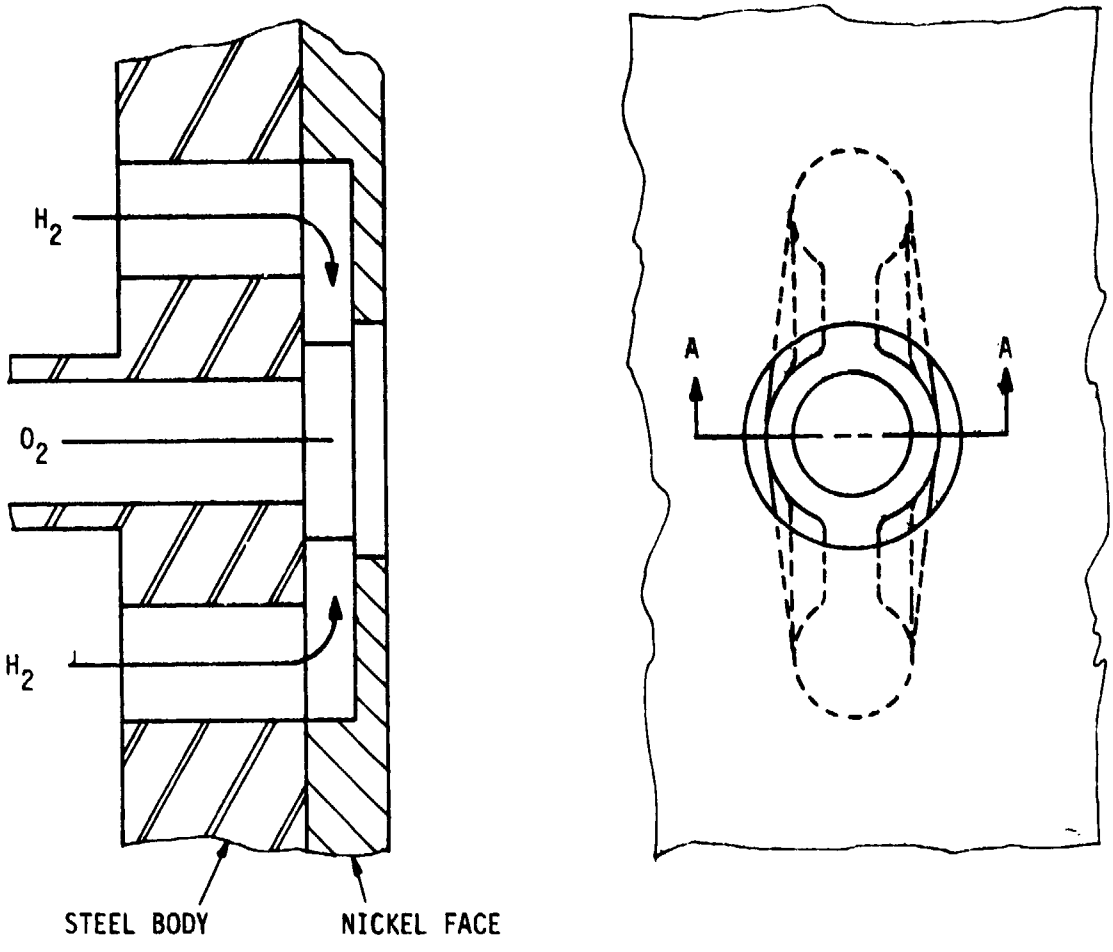

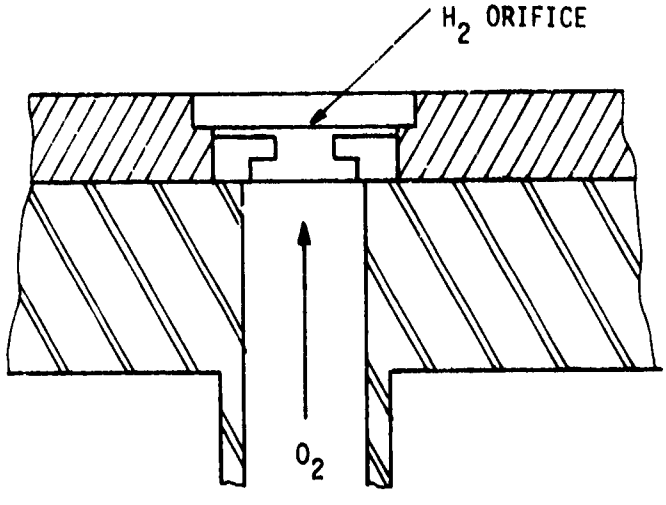

VIEW A-A

Figure 18. Modified I Premix Injector Element

IV, C, Pre-Test Structures Analysis (cont.)

where:

σ_T = Thermal stress
T_{aw} = Recovery or adiabatic wall temperature
E = Modulus of elasticity at T_{aw}
α = Coefficient of expansion at T_{aw}
T_o = Initial wall temperature
ν = Poisson's ratio
β = Biots Number = $\frac{ht_w}{k}$
h = heat transfer coefficient
k = Thermal conductivity
t_w = Wall thickness

In order to allow comparisons between the calculated stresses and the available fatigue life information for Haynes 188, it was necessary to define an equivalent alternating stress. This was done using a modified Goodman diagram (Ref. 6) as illustrated on Figure 19.

$$\sigma_{eq} = \frac{\sigma_a}{1 - \frac{\sigma_m}{F_{tu}}} = \left(\frac{\sigma_a}{F_{tu} - \sigma_m} \right) F_{tu} \qquad (2)$$

where:

σ_{eq} = Equivalent alternating stress with $\sigma_m = 0$,
σ_a = Alternating stress component = 1/2 ($\sigma_T - \sigma_{press}$) at the inner wall (critical location)
σ_m = Mean stress = σ_a for thermal cycle loading,
σ_{press} = Stress due to internal pressure loads,
F_{tu} = Ultimate tensile strengh.

The equivalent total strain range was calculated from the following equation:

$$\Delta\varepsilon_T = \frac{2\sigma_{eq}}{E} . \qquad (3)$$

Fully Reversed Loading

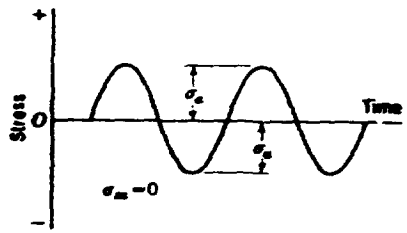

Thermal Cycle Loading

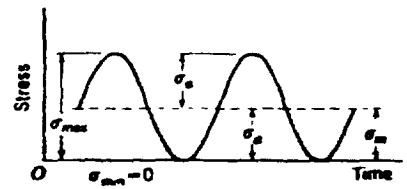

$$\sigma_m = \sigma_a = \frac{1}{2} \quad (\sigma_T - \sigma_p)$$

at Critical N_f Loaction (inner wall)

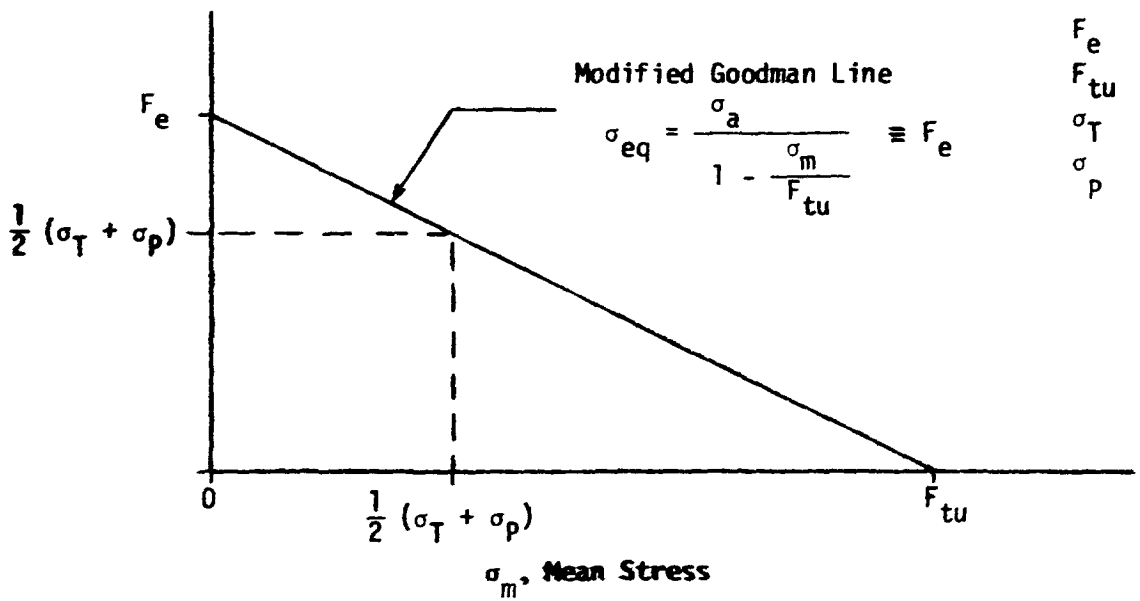

F_e = Endurance Limit
F_{tu} = Ultimate Tensile Strength
σ_T = Thermal Stress
σ_p = Pressure Stress

Figure 19. Structures Analysis Illustrations

IV, C, Pre-Test Structures Analysis (cont.)

For operation at P_c = 20.4 atm, σPress = 48.3 MN/m^2 (7000 psi) at the throat for the ITA design (see Figure 32 of Ref. 7).

Values of cycle life corresponding to the calculated total strains were obtained using Figure 49 of Reference 2 which is derived from the NASA-Manson Universal Slopes Equation (Ref. 8):

$$\Delta\varepsilon_T = \frac{3.5\ F_{tu}}{E} N_f^{-.12} + \left[\ln\left(\frac{100}{100 - RA}\right)\right]^{.6} N_f^{-.6} \qquad (4)$$

where:

N_f = Fatigue Life, cycles,

RA = Area Reduction, %.

The throat cycle life results are summarized on Figure 20 and Table II.

Cycle life decreases very sharply with increased adiabatic wall temperature, consequently the film coolant flow rate must be chosen very carefully. At a given temperature, the ITA cycle life is greater than the APS life because the ITA wall thickness is smaller (see Table I). However, the ITA engine requires more film coolant for a given wall temperature as discussed in Section IV.A.2.

2. Creep Limits

Creep limits were evaluated using the data for Haynes 188 plotted on Figure 21. Chamber wall stress levels were evaluated using Reference 31 data for the ITA engine and by assuming that the stress is inversely proportional to the wall thickness for the APS engine.

The APS design has a thicker nozzle wall, consequently the stress levels are lower and the allowable nozzle temperature is somewhat higher than for the ITA design as shown on Table II. However, the difference is relatively small because of the rapid decrease in creep strength at temperatures above 2000°F. Figure 20 shows that the APS nozzle creep limits correspond to a lower throat adiabatic wall temperature. This is because of the different supersonic entrainment fraction models used for the APS and ITA designs (see Appendix B, Section II).

D. LIFE VS PERFORMANCE PREDICTIONS

Predictions of the life vs performance characteristics of the APS and ITA designs for O/F = 5.5 operation were obtained by combining the results of all three pretest analyses (heat transfer, performance, struc-

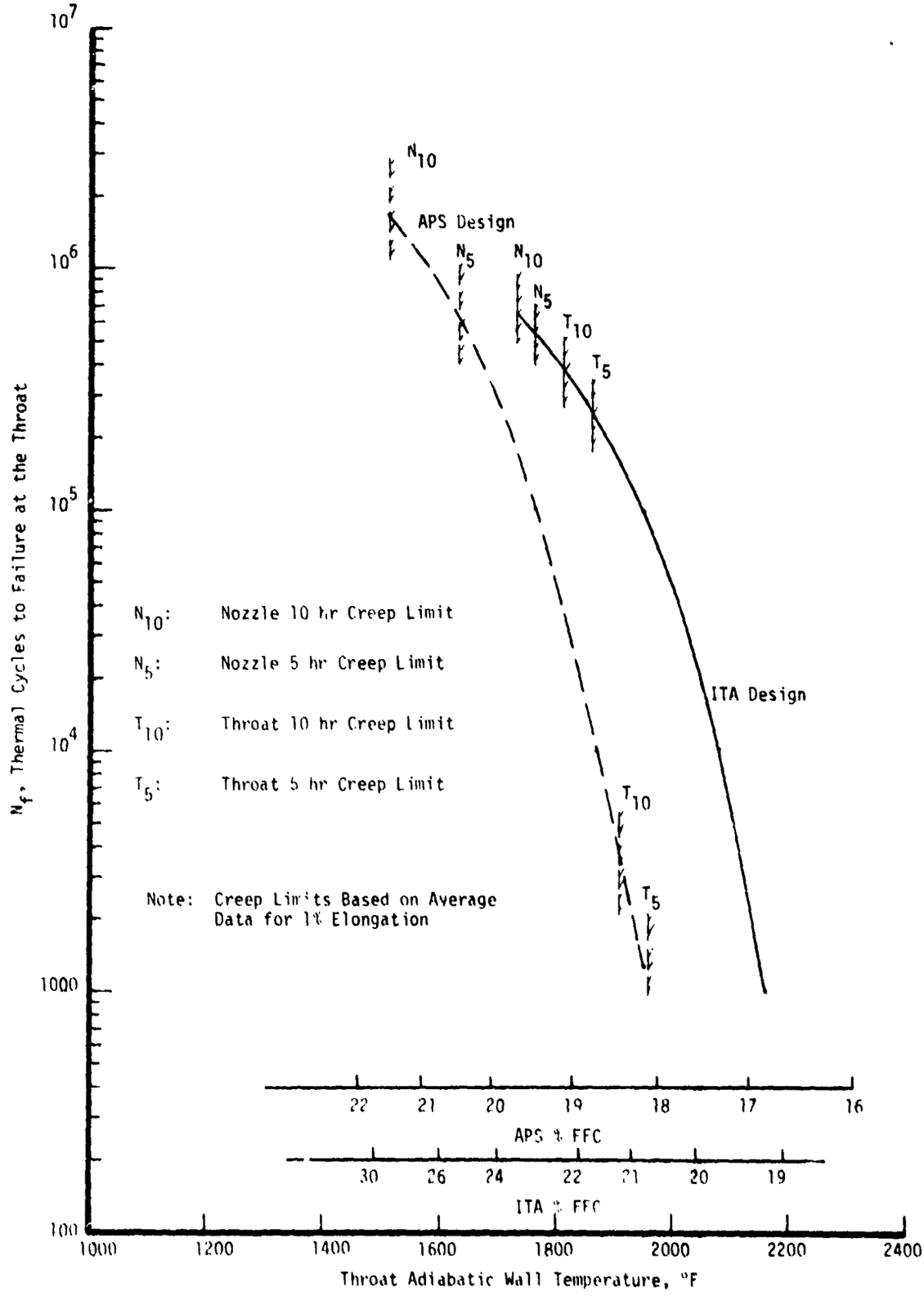

Figure 20. Pretest Stress Analysis Results for the Film Cooled Chamber

TABLE II

PRETEST LIFE VS. PERFORMANCE ANALYSIS RESULTS

THROAT CYCLE LIFE

Design	N_f, Cycles	T_{aw}, °F	% FFC	I_s, sec (1)
ITA	1000	1420 (2100)	19.5	432.7
	2500	1400 (2060)	20.0	432.0
	20,000	1370 (2000)	20.5	431.0
	70,000	1311 (1900)	21.5	429.9
	1.4×10^6	1290 (1860)	22.0	429.1
APS	1200	1310 (1900)	18.5	433.5
	12,000	1260 (1810)	19.0	432.8
	36,000	1230 (1760)	19.5	432.1
	$.25 \times 10^6$	1180 (1660)	20.0	431.4
	$.8 \times 10^6$	1120 (1560)	21.0	430.0
	1.7×10^6	1060 (1450)	22.0	428.4

CREEP LIMITS

Design	Location	Total Life, Hr	T_{max}, °K (°F) (2)	% FFC	I_s, sec (1)
ITA	Throat	10	1260 (1810)	22.5	428.5
	Throat	5	1290 (1860)	22.0	429
	Nozzle	10	1420 (2100)	23.5	427
	Nozzle	5	1440 (2130)	23.0	427.5
APS	Throat	10	1315 (1910)	18.5	433.5
	Throat	5	1345 (1960)	18.0	434
	Nozzle	10	1455 (2160)	21.5	429
	Nozzle	5	1480 (2200)	20.5	430.5

(1) - Vacuum performance with 40/1 nozzle and ambient temperature propellants (estimated to nearest 0.1 sec. for analytical purposes only)

(2) For 1% Elongation

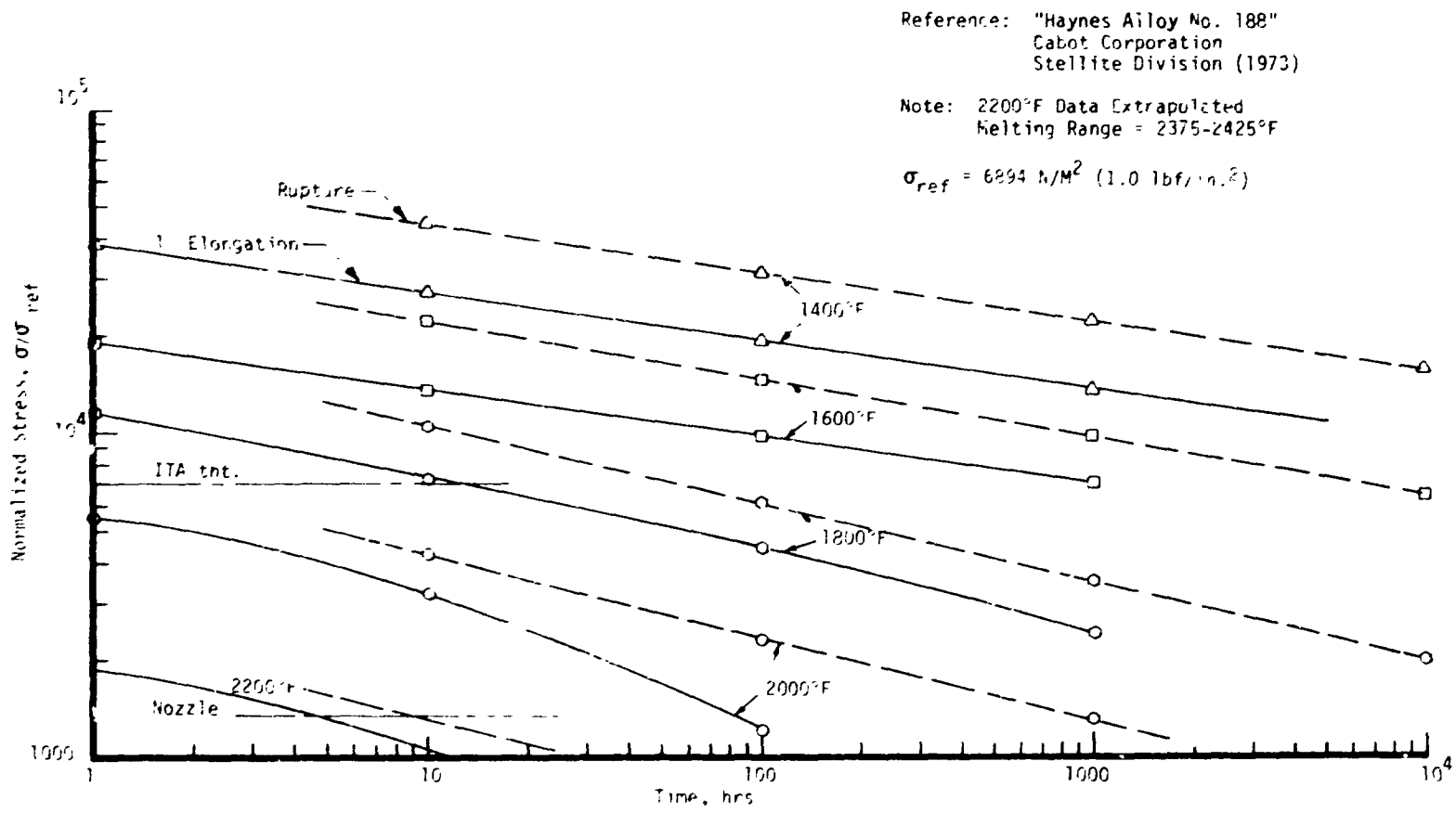

Figure 21. Haynes 188 Creep Strength Data

tures). Figure 20 shows that the predicted performance limit for both designs is due to nozzle creep. For the specified life requirements (1200 thermal cycles and 10 hr total engine life), the predicted maximum performance values obtained from Figures 17 and 20 are 429 sec for the APS design (20.5% FFC) and 427 sec for the ITA design (23.5% FFC). The APS maximum performance is higher because it has a thicker nozzle wall and because less film coolant mixing occurs upstream of the throat.

The life vs performance characteristics were re-evaluated in the post-test analysis based on the experimental heat transfer and performance data. The pretest evaluation provided a preliminary indication of performance potential and was the basis for test planning. During the post-test analysis, the APS injection sleeve design was assumed because it is evidently a more efficient design. The film cooled chamber wall thickness was considered variable in the post-test work.

V. TEST RESULTS AND DISCUSSION OF RESULTS

Two types of tests were performed on this program: performance verification tests and life verification tests. The 8 performance verification tests were generally long duration firings in which steady state performance and thermal data were obtained. The 1220 life verification tests were of relatively short duration firings in which thermal steady state was not achieved but a full thermal strain cycle of the chamber throat was achieved.

A. PERFORMANCE VERIFICATION TESTS

1. Test Objectives

The objective of the performance verification tests was to experimentally determine the effects of fuel film cooling flow rate on specific impulse and thrust chamber wall temperature when the film cooled APS thrust chamber operates at 5.5 overall O_2/H_2 mixture ratio and 300 psia chamber pressure.

2. Testing Approach

The overall approach for the performance verification test series consisted of starting at a relatively high film coolant flow rate and progressively reducing it. After each firing, the chamber wall temperature data were carefully evaluated before proceeding to the next test. The nominal test duration was 10 seconds (steady state P_c, no igniter oxidizer flow). However, the two tests at the lowest film coolant rates were conducted at 2-3 second duration so as to prevent hardware damage by the hot streaks produced by existing cracks in the film coolant sleeve. The O_2/H_2 propellants were stored at ambient temperature and were not temperature conditioned upstream of the thrust chamber assembly.

V, A, Performance Verification Tests (cont.)

The timing of engine flow parameters was patterned after the NAS 3-17813 tests. A typical start sequence is indicated on Figure 22.

3. Test Results

A total of eight tests were conducted at a nominal mixture ratio of 5.5, a nominal chamber pressure of 20.4 atm, and with fuel film coolant flow rates ranging from 34.5% to 18.4% of the total fuel flow.[1] Steady state wall temperatures are listed on Table III. The overall test conditions and measured performance are listed on Table IV. The throat and nozzle exit wall temperature data are plotted on Figures 23 and 24.

Testing was initiated at a 35% fuel film cooling rate in Test 106. The measured chamber wall temperatures were at or very near steady state at the end of this 9 second test. Wall temperatures and performance were both higher than anticipated. In addition, a significant circumferential wall temperature distribution was observed. Throat temperatures ranged from 618°K (625°F) in row C to 819°K (1014°F) in row D. The wall temperature at the nozzle exit ranged from 783°K (949°F) to 1032°K (1398°F).

For the next firing, Test 108, the duration was increased to 10 seconds and the film cooling flow rate was reduced to 30%. Similar wall temperature data were obtained except that the measured temperatures were closer to the predictions. After Test 108, narrow axial streaks were apparent on the nozzle in 4 locations. These streaks correlated with the damaged regions of the injection sleeve. The most severe of these was instrumented at the nozzle exit and designated row E. Figure 25 shows that the 10 second test duration was sufficient to produce thermal steady state. This duration was maintained for the next 4 tests (111, 114, 115, 116).

In Test 111, the film cooling rate was reduced to 27%. The row E temperature measurement was more than 165°K (300°F) higher than other measurements at the same axial position. Additional row E thermocouples were installed prior to the next test, Test 114, which was conducted with 24% film cooling. At this condition, all measured throat and nozzle temperatures except row E were below the predictions. Similar data were subsequently obtained at a 22% film cooling rate in Test 115.

[1] The fuel film coolant flow rate is defined as the percentage of the total fuel flow rate injected as film coolant.

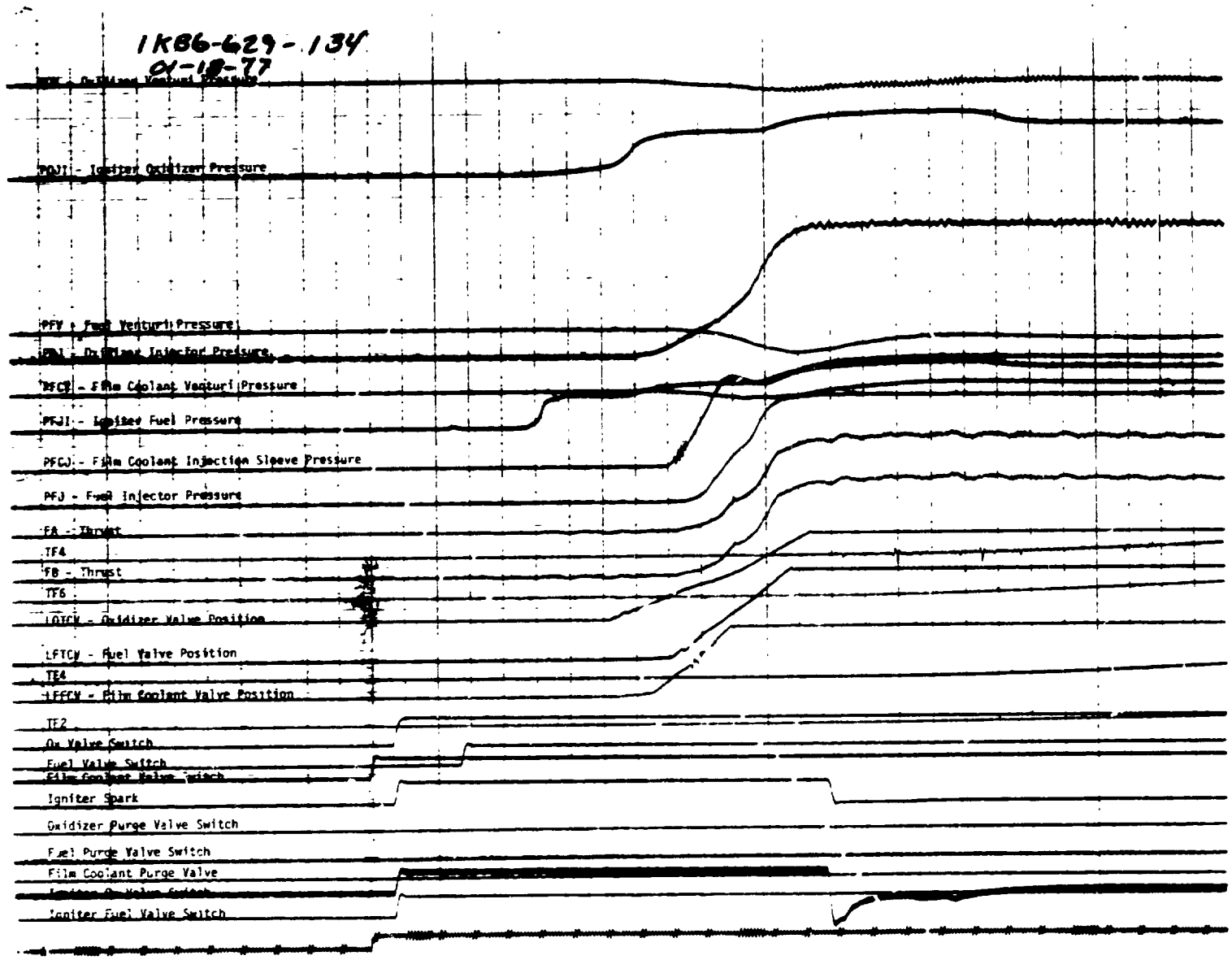

Figure 22. Typical Start Sequence

ORIGINAL PAGE IS
OF POOR QUALITY

TABLE III

STEADY STATE WALL TEMPERATURES

Performance Verification Tests, Test Series 1F 66-629-XXX

Test	Axial Position	Measured Temperature Values, °F: Row A 0	Row F 65	Row B 120	Row G 135	Row H 150	Row C 210	Row D 300	Row E 320	Measured Temperature, °F: Row A 0	Row F 65	Row B 120	Row G 135	Row H 150	Row C 210	Row D 300	Row F 320
	1		-	394	-	-	-	682	-	-		474	-	-	-	634	-
106	2	581	-	578	-		495	792	-	578	-	549	-	-	531	696	
34.5% FFC	3	-	-	769	-	-	-	934		-	-	683	-	-	-	774	-
O/F=5.75	4	828	-	838	-	-	652	1014	-	716	-	721	-	-	618	819	-
Pc=21.1 atm	5	-	-	1019	-	-	810	1208	-	-	-	872	-	-	706	927	-
9 sec dur	6	1158	-	1147	-	-	949	1398	-	899	-	893	-	-	783	1032	-
	1	-	-	439	-	-	-	759	-	-	-	499	-	-	-	677	-
108	2	617	-	593			535	845	-	598	-	595	-	-	553	725	-
29.4% FFC	3	-	-	871	-	-		1026	-	-	-	739	-	-	-	826	-
O/F=5.5?	4	926	-	945	-	-	-	1104	-	770	-	791	-	-	-	869	-
Pc=20.8 atm	5	-	-	1100	-	-	684	1278	-	-	-	311	-	-	747	966	
10 sec dur	6	1256	-	1218	-	-	1033	1477		953	-	932	-	-	829	1076	-
	1	-	-	459	-	-	-	795	-	-	-	511	-	-	-	697	-
111	2	639	-	625	-	-	561	969	-	611	-	603	-	-	567	738	-
27.2% FFC	3	-	-	916	-	-	-	1053	-	-		764	-	-	-	841	-
O/F=5.39	4	977	-	992	-	-	772	1134	-	798	-	807	-	-	684	896	-
Pc=20.3 atm	5	-	-	1132	-	-	-	1289	-	-	-	884	-	-	-	972	-
10 sec dur	6	1273	-	1246	-	-	1070	1491	1792	963	-	948	-	-	850	1078	1251
114	1	-	-	482	-	-	699	890	834	-		523	-	-	644	750	719
24.4% FFC	2	683	-	663	-	-	594	960	672	635	-	624	-	-	586	789	629
O/F=5.29	4	1066	-	1058	-	-	847	1220	1440	848	-	843	-		726	933	1056
Pc=20.1 atm 10 sec dur	6	1320	-	1289	-	-	1130	1493	1767	989	-	972	-	-	883	1085	1237
115	1	-	-	523	-	-	759	966	904	-	-	546	-	-	677	792	758
22% FFC	2	866	-	742	-	-	667	1039	737	737	-	668	-	-	626	833	665
O/F=5.27	4	1109	-	1161	-	-	972	1331	1584	983	-	901	-	-	796	995	1136
Pc=19.9 atm 10 sec dur	6	1575	-	1381	-	-	1240	1600	1881	1131	-	1023	-	-	944	1144	1073
116 22.1% FFC	2	787	-	748	-	-	680	1051	746	693	-	672	-	-	633	839	670
O/F=5.43	4	1247		1181	-	-	793	1353	1636	948	-	912	-	-	807	1007	1164
Pc=20.5 atm 10 sec dur	6	1519	1840	1401	-	1578	1271	1629	1937	1099	1278	1034	-	1132	962	1162	1332
117* 19.7% FFC	2	920	-	870	-	-	795	1180	845	767		739	-		697	911	725
O/F=5.40	4	1420	-	1330	-	-	1170	1510	1810	1044	-	994	-	-	906	1094	1261
Pc=19.9 atm 3 sec dur	6	1605	1815	1425	1915	1650	1410	1700	2040	1147	1264	1047	1264	1172	1039	1200	1389
118* 15.4% FFC	2	970	-	920	-		865	1120	905	794	-	767	-	-	736	878	758
O/F=5.41	4	1495	-	1415		-	1275	1510	1860	1086	-	1041	-	-	964	1094	1289
Pc=19.5 atm 2 sec dur	6	1620	1835	1540	1940	1660	1475	1675	2030	1156	1281	1111	1278	1178	1075	1186	1383

*Steady State Temperatures Estimated from Transient Data

TABLE IV

TEST PERFORMANCE SUMMARY

Test Series	-	1K 86-629-XXX →														
Test No.	-	106 →		108 →		111 →		114 →		115 →		116 →		117 →		118 →	
Summary Period, t	(sec	5-9		5-10		5-10		5-10		5-10		5-10		2.75-3.0		1.75-2.0	
Chamber Pressure, Pc	(psia)	310.4		305.7		299.2		296.2		292.7		300.6		291.5		286.3	
Test Mixture Ratio, O/F	-	5.755		5.520		5.392		5.288		5.267		5.433		5.405		5.414	
% FFC, $W_{ffc}/W_{f,tot}$		24.45		29.35		27.21		24.41		21.96		22.06		19.66		18.44	
Corrected Thrust, F_{vac}	lbf	1338.7	1690.5	1316.1	1658.4	1288.0	1632.8	1279.9	1627.4	1262.6	1605.8	1305.2	1649.2	1261.8	1606.8	1242.6	1580.9
Oxid. Flowrate, $\dot{W}_o$	lbm/sec	3.5763		3.4057		3.2752		3.1980		3.1319		3.2642		3.1405		3.0805	
Fuel Flowrate, $\dot{W}_{f,core}$	lbm/sec	.3976		.4257		.4320		.4468		.4537		.4578		.4566		.4540	
Igniter Flow, $\dot{W}_{f,ign}$	lbm/sec	.0098		.0102		.0101		.0103		.0104		.0105		.0103		.0100	
FFC, $\dot{W}_{ffc}$	lbm/sec	.2140		.1811		.1653		.1476		.1306		.1325		.1142		.1049	
Total Flowrate, $\dot{W}_t$	lbm/sec	4.1977		4.0227		3.8827		3.8027		3.7265		3.8651		3.7216		3.6495	
Char. Exhaust Vel. C*	ft/sec	6795.0		6982.4		7080.4		7158.8		7216.3		7152.3		7203.1		7214.1	
Specific Impulse, Isp	sec	318.9	402.7	327.2	412.3	331.7	420.5	336.6	428.0	338.8	430.9	337.7	426.7	339.0	431.7	340.5	433.2
AT TEST CONDITIONS																	
Nozzle Exit Area Ratio, ϵ	-	4.43	40	4.43	40	4.43	40	4.43	40	4.43	40	4.43	40	4.43	40	4.43	40
$I_{sp,vac}$	sec	395.0	464.3	397.9	466.0	399.4	466.8	400.3	467.4	400.7	467.6	398.8	466.4	399.3	467.0	399.2	466.9
$I_{sp,ODK}$	sec	392.1	457.4	394.9	459.6	396.3	460.7	397.2	46 .3	397.6	461.6	395.8	460.1	395.2	460.8	396.1	460.7
t_{KL}	sec	2.9	6.9	3.0	6.4	3.1	6.1	3.1	6.1	3.1	6.0	3.0	6.3	3.1	6.2	3.1	6.2
t_{BLL}	sec	2.0	6.5	2.0	6.5	2.0	6.5	2.0	6.5	2.0	6.5	2.0	6.5	2.0	6.5	2.0	6.5
t_{CCL}	sec	32.8	4.3	33.7	4.4	34.1	4.4	34.6	4.5	34.9	4.5	34.7	4.5	34.9	4.5	35.0	4.5
t_{FFCL}	sec	35.2	35.2	28.0	28.7	25.2	23.4	21.6	19.3	18.6	16.7	19.8	16.2	15.9	13.3	14.5	12.1
t_{EPL}	sec	3.2	8.7	4.0	9.7	3.3	5.9	2.4	3.0	3.3	3.6	2.6	6.2	4.4	4.8	4.1	4.4
EPE	%	99.19	98.12	98.99	97.91	99.17	98.73	99.40	99.35	99.18	99.24	99.35	98.67	98.90	98.98	98.97	99.05
Mixing Eff., E_m	%	75.2	75.2	77.0	77.0	81.0	81.0	86.0	86.0	84.4	84.4	80.0	80.0	82.0	82.0	82.5	82.5
AT NOMINAL OPER. POINT																	
$I_{sp,ODK}$	sec	395.7	460.7	395.7	460.7	395.7	460.7	395.7	460.7	395.7	460.7	395.7	460.7	395.7	460.7	395.7	460.7
$I_{sp,NOM}$	sec	322.5	406.0	328.9	413.4	331.1	420.5	335.1	427.4	336.9	430.0	337.6	427.3	338.5	431.6	340.1	433.2
F_{vac}	lbf	1353.8	1704.3	1319.3	1662.9	1285.7	1632.8	1274.2	1625.2	1255.5	1602.5	1304.8	1651.5	1259.9	1606.5	1241.1	1580.9

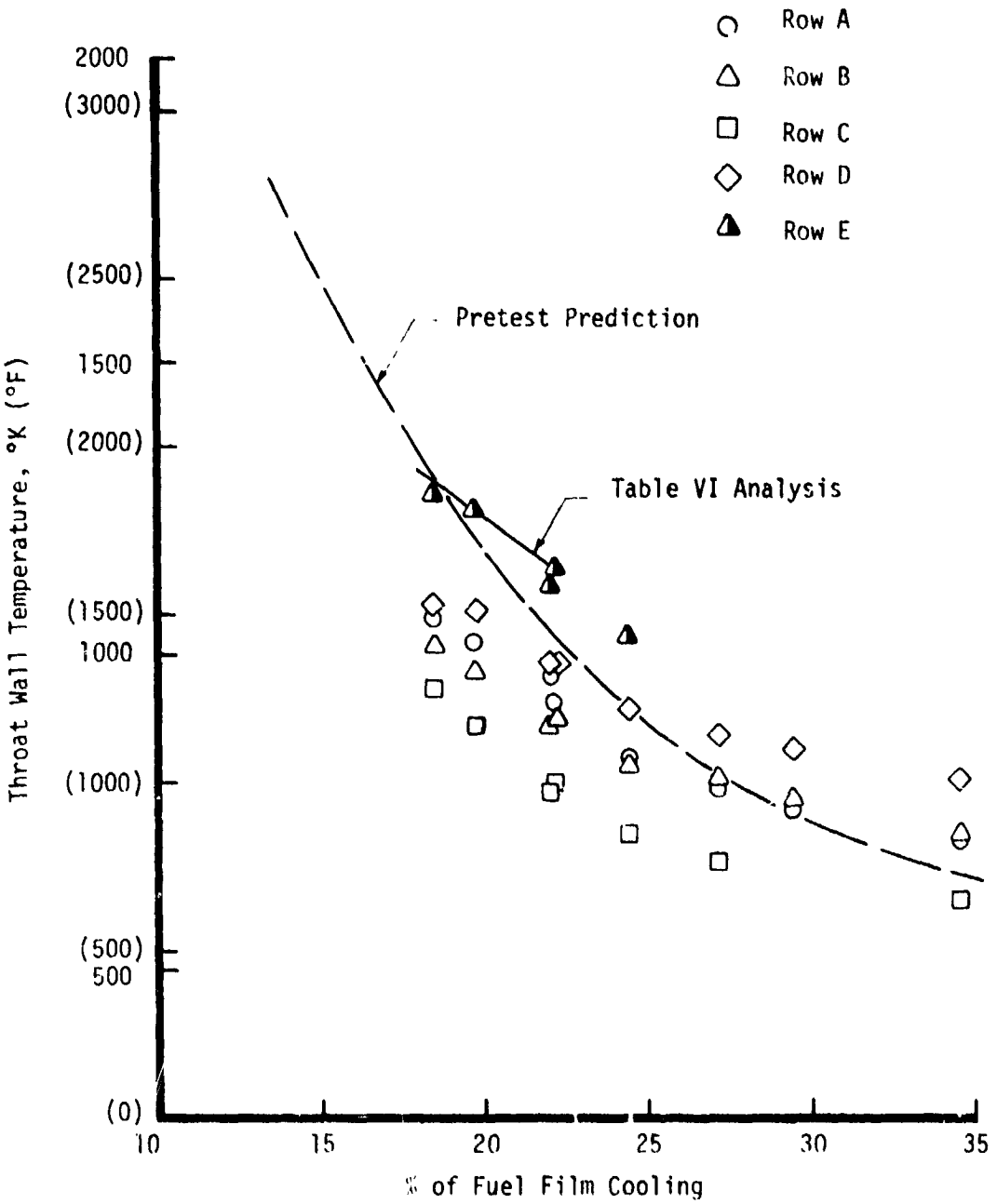

Figure 23. Effect of Film Cooling on Throat Wall Temperature

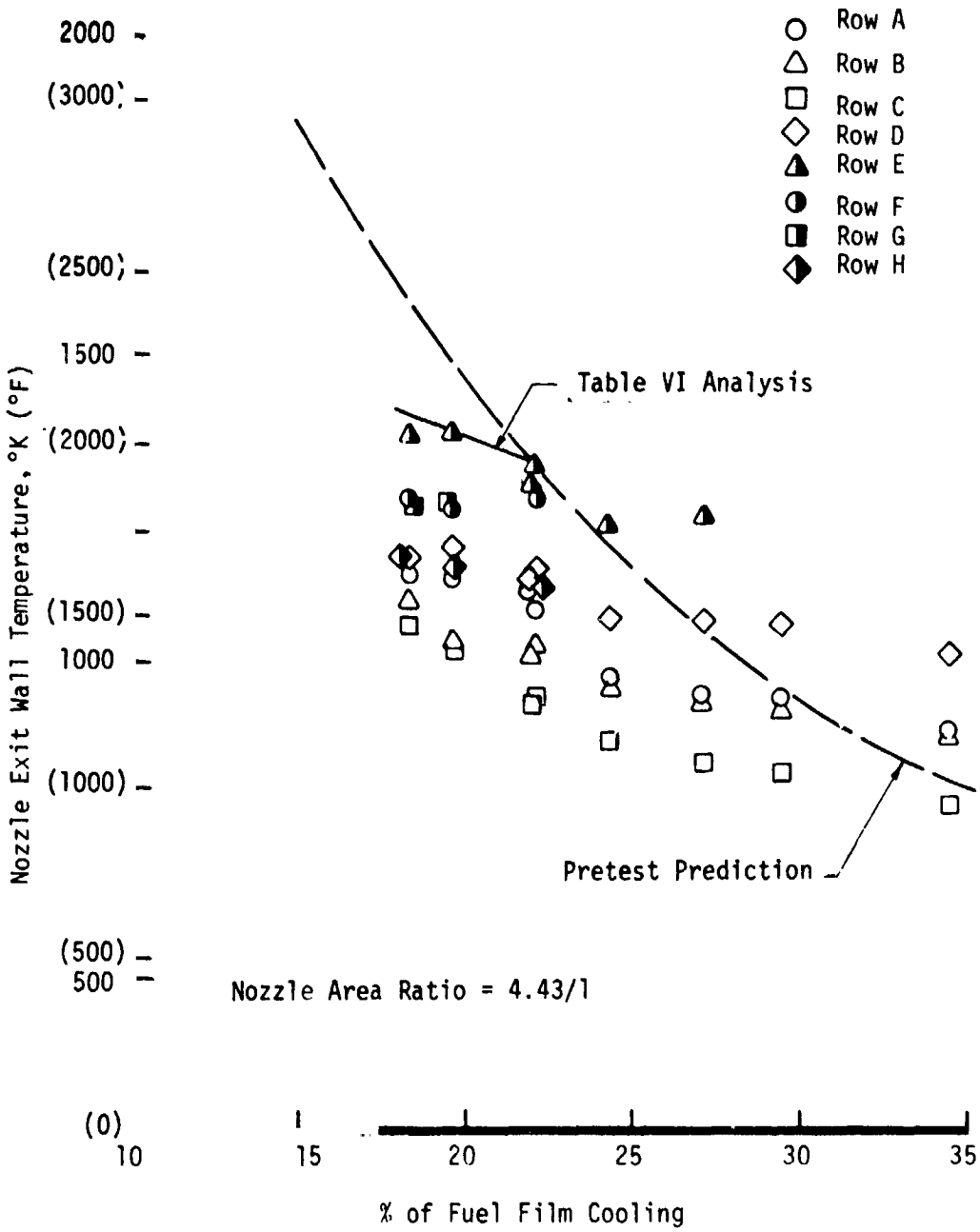

Figure 24. Effect of Film Cooling on Nozzle Exit Wall Temperature

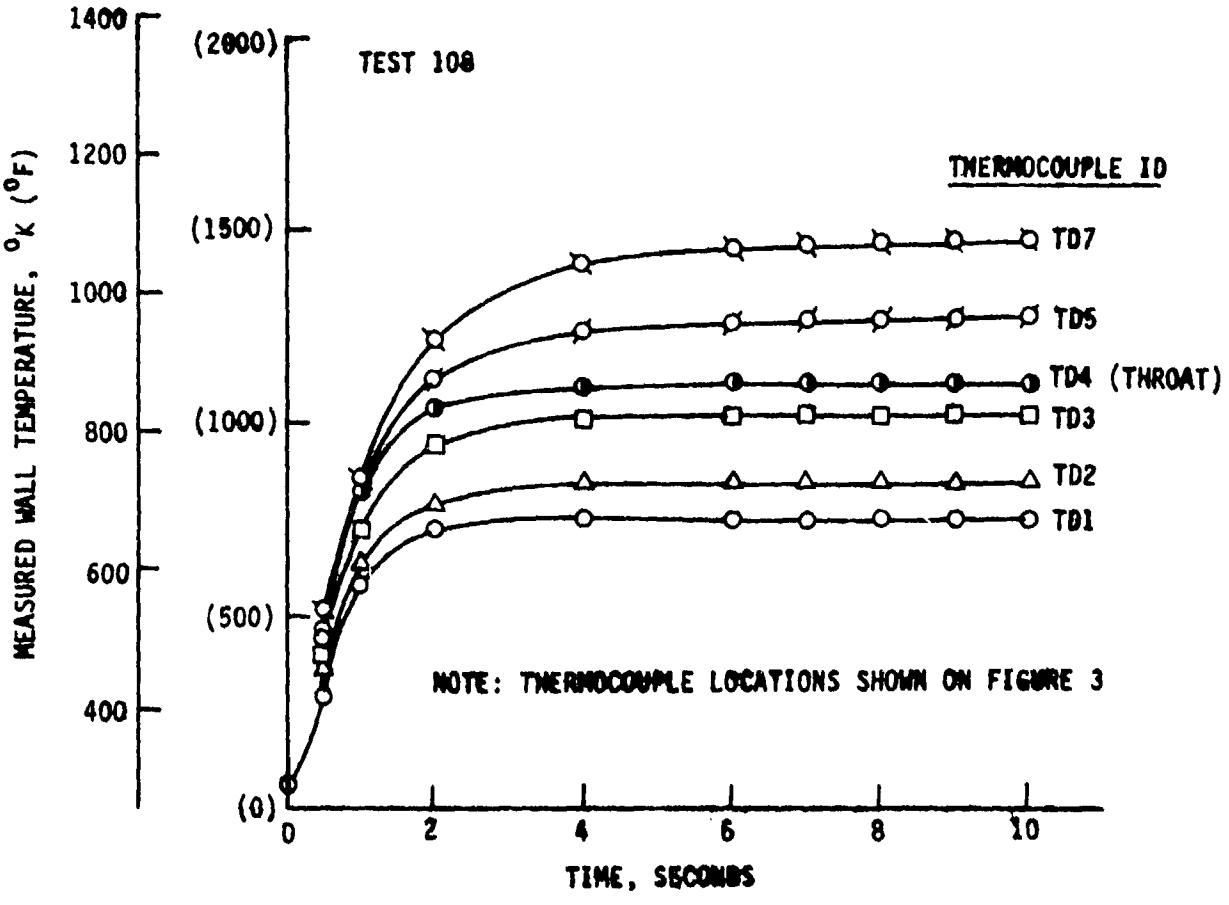

Figure 25. Wall Temperature Transient, Test 108

V, A, Performance Verification Tests (cont.)

The nominal conditions of Test 115 were repeated in Test 116. Prior to Test 116, additional thermocouples were installed on the other visible streaks at the nozzle exit. The data from these added thermocouples verified that row E was the maximum temperature location.

Two tests were conducted with a film cooling rate less than 20% - Test 117 at 19.7% and Test 118 at 18.4%. These tests were run with short durations (2-3 seconds) to preclude any hardware damage due to high temperatures since no backup hardware was available for the life verification test series. Steady state wall temperatures were estimated from the Test 117 and 118 transient data using the Test 116 steady state and transient data as indicated on Figure 26. The estimated steady state temperatures are believed to be accurate within $\pm$ 10°K.

These eight performance verification tests yielded the desired experimental relationships between performance, chamber wall temperature, and film coolant flow rate which were subsequently used to establish the operating conditions for the life verification test series which is discussed in the following section.

B. LIFE VERIFICATION TESTS

1. Test Objectives

The objective of the life verification tests was to demonstrate the life potential of a thruster during a series of 1200 full thrust steady state cycles at a single film coolant flow rate and at 5.5 overall O_2/H_2 mixture ratio and 20.4 atm chamber pressure.

2. Testing Approach

The life verification tests were conducted for a duration ranging from 1.0 to 0.4 seconds. All tests were sufficiently long enough to produce a full thermal strain cycle in the throat region. The throat region was cooled to ambient temperature between firings by utilizing a film coolant lag at shutdown and by flowing a gaseous nitrogen purge through the film cooling circuit for about 30 seconds.

3. Test Results

A total of 1220 test firings of the APS Thrust Chamber Assembly were conducted during the Life Verification Test Series. The nominal performance level ranged from 430 to 432 seconds.[2] A photograph of the engine operating after over 1200 of the firings has been made is shown as Figure 27 (Test 151).

[2]Based on ambient temperature propellants and 40/1 nozzle.

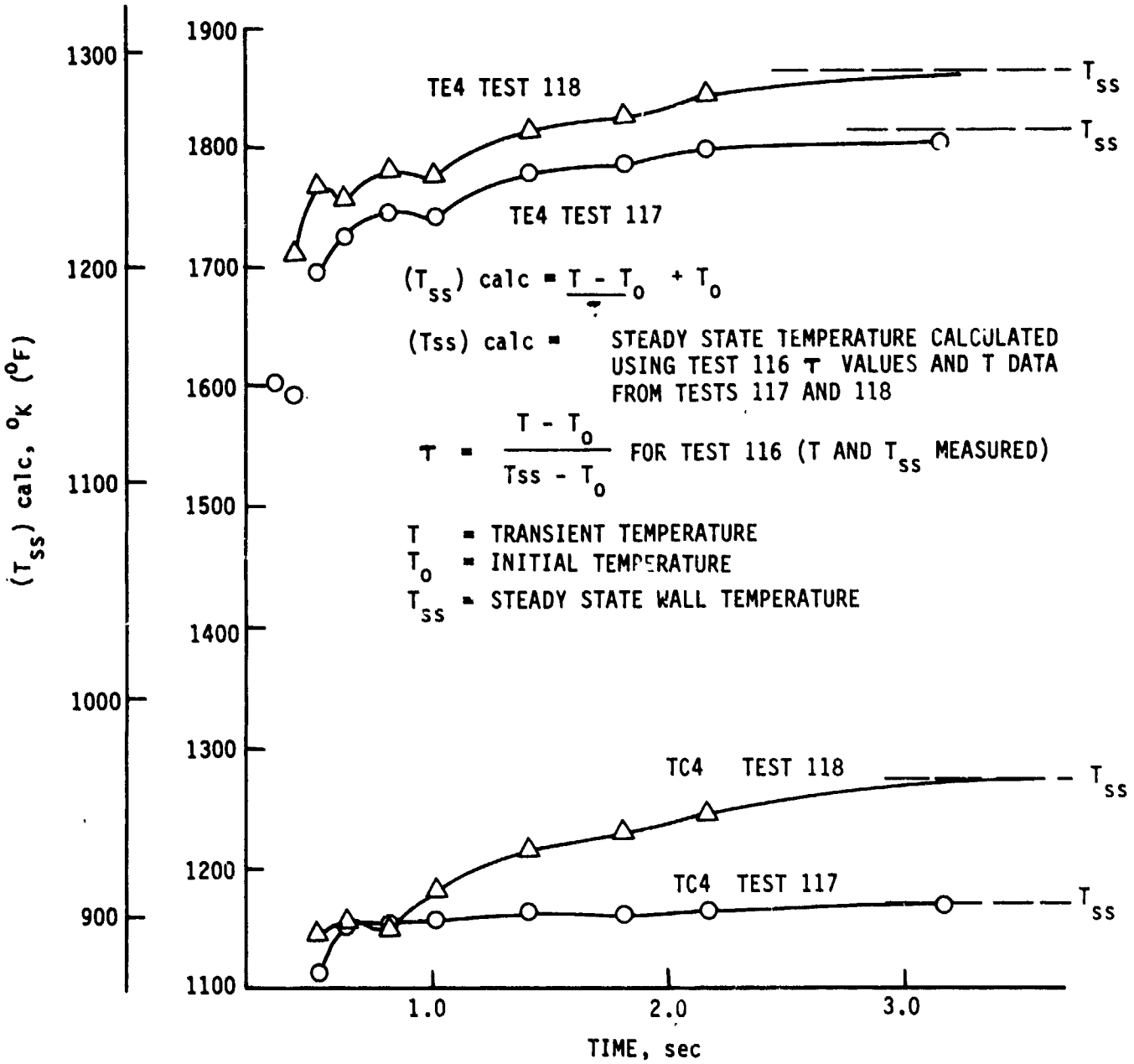

Figure 26. Technique for Estimating Steady State Wall Temperature From Transient Data of Tests 117 and 118

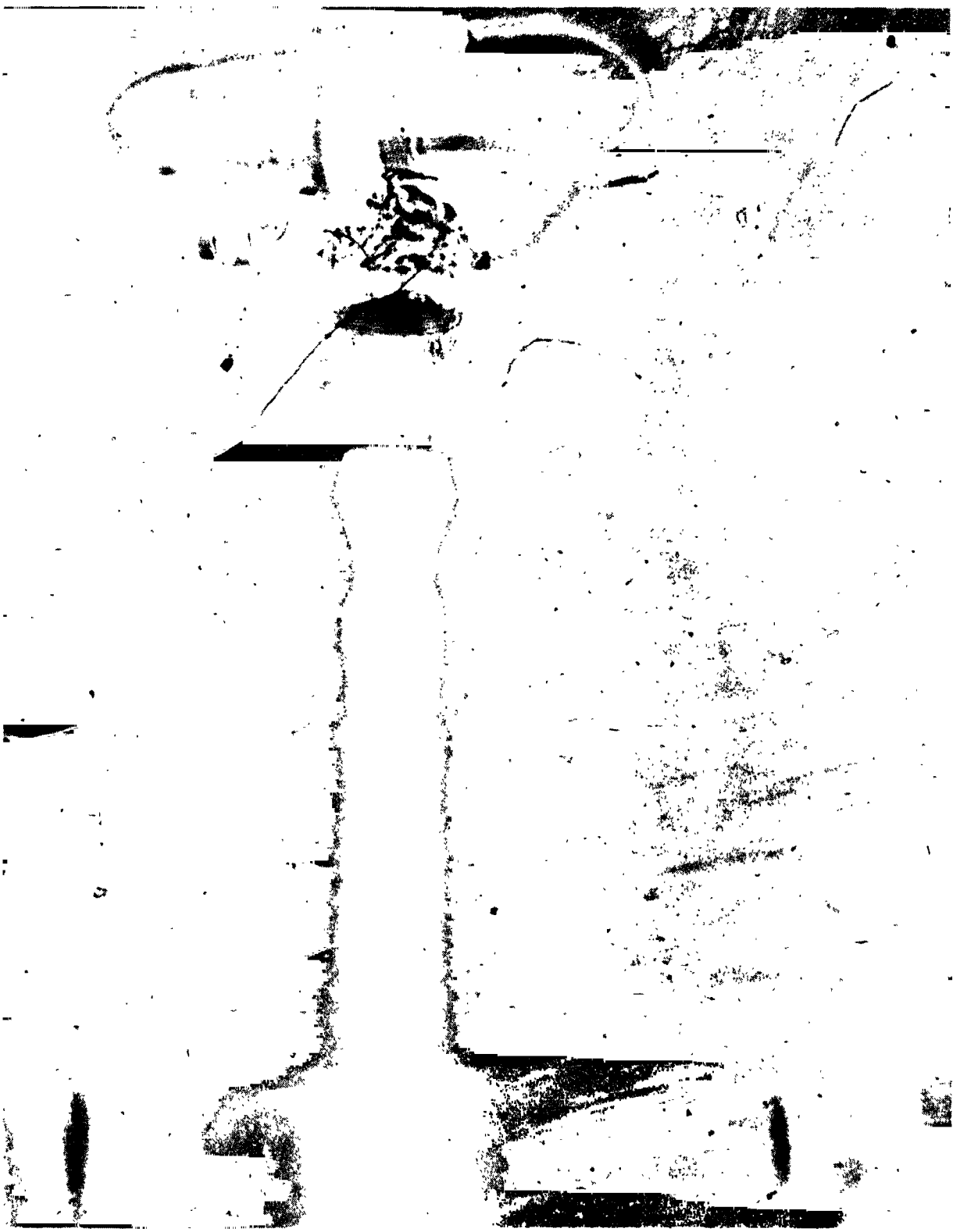

Figure 27. Plug Cluster Module Engine Firing After Over 1200 Previous Firings at O/F = 5.5

V, B, Life Verification Tests (cont.)

The nominal test conditions were as follows:

O_2/H_2 Mixture Ratio	=	5.5
Chamber Pressure	=	20.4 atm
Fuel Film Coolant Flow Rate	=	19.5% to 21.5% of the total H_2 Flow Rate

The actual test conditions are summaried on Table V.

The initial 19.5% nominal film coolant flow rate corresponds to a performance level of 432 seconds.[3] This flow rate was selected by evaluating wall temperature data from the performance verification tests on the basis of the pre-test structures analysis results. The evaluation yielded the prediction of cycle life vs film coolant flow rate indicated on Table VI. The critical wall temperature with regard to cycle life was TE4 (Row E at the throat).

Since it was required to demonstrate 1200 thermal strain cycles, it was determined that the operating condition for the life verification tests should be chosen so that the calculated cycle life is at least 5000 cycles. The difference between 5000 cycles and 1200 cycles accounts for cycle life data scatter (factor of 4 on 1200 cycles) and the previous test history of the S/N 6 APS film cooled chamber (4% of film cooled chamber life used). The cycle life calcualted for the 19.5% flow rate was 7000 cycles. This is somewhat higher than was required but in view of the very steep decrease in cycle life and moderate increase in performance with coolant flow rate, the 19.5% condition was chosen as a safe operating point.

The initial test duration of 1.0 seconds was chosen somewhat arbitrarily and is in excess of the minimum duration required to produce maximum strain during each firing. The thermal strain is proportional to the ΔT through the chamber wall. Figure 28 shows that when an instantaneous convective boundary condition is assumed this ΔT maximizes in about 0.1 seconds. Figure 7.1 of Reference 5 also shows that this corresponds to the time at which maximum stress occurs. Consideration of the start transient period indicates that about 0.15 sec test duration is sufficient to yield a full thermal strain cycle at the throat.

During previous testing at ALRC and NASA-Lewis with overall O/F = 4, the copper sleeve through which the hydrogen film coolant is injected had been damaged. Several small cracks had developed in the sleeve at the

[3] Based on ambient temperature propellants and 40/1 nozzle.

TABLE V

SUMMARY OF LIFE VERIFICATION TEST CONDITIONS

TEST SERIES 1K B6 - 629 - XXX

Test No.	O/F	Pc psia	% FFC	Firing Duration	Date	Thermal Cycles	Total Thermal Cycles	Remarks
119-126	5.51-5.87	300-313	19.4-20.2	1.0	1/7-11/77	9	9	Sequence checkout tests (Test No. 119,122, 123, 125,126)
127	5.33-5.42	300-308	19.4-19.5	1.0	1/11/77	37	46	
128	5.2-5.56	295-309	19.4	1.0	1/11/77	6	52	
129	5.4-5.58	301-311	19.5-19.8	1.0	1/11/77	30	82	
130	5.47-5.63	301-309	19.3-19.7	1.0	1/11/77	50	132	Cu Sleeve Cracks enlarged, Cu Erosion at Row F and Cu deposited on Haynes 188 wall
131	5.44-5.6	301-308	19.2-19.5	1.0	1/11/77	20	152	Cu Erosion, Surface Crack in Haynes Wall where Cu deposited (Row F)
132	5.4	298-302	19.1-19.5	1.0	1/13/77	5	157	Normal Temperatures Measured in Region of Surface Crack
133	5.31-5.41	309-314	20.2-20.6	1.0	1/18/77	20	177	Increased % FFC and Reduced FFC Valve Opening Time from 70 ms to 35 ms
134	5.26-5.52	305-313	20.6-21.7	1.0	1/18/77	45	222	
135	5.42-5.56	302-309	21.3-21.5	1.0	1/18/77	50	272	Cu Crack Eroded at 345°
136	5.4-5.65	306-315	21.1-21.9	1.0	1/18/77	50	322	Cu Cracks Eroded at Row F, 345°, 310°
137	5.39-5.57	301-312	21.3-21.9	1.0	1/18/77	40	362	Small Amounts of Cu Erosion (Row F, 310°)
138	5.4-5.57	303-312	21.1-21.7	1.0	1/21/77	50	412	Cu Deposits on Haynes Wall at Row F,345°,310°
139	5.31-5.55	303-312	20.8-21.7	1.0	1/21/77	72	484	Shutdown Due to Throat Erosion at 345° (Streak Visible in Exhaust)
140	5.34-5.45	296-304	21.4-21.6	0.5	1/24/77	50	534	Reduced Test Duration, Throat Erosion Rate Reduced
141	5.37-5.43	295-301	21.6-21.8	0.4	1/24/77	50	584	Throat Erosion Rate Small (345°) Small Amounts of Cu Erosion (Row F, 345°, 310°)
142	5.31-5.45	297-305	21.3-21.6	0.4	1/25/77	50	634	
143	5.27-5.41	296-300	21.3-21.6	0.4	1/25/77	50	684	
144	5.27-5.52	301-306	20.9-21.7	0.4	1/25/77	50	734	
145	5.33-5.51	303-307	21.2-21.6	0.4	1/25/77	50	784	
146	5.40-5.54	302-310	21.2-21.6	0.4	1/25/77	100	884	
147	5.41-5.53	299-304	21.5-21.9	0.4	1/25/77	50	934	
148	5.46-5.60	296-306	21.3-21.8	0.4	1/26/77	50	984	
149	5.46-5.56	298-308	21.4-21.9	0.4	1/26/77	100	1084	
150	5.41-5.52	299-309	21.4-21.7	0.4	1/26/77	116	1200	
151, 152	5.36-5.44	298-302	21.5-21.7	0.4	1/28/77	20	1220	

TABLE VI

CYCLE LIFE PREDICTIONS BASED ON ROW E MEASURED WALL TEMPERATURES

O/F = 5.5, O_2/H_2

Pc = 20.41 atm.

% FFC	(1) TE4, ^{o}K (^{o}F)	(2) N_f, cycles	(3) Nominal I_s, sec	(4) TE6, ^{o}K (^{o}F)
21.5	1189 (1680)	1.7×10^5	430	1350 (1970)
20.5	1228 (1750)	45,000	431	1372 (2010)
19.5	1272 (1830)	7,000	432	1394 (2050)
18.5	1311 (1900)	800	433.5	1422 (2100)

NOTES:

(1) From Figure 23 plot of test data

(2) New Chamber Assumed

(3) Ambient Temperature Propellants
40/1 Nozzle Area Ratio

(4) From Figure 24 plot of test data
(10 hr 1% creep limit = $2160^{o}F = 1455^{o}K$)

Twg = Gas-Side Wall Temperature

Twb = Back-Side Wall Temperature

Taw = Adiabatic Wall Temperature

T_i = Initial Temperature

h_g = .0026 Btu/in^2-sec = 0.00038 Kw/cm^2

t_{wall} = .045" = 0.11 cm

Haynes 188 Wall

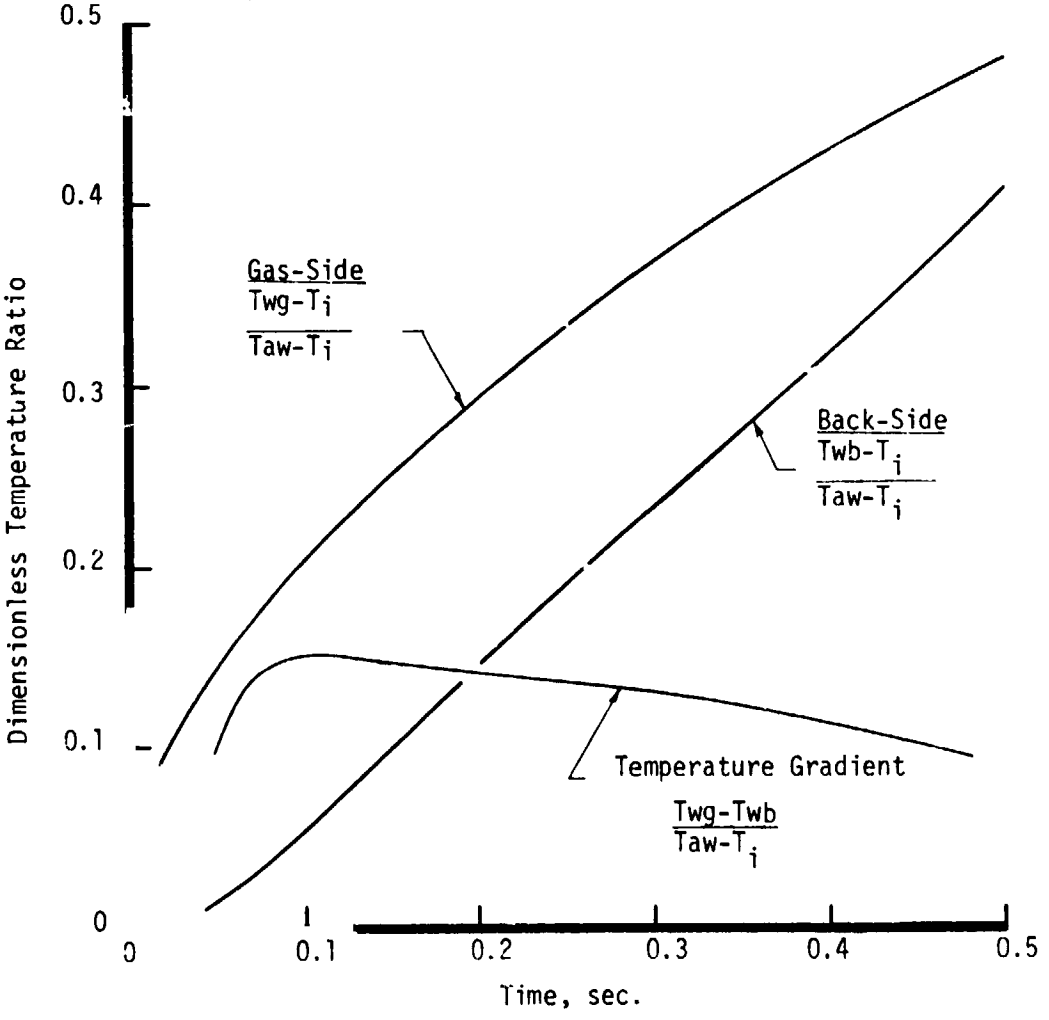

Figure 28. Typical Wall Temperature Transients

coolant injection point. This damage worsened during the course of the life verification test series and, as a result, the film coolant flow rate was increased from the initial value of 19.5% to 21.5% and the firing duration was decreased from 1.0 sec to 0.4 sec. Even with this change in test conditions the chamber experienced a full thermal strain cycle on each firing, so that the cycle life demonstration remained valid.

4. Testing Narrative

The life verification tests are summarized on Table V. During the initial firings (Tests 119-126), the test sequence was finalized and the chamber was thermally cycled 9 times. It was found that the throat region wall could be cooled to ambient temperature between firings by utilizing a 0.5 second hydrogen film coolant lag at shutdown followed by a 30 sec gaseous nitrogen purge in the film coolant circuit. The nitrogen purge pressure was 19.7 atm.

In the next 4 tests (Tests 127-130) the number of chamber thermal strain cycles was increased to 132. During these firings, the existing cracks in the copper injection sleeve visibly enlarged both in length and width. After Test 130, the cracks, which were originally less than 0.6 cm long, extended from the tip of the injection sleeve to about 2.5 cm upstream. Erosion of the copper sleeve had occurred in the crack situated at Row F (65° circumferential position - see Figure 5) and some of the copper had deposited on the film cooled chamber wall about 1.3 cm downstream of the film coolant injection point.

After Test 131 (152 thermal strain cycles), a small surface crack was found in the Haynes 188 film cooled chamber wall in the area where the copper deposition had been found. Additional thermocouples were installed in Row F in the vicinity of the crack prior to the next test. Data from the next 5 firings, Test 132, showed that no unusual temperature existed in the area of this surface crack. It was concluded that the surface crack in the film cooled chamber wall was related to liquid metal (copper) corrosion. In subsequent tests, copper deposits were removed with sandpaper whenever they were found. Before proceeding to Test 133, the nominal film coolant flow rate was increased from 19.5% to 21.5% and the opening time of the film coolant valve was decreased from 70 ms to 35 ms. These two steps were taken in an attempt to minimize future additional damage to the film coolant sleeve. In addition, the insulation behind the surface crack was removed so that the backside wall could be observed during the test for evidence of burn through.

V, B, Life Verification Tests (cont.)

During the next 5 tests, Tests 134-138, the engine was fired 240 times ard the total number of thermal strain cycles was increased to 412. As the testing proceeded, additional erosion of the copper sleeve occurred in the crack at Row F and in two cracks in the general vicinity of Row E. As shown on Figure 4, Row E was located at 320°. The additional copper erosion occurred at 345° and 310°. New "hot streaks" were evident on the film cooled chamber downstream of these two eroded cracks. There was no indication that this erosion influenced wall temperatures along Row E.

Erosion of the Haynes 188 throat occurred directly downstream of the eroded copper crack located at 345° during Test 139. The test was terminated after 77 firings when a bright streak was noticed in the nozzle exhaust. The erosion did not penetrate through the throat wall. Insulation in the eroded area was removed for visual monitoring during future tests.

The firing duration was reduced to 0.5 seconds for Test 140 and the engine was fired 50 times. No unusual exhaust streaks were seen. The throat erosion continued but at a much lower rate.

A duration of 0.4 seconds was utilized for the 50 firings of Test 141 (634 total cycles). This duration reduced the amount of throat and copper sleeve erosion to acceptable levels. Figure 28 shows that this duration was also sufficient to produce a full thermal cycle at the chamber throat.

The test series was completed using the 0.4 second duration. A total of 1220 thermal strain cycles were applied to the chamber and no evidence of thermal fatigue cracking in the film cooled chamber was ever observed. Neither the surface crack at Row F or the throat erosion at 345° propagated through the wall. A post-test photograph of the chamber throat region is shown on Figure 29.

C. PERFORMANCE DATA ANALYSIS AND CORRELATION

1. Post-Test Analysis and Correlation

The scope of the performance data analysis and correlation work which was done is outlined on Figure 30. Table IV contains a detailed performance summary for each of the performance verification tests. Test operating conditions, measure performance, flowrates, thrust, and other performance parameters are listed.

The measured performance values are plotted as a function of film coolant flow rate on Figure 31. The actual test data are shown as open circles. The half-shaded circles shown are the test data adjusted to

Figure 29. Post-Test Photograph of the Chamber Throat Region After Completion of the Life Verification Test Series

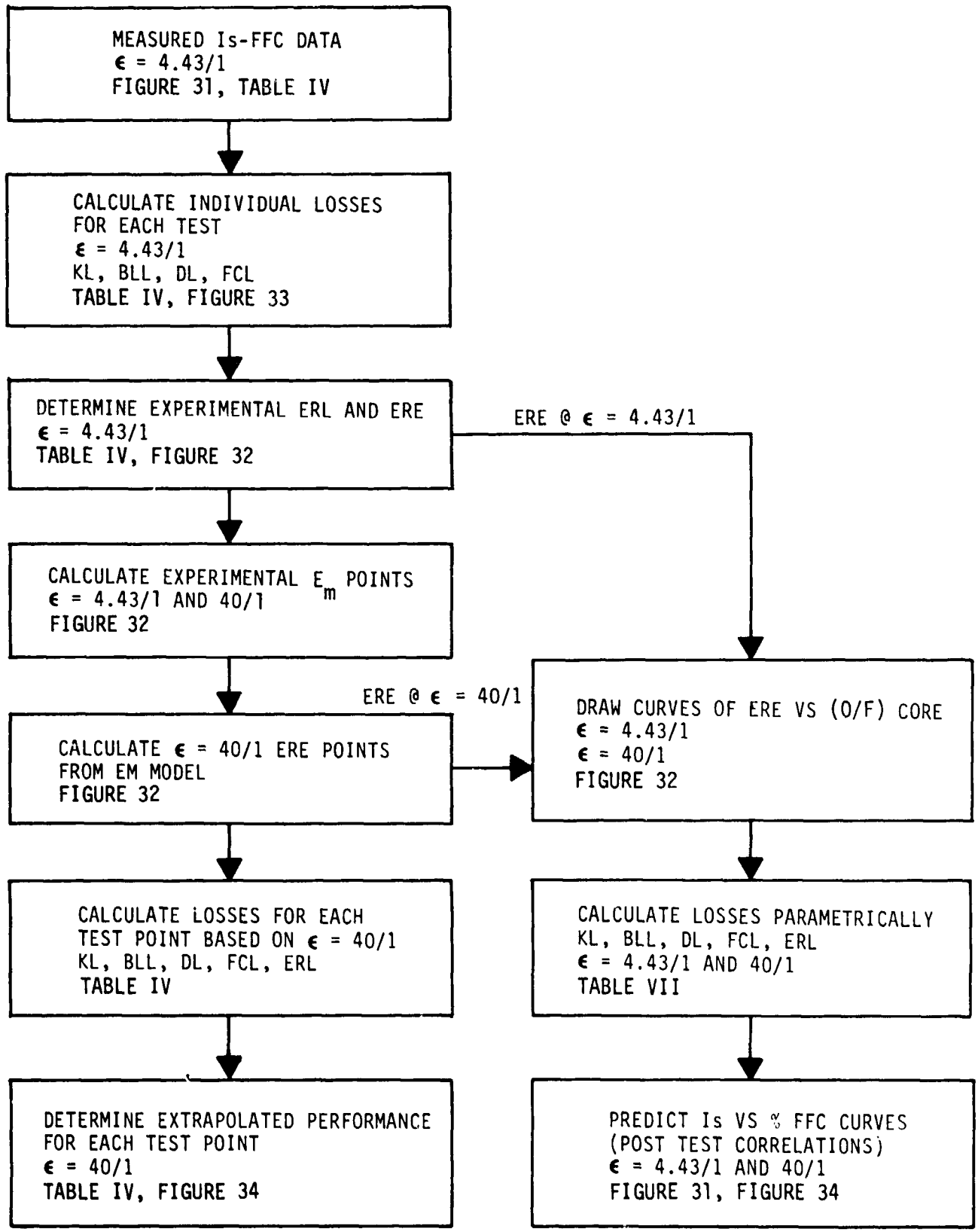

Figure 30. Performance Data Analysis Approach

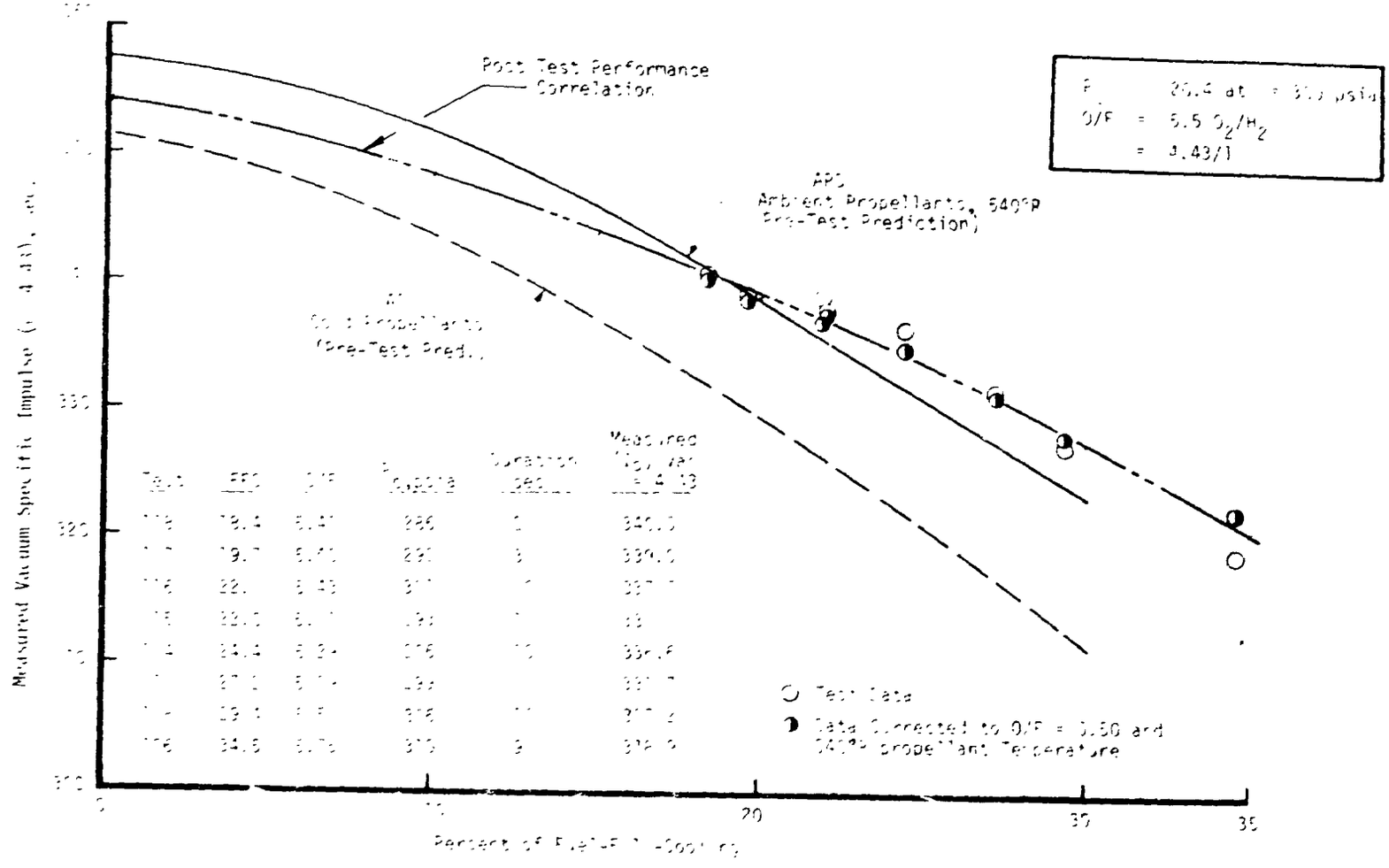

Figure 31. Film Cooling Effect on Sea Level Nozzle Test Performance

a nominal ambient temperature (300°K) and the nominal 5.50 O_2/H_2 mixture ratio. The data adjustment consisted of adding or subtracting differences in ODK performance evaluated at the nominal and actual test conditions. This "nominal operating point" performance is listed as Isp, nom on Table IV. In calculating Isp, nom it was assumed that boundary layer, divergence, film cooling and energy release losses remain constant for the small changes in overall mixture ratio and inlet temperature.

The measured performance is higher than the pre-test prediction because the energy release efficiency of the Modified I injector did not increase, as predicted in the pre-test analysis, when the core mixture ratio increased. The energy release efficiency values determined from the test data are plotted as a function of core mixture ratio (main injector O/F) on Figure 32. The experimental ERE was virtually constant at 99.14% $\pm$ .25% over the entire ranged test conditions.

The pre-test ERE prediction, also plotted on Figure 32, was based on an evaluation of the 40/1 ERE data available at the start of this program. The disagreement between the experimental ERE values measured with ε = 4.43/1 and the ε = 40/1 data is evidence of the fact that ERE is not a sufficiently general parameter for characterizing injector performance with different area ratio nozzles. Previous work at ALRC (Ref. 4) has shown that the mixing efficiency E_m described in Appendix C provides a more general characterization of injector performance for fixed injector mixture ratio but variable nozzle area ratio conditions.

The E_m values calculated from the test data and ERE values for a 40/1 engine which were calculated using the E_m model a also plotted on Figure 31. The 40/1 ERE values are in reasonable agreement with the pretest ERE prediction which was based on the 40/1 data obtained in the APS and ITA programs.

In calculating the experimental ERE values, it was necessary to analytically evaluate the performance losses due to kinetics, boundary layer effects, divergence, and film cooling. This was done using the methodology of the pre-test analysis (Appendix C) and the various loss components are listed on Table IV.

The One Dimensional Equilibrium (ODE) and Kinetic (ODK) specific impulses were determined at the tested overall engine mixture ratios. The oxygen and hydrogen inlet temperatures ranged from 267°K to 286°K (480°R to 515°R) and the ODE/ODK test performance account for the appropriate propellant enthalpy corrections. The procedures for defining the test nozzle kinetic loss (KL) and boundary layer loss (BLL) are identical to those used in the pre-test analysis.

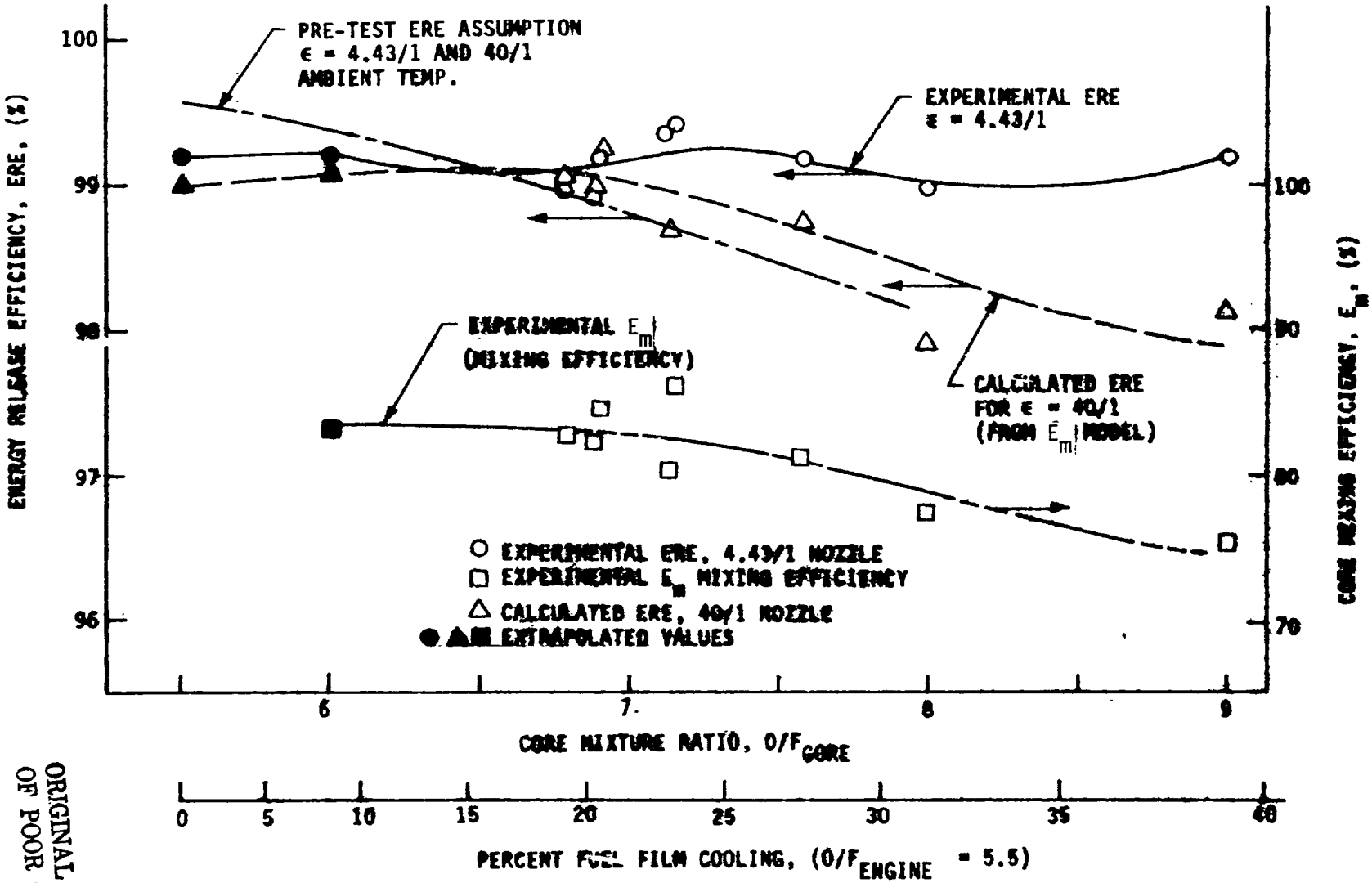

Figure 32. Energy Release Efficiency Correlation

V, C, Performance Data Analysis and Correlation (cont.)

The divergence loss estimated during the pre-test analysis for the 30% FFC case was generalized to other film cooling flow rated by using the following relationship which follows from Equation C-2 of Appendix C.

$$\frac{DL}{I_{sp\ Delivered}} = \text{a constant} \qquad (5)$$

The tests were conducted with a Rao nozzle which was originally contoured for ε = 40/1 and subsequently truncated to ε = 4.43/1. This accounts for the large nozzle divergence performance loss (CDL) listed in Table IV for the sea level test condition.

The film-cooling loss (FCL) was calculated using the HOCOOL model and the posttest entrainment fraction correlation described in Appendix C. The film-cooling loss is plotted as a function of film coolant flow rate and area ratio on Figure 33 The post-test FCL values are higher than initially predicted in the 10-20% FFC range because the experimental entrainment fractions were less than predicted (less film coolant mixing, lower wall temperatures).

The experimental performance data were extrapolated to a 40/1 area ratio nozzle condition by utilizing the ERE values calculated from the E_m model and by re-evaluating each of the other loss components for a 40/1 configuration. The pertinent parameters are listed on Table IV and the extrapolated data points are plotted on Figure 34. These extrapolated data compare reasonably well with the pretest prediction.

A parametric analysis of delivered performance as a function of film cooling percentage was made using the curves faired through the ERE data on Figure 31 and the results are listed on Table VII and plotted on Figures 31 and 34. The curves plotted represent the posttest performance correlations for the plug cluster engine operating with 4.43/1 and 40/1 area ratio nozzles at an engine O/F = 5.5 with 300°K propellants. Typically, these correlations pass through the middle of the test data and predict a slightly lower performance in the 0 - 20% FFC range than was predicted originally.

2. Energy Release Efficiency

Figure 31 shows the experimentally measured ERE, which was obtained with the truncated sea level nozzle, as a function of the core mixture ratio. Also shown in Figure 31 is the inferred test value of E_m which correlates the test sea level ERE. Increasing core O/F

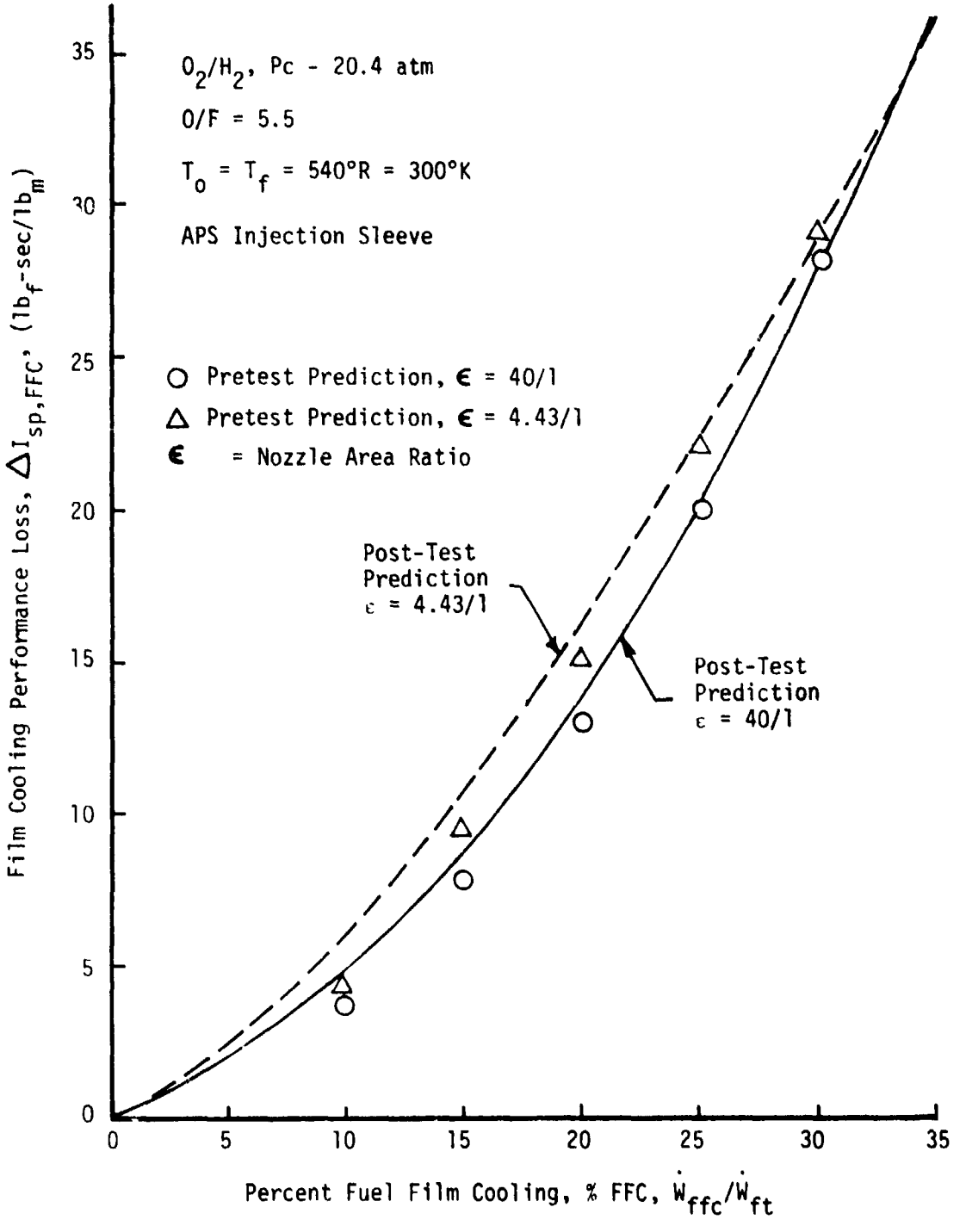

Figure 33. Post Test Prediction of Film Cooling Performance Loss From HOCOOL Computer Program

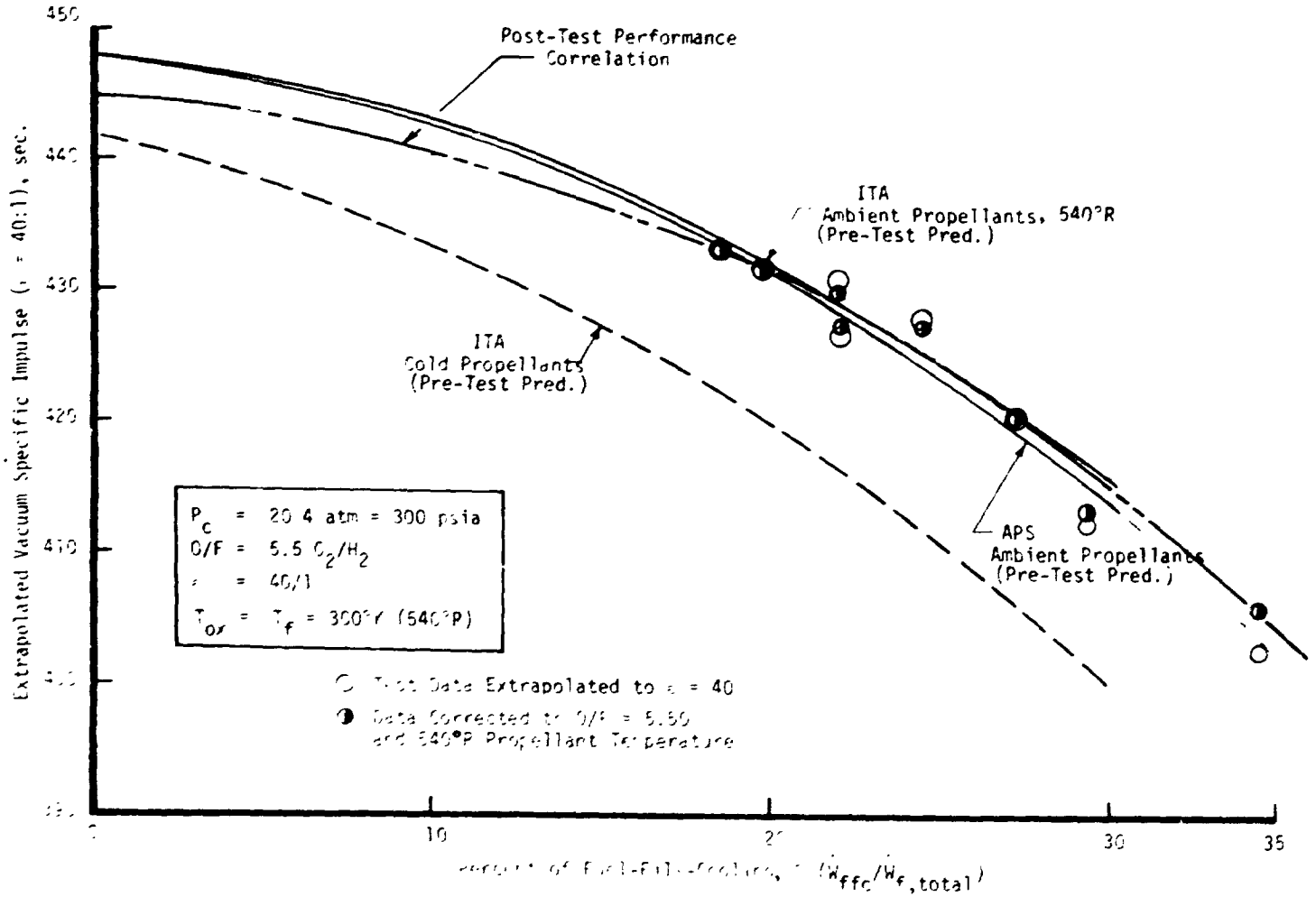

Figure 34. Film Cooling Effect on 40/1 Nozzle Extrapolated Performance

TABLE VII

PLUG CLUSTER PERFORMANCE CORRELATION

Engine Mixture Ratio, O/F	-	5.50	←					5.50
% FFC, $W_{ffc}/W_{f,total}$	%	0	10	15	20	25	30	35
Core Mixture Ratio, $(O/F)_{core}$	-	5.50	6.111	6.471	6.875	7.333	7.857	8.462
S.L. Noz. Exit Area Ratio, ε_{SL}	-	4.43	←					4.43
Theo Va. Spec. Imp., $Isp_{,ODE}$	sec.	398.8	←					398.8
Kinetic Impulse, $Isp_{,ODK}(O/F)_{core}$	sec.	395.7	388.2	383.4	378.0	371.7	364.4	
Kinetic Loss, ΔKL	sec.	3.1	3.1	3.1	3.1	3.1	3.1	3.1
Boundary Layer Loss, ΔBLL	sec.	2.0	2.0	2.0	2.0	2.0	2.0	2.0
Nozzle Div. Loss, ΔCDL	sec.	36.4	35.9	35.4	34.9	34.3	33.7	33.0
FFC Loss, ΔFFCL	sec.	0.0	6.1	10.8	16.2	22.3	28.8	36.0
Energy Release Loss, ΔERL	sec.	3.2	3.2	3.6	3.6	3.2	3.6	4.0
Energy Release Efficiency, % ERE	%	99.2	99.2	99.1	99.1	99.2	99.1	99.0
Predicted Performance, $Isp_{,pred}$	sec.	354.1	348.5	343.9	339.0	333.9	327.6	320.7
Vac. Noz. Exit Area Ratio, ε_{vac}	-	40	←					40
Theo. Vac. Spec. Imp. $Isp_{,ODE}$	sec.	467.1	←					467.1
Kinetic Impulse, $Isp_{,ODK,O/F_{core}}$	sec.	460.7						
Kinetic Loss, ΔKL	sec.	6.4	6.4	6.4	6.4	6.4	6.4	6.4
Boundary Layer Loss, ΔBLL	sec.	6.5	6.5	6.5	6.5	6.5	6.5	6.5
Noz. Div. Loss, ΔCDL	sec.	4.7	4.6	4.6	4.5	4.5	4.4	4.2
FFC Loss, ΔFFCL	sec.	0.0	4.9	8.9	13.7	20.2	27.8	36.1
Energy Release Loss, ΔERL	sec.	4.7	4.3	4.2	4.3	5.1	7.5	8.9
Energy Release Efficiency, % ERE (ε = 40)	%	99.0	99.07	99.1	99.07	98.9	98.4	98.1
Predicted Performance, $Isp_{,pred}$	sec.	444.8	440.4	436.5	431.7	424.4	414.5	405.0

decreases the fuel to oxidizer injection momentum ratio which decreases the fuel stream penetration into the oxidizer jet of the modified "I" triplet injection element (see Figure 18). The test data show that this degrades mixing efficiency at higher O/F. Despite this, the sea level ERE remains nearly constant due to the offsetting effect of more linear Isp vs O/F at higher mixture ratios. When the experimental E_m values are used to calculate ε = 40/1 vacuum ERE, however, it does decrease from 99% ERE at (O/F) = 7 to 98% ERE at (O/F) = 9 which is the trend which was predicted during the pre-test analysis.

Although the test data shows that the ERE of the Modified I injector decreases at high mixture ratio, no redesign of the injector is necessary for plug cluster applications with 300°K propellants because no significant decrease occurs in the range of core O/F required (≤ 7.0).

D. WALL TEMPERATURE DATA CORRELATION

1. Correlation Approach

The adiabatic wall temperature correlation approach is indicated on Figure 35. The data, listed on Table III, were correlated in terms of the ALRC entrainment model described in Reference 3. The ALRC entrainment film cooling model is basically a two stream tube mixing model as illustrated in Figure 36. Core gases or combustion gases emanating from the main propellant injector are considered to be entrained by and to mix with film coolant gases which have been injected onto the chamber wall. The mixing is assumed to occur in an annular mixing layer adjacent to the thrust chamber wall. This mixing layer comprises one of the stream tubes. The other stream tube is the central flow region where the unmixed core gases are located. The rate at which core gases are entrained into the mixing layer is defined in terms of an entrainment fraction, k, as follows:

$$\begin{pmatrix}\text{Entrained}\\ \text{Core Gas}\\ \text{Mass Flux}\end{pmatrix} = k \begin{pmatrix}\text{Axial Flow}\\ \text{Core Gas}\\ \text{Mass Flux}\end{pmatrix} \qquad (6)$$

The k values are model inputs and appropriate values for design calculations are determined from test data. Equation 6 defines a bulk mixing process between the core gas and film coolant gas. The effects of enthalpy and concentration profiles through the mixing layer are accounted for in the ALRC entrainment model by the use of a profile shape factor which relates bulk mixing layer conditions to adiabatic wall conditions.

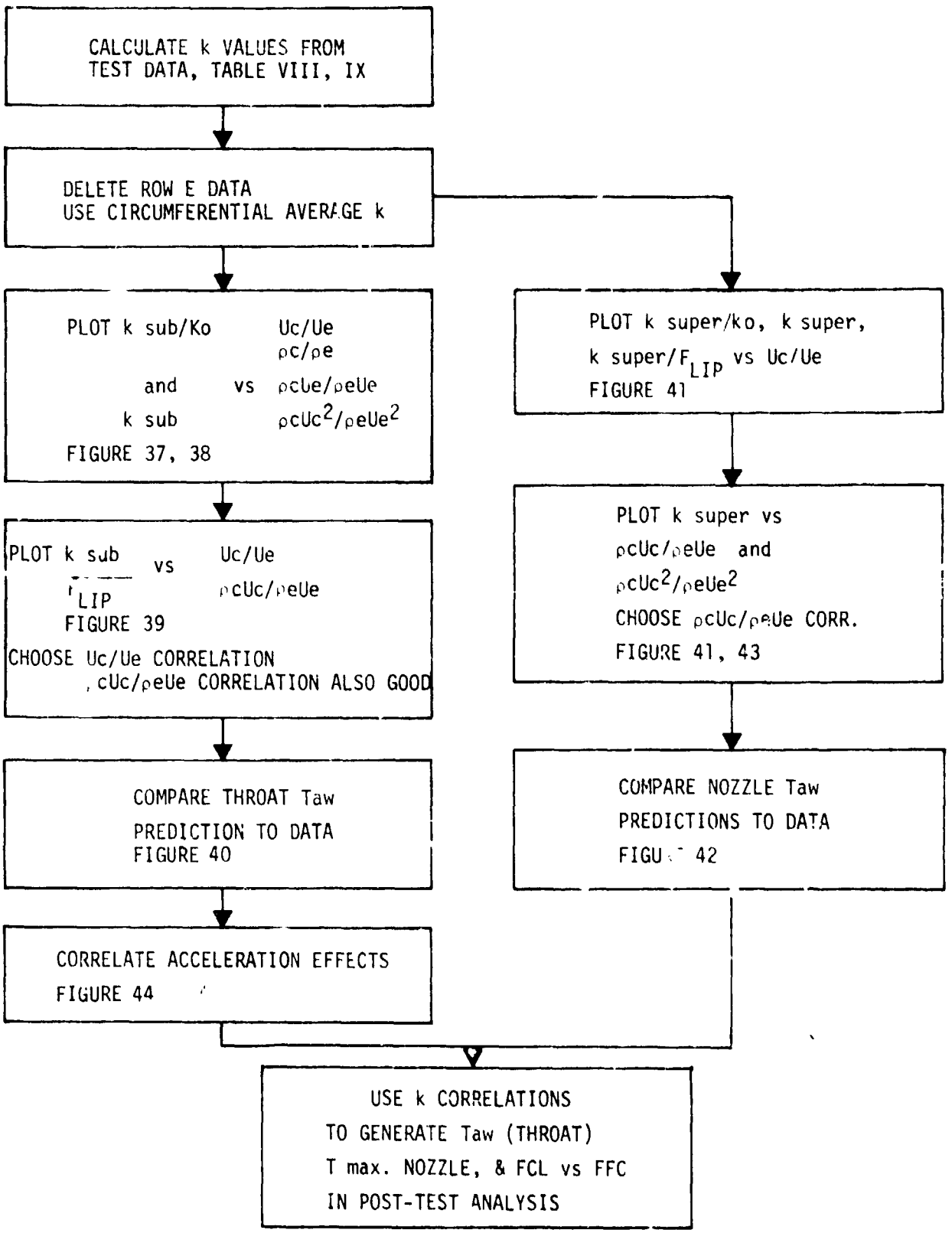

Figure 35. Wall Temperature Data Correlation Approach

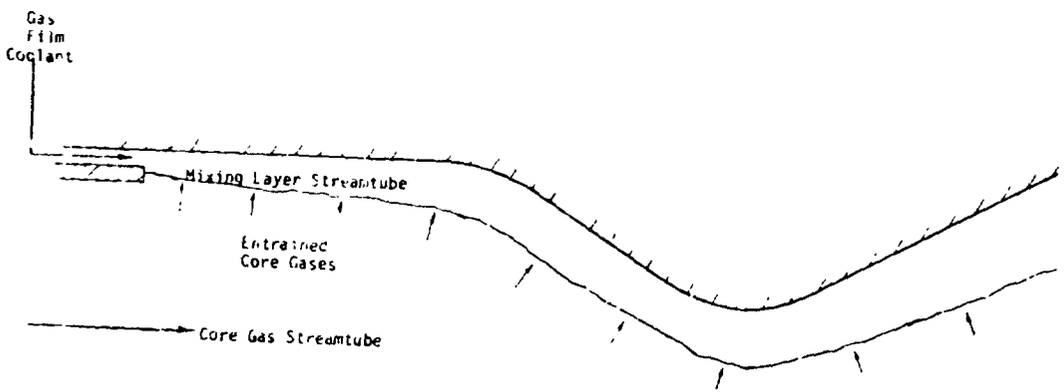

ENTRAINMENT FILM COOLING MODEL SCHEMATIC

ANALYTICAL APPROACH

2 STREAMTUBE FLOW MODEL

CORE GASES ENTRAINED AND MIX

$$\text{ENTRAINED MAX FLUX} = k \; \text{AXIAL MASS FLUX}$$

EQUILIBRIUM CHEMISTRY

MODEL PREDICTIONS

ADIABATIC WALL TEMPERATURE

GAS COMPOSITION AT WALL

PERFORMANCE LOSS

Figure 36. Entrainment Film Cooling Model Features

V, D, Wall Temperature Data Correlation (cont.)

The general analysis approach followed in the ALRC entrainment model is as follows: (1) the total entrained core gas flow rate between the coolant injection point and the point of interest is calculated by integration of Equation 6, (2) the film cooling effectiveness is calculated using previously established correlations between the ratio of entrained flow rate to injected coolant flow rate and effectiveness, (3) adiabatic wall temperature and gas composition at the wall are calculated using appropriate effectiveness definitions.

2. Entrainment Fraction Data

The entrainment fractions calculated directly from the Table III wall temperatures are listed on Table VIII. The parameter listed is k/ko which is the entrainment fraction k, divided by a reference entrainment fraction, ko, calculated from the correlation developed from flatplate lab data (Reference 9). The k/ko parameter was utilized to correlate entrainment fraction data in Reference 3. The equation which defines ko is shown on Figure B-4 in Appendix B.

In examining the data, it was found that the Row E k values were consistently higher than the other data due to the "streaking" which occurred as a result of the damaged film coolant sleeve. Consequently, the Row E data were not considered in establishing post-test entrainment fraction correlations.

Entrainment fractions indicated by the other prime data Rows (A, B, C, and D) generally agreed within + 25%. This is consistent with the Combustion Effects data (Reference 3) and probably representative of the variation which can be expected in a real rocket engine. The prior coolant damage had distorted the circumferential film coolant distribution somewhat, and this is probably why some rows were consistently hotter than others. It was assumed that the circumferential average of the Row A, B, C, and D entrainment fraction adequately describes the overall coolant/core gas mixing in the engine tested. Consequently, the entrainment fractions correlated were the circumferential average values which are listed on Table IX. This is the same approach used in the Combustion Effects data analysis (Reference 3).

In order to simplify the data evaluation and the subsequent analysis, it was decided to correlate the overall subsonic region data, and the overall supersonic region data, rather than attempt correlating an axial distribution of k within the test engine. The subsonic region is bounded by the injection point and the nozzle throat (Thermocouple No. 4). The supersonic region is bounded by the throat and Thermocouple No. 6.

TABLE VIII

NORMALIZED ENTRAINMENT FRACTION DATA

Experimental k/ko Values

k = Entrainment Fraction = Entrained Core Gas Mass Flux/Axial Core Gas Mass Flux

Test	% FFC	O/F	Average U_c/U_e	ρ_c/ρ_e	$T_{inj.}$, °R	ko	Row	Thermocouple Pair (i = Injection Point) i -2	2-4	4-5	5-6	i-4	4-6	i-6
106	34.45	5.76	1.15	1.23	608	.00690	A	3.59	1.58	-	-	2.49	2.07	2.31
							B	3.15	2.00	2.38	1.56	2.52	1.97	2.28
							C	2.91	1.1	1.79	1.78	1.92	1.79	1.86
							D	5.18	1.55	2.47	2.08	3.19	2.27	2.79
108	29.35	5.52	1.00	1.24	652	.00692	A	3.14	1.80	-	-	2.41	1.93	2.20
							B	2.96	2.07	1.93	1.42	2.48	1.67	2.13
							C	2.57	2.02	-	-	2.27	1.10	1.76
							D	4.68	1.66	2.11	1.92	3.02	2.02	2.59
111	27.21	5.39	0.94	1.25	671	.00733	A	2.85	1.81	-	-	2.27	1.61	1.99
							B	2.76	1.97	1.61	1.28	2.32	1.11	1.94
							C	2.34	1.18	-	-	1.71	1.52	1.62
							D	4.24	1.54	1.78	1.70	2.75	1.74	2.32
							E	-	-	-	-	-	-	2.89
114	24.41	5.29	0.86	1.24	700	.00793	A	2.50	1.77	-	-	2.10	1.23	1.72
							B	2.40	1.82	-	-	2.08	1.16	1.68
							C	2.00	1.18	-	-	1.55	1.28	1.43
							D	3.91	1.31	-	-	2.48	1.26	1.95
							E	2.44	3.53	-	-	3.04	1.53	2.38
115	21.96	5.27	0.78	1.22	729	.00854	A	2.80	1.74	-	-	2.22	1.09	1.73
							B	2.24	1.66	-	-	1.92	.94	1.49
							C	1.90	1.16	-	-	1.49	1.10	1.32
							D	3.56	1.21	-	-	2.27	1.10	1.76
							E	2.22	3.26	-	-	2.78	1.35	2.16
116	22.06	5.43	0.78	1.20	726	.00856	A	2.39	1.74	-	-	2.03	1.03	1.60
							B	2.21	1.65	-	-	1.91	.90	1.46
							C	1.91	1.16	-	-	1.49	1.09	1.32
							D	3.52	1.21	-	-	2.26	1.07	1.74
							E	2.20	3.29	-	-	2.80	1.38	2.18
							F	-	-	-	-	-	-	2.02
							H	-	-	-	-	-	-	1.68

TABLE [illegible]

								[illegible] Pair [illegible] Injection Pair						
[illegible]	[illegible]	[illegible]	[illegible]	[illegible]	[illegible]	[illegible]	Row	[illegible]	[illegible]-4	4-5	5-6	1-4	4-6	1-6
[illegible]	[illegible]	[illegible]	[illegible]	[illegible]	[illegible]	[illegible]	A	2.34	[illegible]	-	-	1.94	.69	1.39
							B	[illegible]	[illegible]	-	-	[illegible]	.49	1.22
							C	[illegible]	[illegible]	-	-	[illegible]	.80	[illegible]
							D	[illegible]	[illegible]	-	-	[illegible]	.73	1.50
							E	[illegible]	[illegible]	-	-	[illegible]	1.06	.93
							F	-	-	-	-	-	-	[illegible]
							G	-	-	-	-	-	-	1.61
							H	-	-	-	-	-	-	[illegible]
[illegible]	[illegible]	[illegible]	[illegible]	[illegible]	[illegible]	[illegible]	A	[illegible]	[illegible]	-	-	[illegible]	.51	[illegible]
							B	[illegible]	[illegible]	-	-	[illegible]	.47	1.17
							[illegible]	[illegible]	[illegible]	-	-	1.49	.63	[illegible]
							[illegible]	[illegible]	[illegible]	-	-	[illegible]	.60	[illegible]
							E	2.91	[illegible]	-	-	2.37	.81	1.70
							F	-	-	-	-	-	-	1.47
							G	-	-	-	-	-	-	1.46
							H	-	-	-	-	-	-	1.29

TABLE IX

CIRCUMFERENTIAL AVERAGED ENTRAINMENT FRACTION RESULTS

INJECTOR S/N 6, CHAMBER S/N 2

Test	Uc/Ue	Pc/Pe	$\frac{k_{sub}}{ko}$ (1)	k_{sub}	k_{sub} Circum. Variation	$\frac{k_{super}}{ko}$ (2)	k_{super}	k_{super} Circumf. Variation, %
106	1.15	1.23	2.53	.0179	±26	2.025	.0143	±17
108	1.00	1.24	2.55	.0181	±18	1.68	.0119	±35
111	0.94	1.25	2.26	.0170	±24	1.50	.0113	±25
114	0.86	1.24	2.05	.0167	±24	1.23	.0100	±6
115	0.78	1.22	1.97	.0172	±24	1.06	.00927	±27
116	0.78	1.20	1.92	.0168	+22	1.02	.00894	±12
117	0.70	1.18	1.83	.0174	±17	0.68	.00646	±28
118	0.66	1.17	1.72	.0172	±15	0.55	.00550	±15

Notes:

(1) k_{sub} = Average Entrainment Fraction Between Injection Point and Nozzle Throat (Thermocouple No. 4)

(2) k_{super} = Average Entrainment Fraction Between Nozzle and Thermocouple No. 6 (APS region 15% longer)

(3) k_{sub} and k_{super} based on Row A, B, C, and D data

V, D, Wall Temperature Data Correlation (cont.)

An acceleration effect was not assumed in reducing the data as it was in the Combustion Effects analysis. This allows the data to indicate directly any effects of core gas flow acceleration. Examination of the Table VIII data reveals that there were some very significant acceleration effects upstream of the throat as the k value between the injection point and Thermocouple No. 2 was consistently higher than the k between Thermocouples 2 and 4. An acceleration effect correlation was developed from these data and it is discussed in Section V.D.5.

3. Subsonic Region Entrainment Fraction Correlation

Four correlating parameters were considered for correlating the subsonic region entrainment fraction: injection velocity ratio, u_c/u_e, density ratio, ρ_c/ρ_e, injection mass flux ratio, $\rho_c U_c/\rho_e U_e$, and injection momentum flux ratio, $\rho_c \rho_c^2/\rho_e U_e^2$. The velocity ratio has historically been used to characterize film cooling at ALRC (Reference 3). The results of other studies have been characterized in terms of the injection mass flux ratio (Reference 10), hence the density ratio influence is also pertinent. In the Reference 11 work, the momentum flux ratio was found to have a significant effect on the mixing of cold gas jets injected normally into a hot confined crossflow.

In establishing a data correlation, both the Plug Cluster Program data and APS data were considered since they were obtained with identical hardware and some of the APS data were obtained with cold propellants. The first attempt at correlating the subsonic region entrainment fraction consisted of plotting the k/ko parameter as a function of the four correlating parameters considered. The results are shown on Figure 37. None of these plots provided a precise correlation; however, the mass flux ratio did yield a reasonable grouping for the two sets of data.

The data are plotted in a similar way on Figure 38 except that the absolute value of entrainment fraction, k, is plotted instead of the normalized ratio k/ko. Comparison of Figures 37 and 38 indicated that use of the parameter ko was not conclusive to the establishment of a correlation, therefore, it was not considered any further. It is not necessary to normalize k since it is by definition a dimensionless parameter. None of the Figure 38 plots provide a good correlation of both sets of data; however, the velocity ratio does provide an adequate correlation for the two individual sets of data.

It was found that if the so called lip effects identified in the Reference 3 program were accounted for, the APS and Plug Cluster Program data grouped together reasonably well and satisfactory correlations were obtained by plotting k/Flip vs velocity ratio and mass flux ratio as shown on Figure 39.

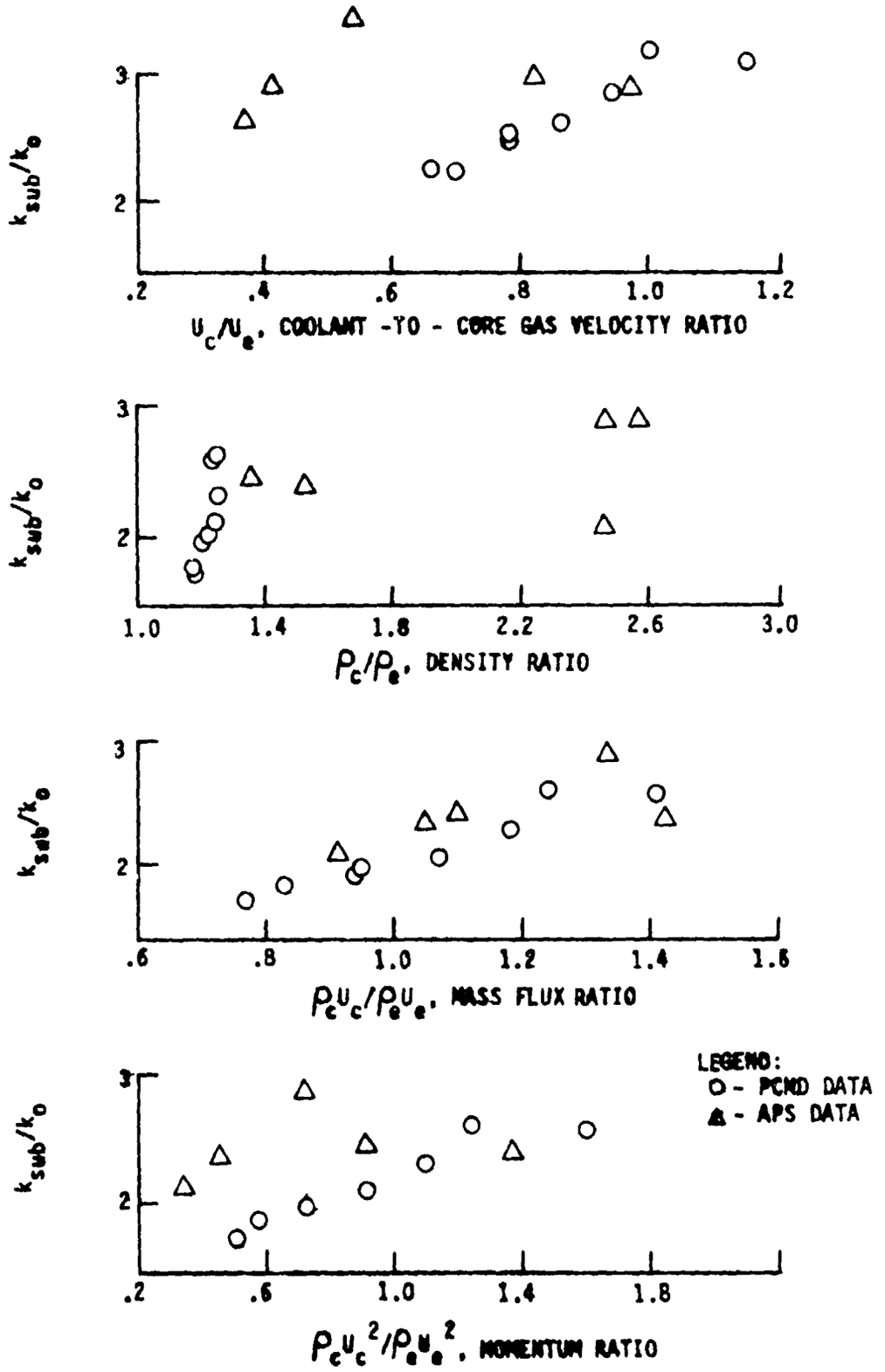

Figure 37. Subsonic Region Entrainment Fractions Correlated with Ko Parameter

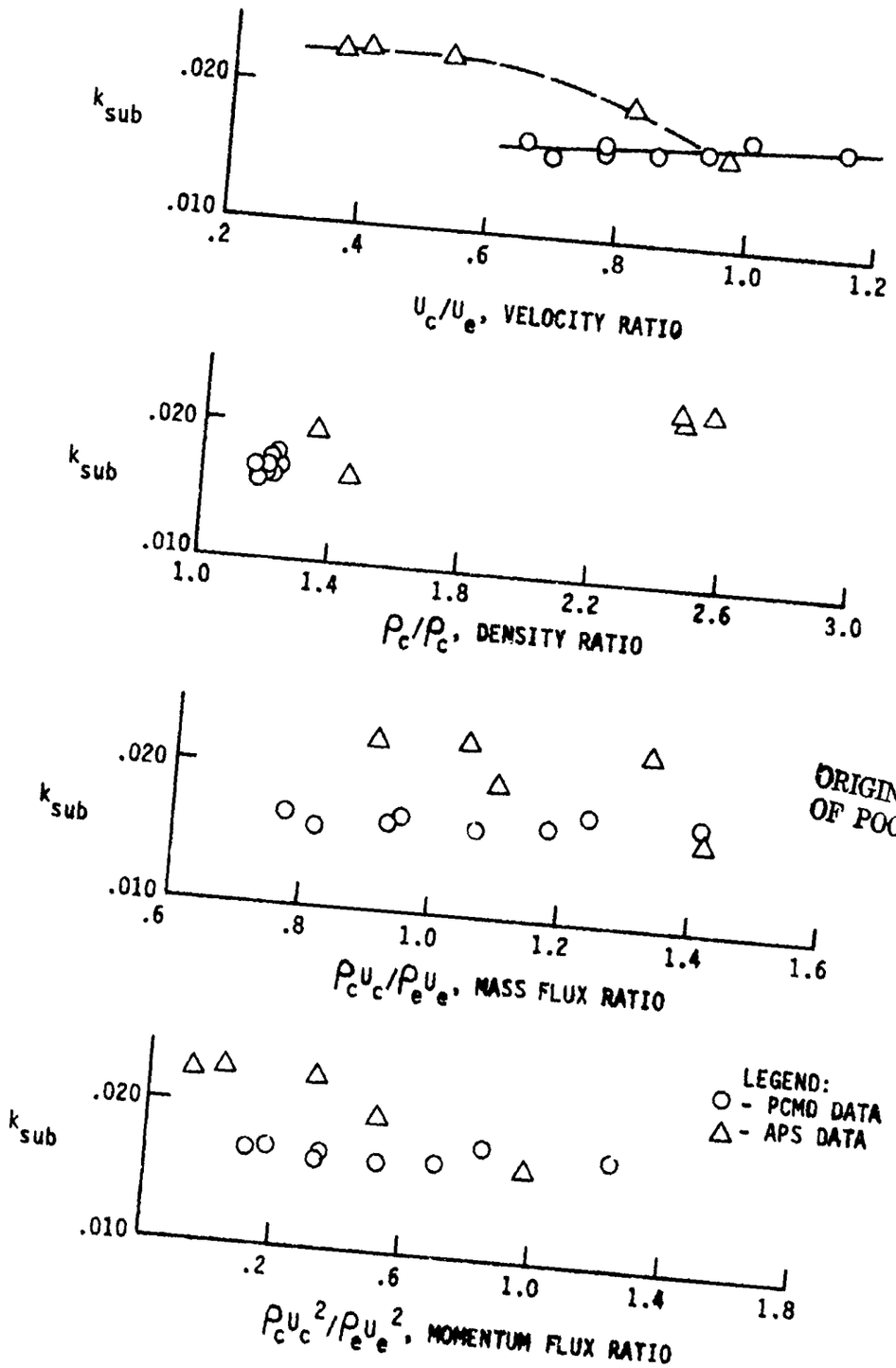

Figure 38. Subsonic Region Entrainment Fraction Data

$F_{11p} = 2.81 - 0.96\ (u_c/u_e)$. FIGURE 28 OF REFERENCE 3

$u_c/u_e > .8$: $k_{sub}/F_{11p} = .00314 + .00634\ (U_c/U_e)$

$u_c/u_e < .8$: $k_{sub}/F_{11p} = .0081$

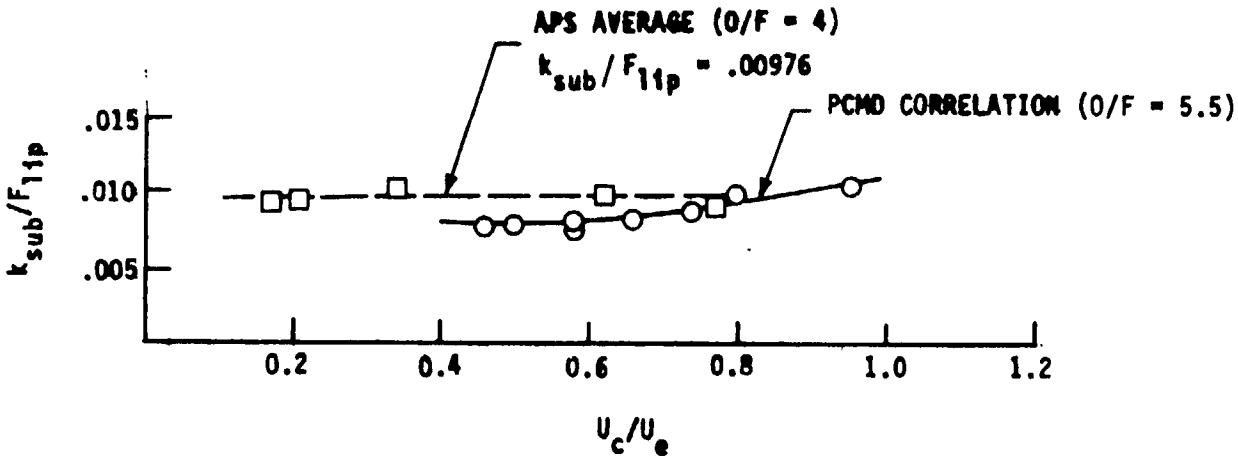

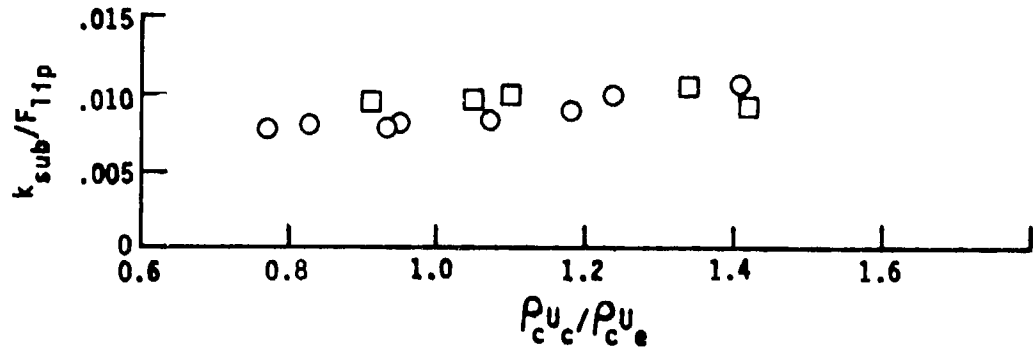

Figure 39. Subsonic Region Correlations for Entrainment Fraction

V, D, Wall Temperature Data Correlation (cont.)

The Flip factor accounts for turbulent mixing caused by the wake of the injection slot. In the Reference 3 tests, the lip effect was noticeable for about 3 cm downstream of the injection slot. Use of the Combustion Effects Program data for F_{lip} on Figure 39 is justified because the subsonic region was about 3 cm long and the slot lip thickness was about the same as in the combustion effects tests. Larger F_{lip} factors are probably appropriate if the lip thickness is greater than about .05 cm. Even when lip effects are accounted for there is still some separation between the APS and the Plug Cluster Program data. This could be due to core mixture effects which were also found to be significant in the Reference 3 work and which probably relate to the free stream turbulence level of the core combustion gases. The design of the ALRC premix injector is such that low O/F values are conducive to high free stream turbulence levels (see Figure 12).

The velocity ratio correlation shown on Figure 39 was considered most convenient of the two shown and was utilized in the post-test analyses described in Section VI. The prediction from the HOCOOL computer model and the Figure 39 velocity ratio correlation compares very well with the data as shown on Figure 40. Both the Figure 39 correlations are recommended for future work; however, it should be noted that these graphs include the effects of acceleration for the specific geometry tested. Analysis of other geometries should include a specific evaluation of acceleration effects using the correlation of Section V.D.5. or some other suitable correlation.

4. Supersonic Region Entrainment Fraction Correlation

The correlation of the supersonic region entrainment fraction data paralleled the subsonic data correlation. The supersonic data are plotted as a function of velocity ratio, mass flux ratio, and momentum flux ratio on Figure 41. The conclusions drawn from Figure 41 are:

a. The F_{lip} factor does not group the supersonic data as well as the subsonic data. This is not surprising since the supersonic region is beyond the 3 cm distance where lip effects disappear in the Combustion Effects data (top graph).

b. As in the subsonic case, the parameter ko does not aid in correlating the data (see graph of k and k/ko vs uc/ue).

c. The velocity ratio provides reasonable correlations of the individual sets of data but the two sets do not correlate very well.

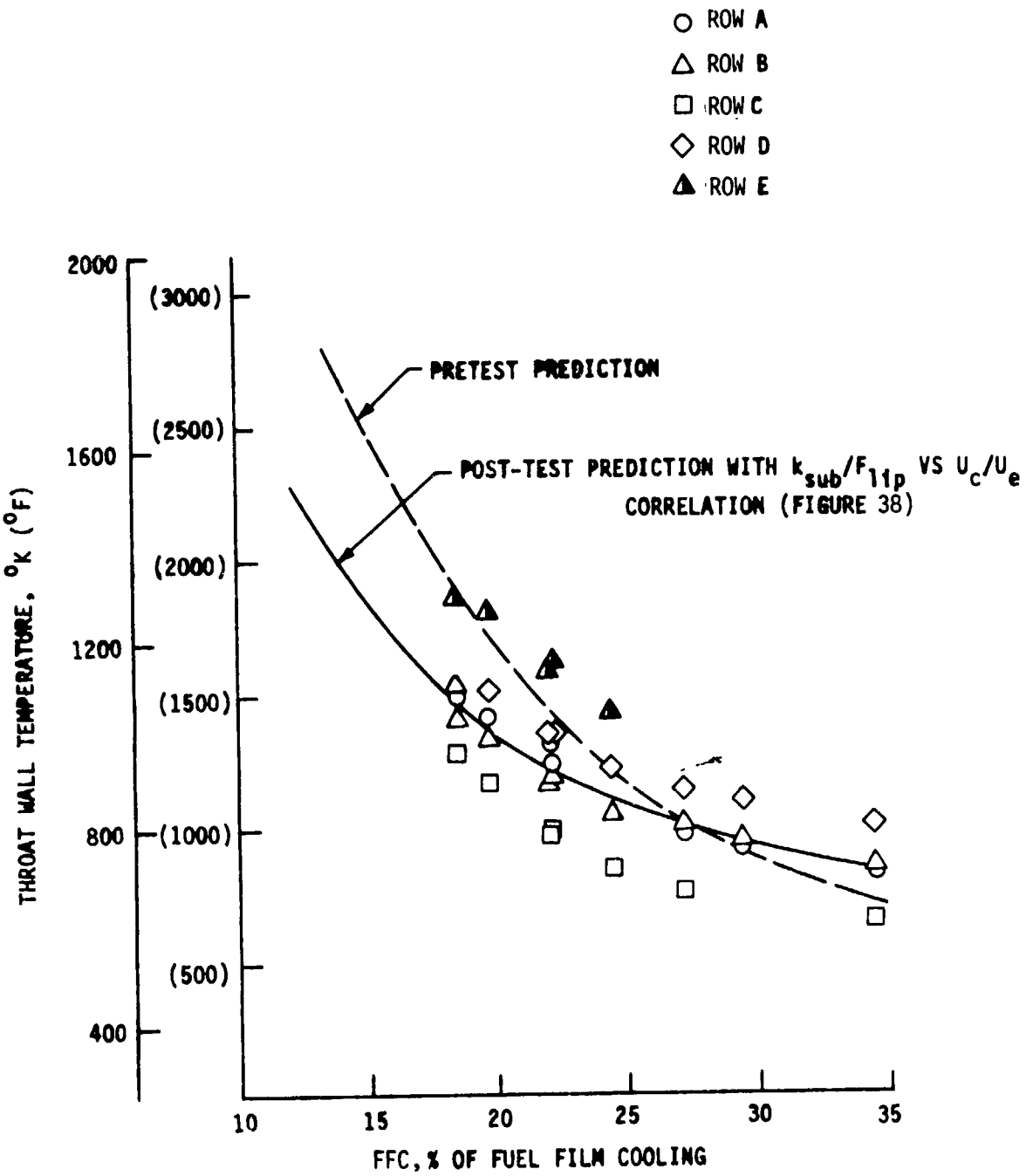

Figure 40. Comparison of Throat Wall Temperature Data and Post-Test Prediction

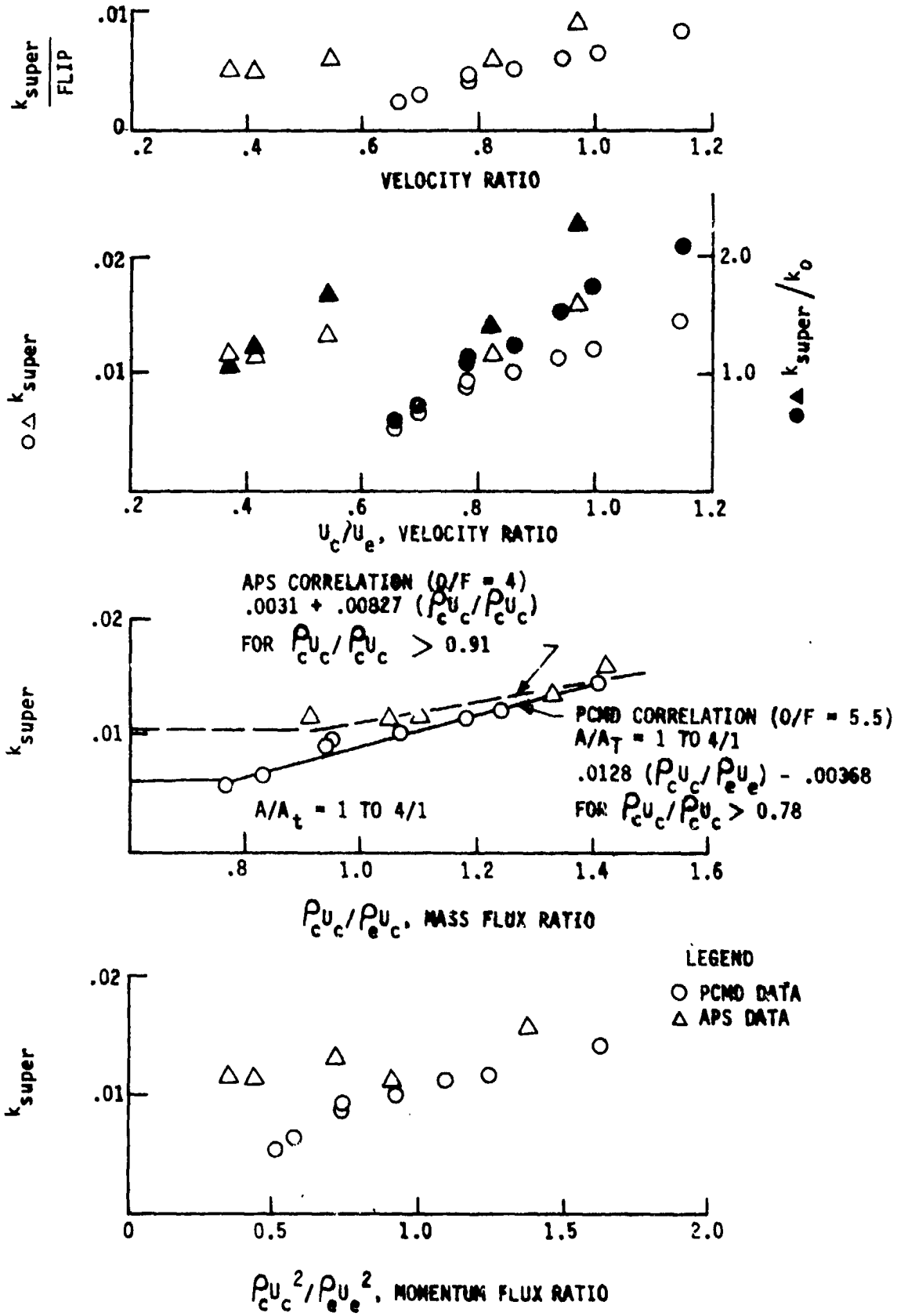

Figure 41. Supersonic Region Entrainment Fraction Data and Correlations

d. The mass flux ratio provides the best correlation of both sets of entrainment fraction data, although there is still some separation between the two sets as noted for the subsonic region. This is possibly related to the difference in core gas O/F.

e. The momentum flux ratio did not correlate the data as well as mass flux ratio.

The mass flux ratio correlations drawn on Figure 41 were chosen for use in the post-test analysis discussed in Section VI. Predictions for the thermocouple 6 location generated using the PCMD subsonic correlation of Figure 39 and the PCMD supersonic correlation of Figure 41 compared well with the test data as shown on Figure 42. The Figure 41 correlations are for the average entrainment fraction in the A/A_t = 1.0 to 4.0 region of the APS/ITA nozzle. For higher area ratios, only APS data are available. These data also correlate with mass flux ratio as shown on Figure 43. The Figure 43 correlations were also used for the post-test analysis.

5. Acceleration Effects

The effect of core gas acceleration on the entrainment fraction is the subsonic region of a converging-diverging nozzle was investigated during the Hydrogen Film Cooling Investigation (Reference 13) using heated nitrogen core gas. The data were correlated with the following equation:

$$k_o = k_i \left[\frac{(\rho_e u_e)}{(\rho_e u_e)_i}\right]^{-m} = k_i \left(\frac{r}{r_i}\right)^{2m} \left(\frac{\phi}{\phi_i}\right)^{-m} \qquad (7)$$

where:

k_o = entrainment fraction

$\rho_e u_e$ = core gas mass flux adjacent to mixing layer

r = nozzle radius

ϕ = $(\rho_e u_e)_{2D}/(\rho_e u_e)_{1D}$, accounts for two dimensional flow effects

Subscript i: refers to the injection point

m = 0.65 (see Figure 34 of Reference 13)

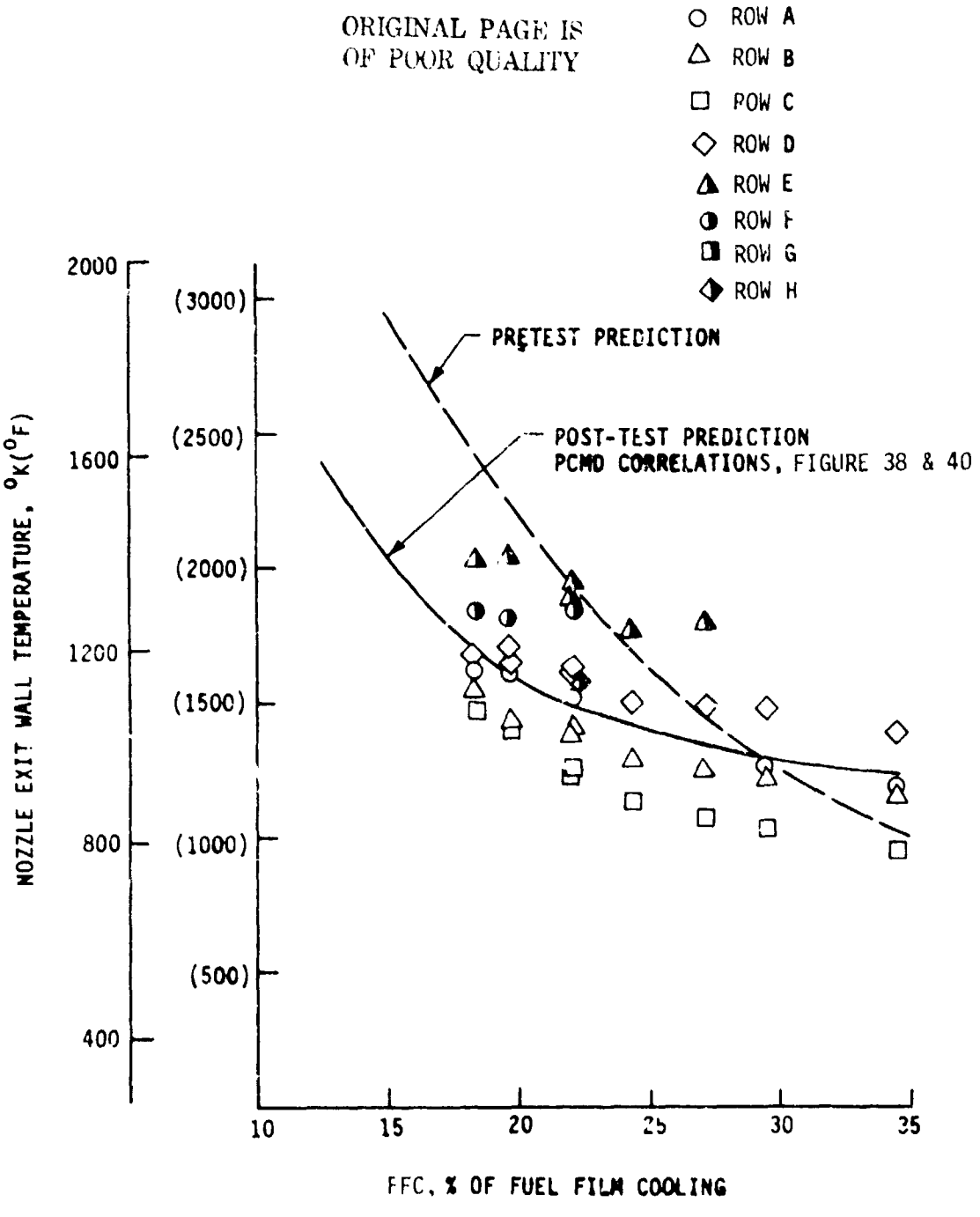

Figure 42. Comparison of Nozzle Wall Temperature Data and Post-Test Predictions

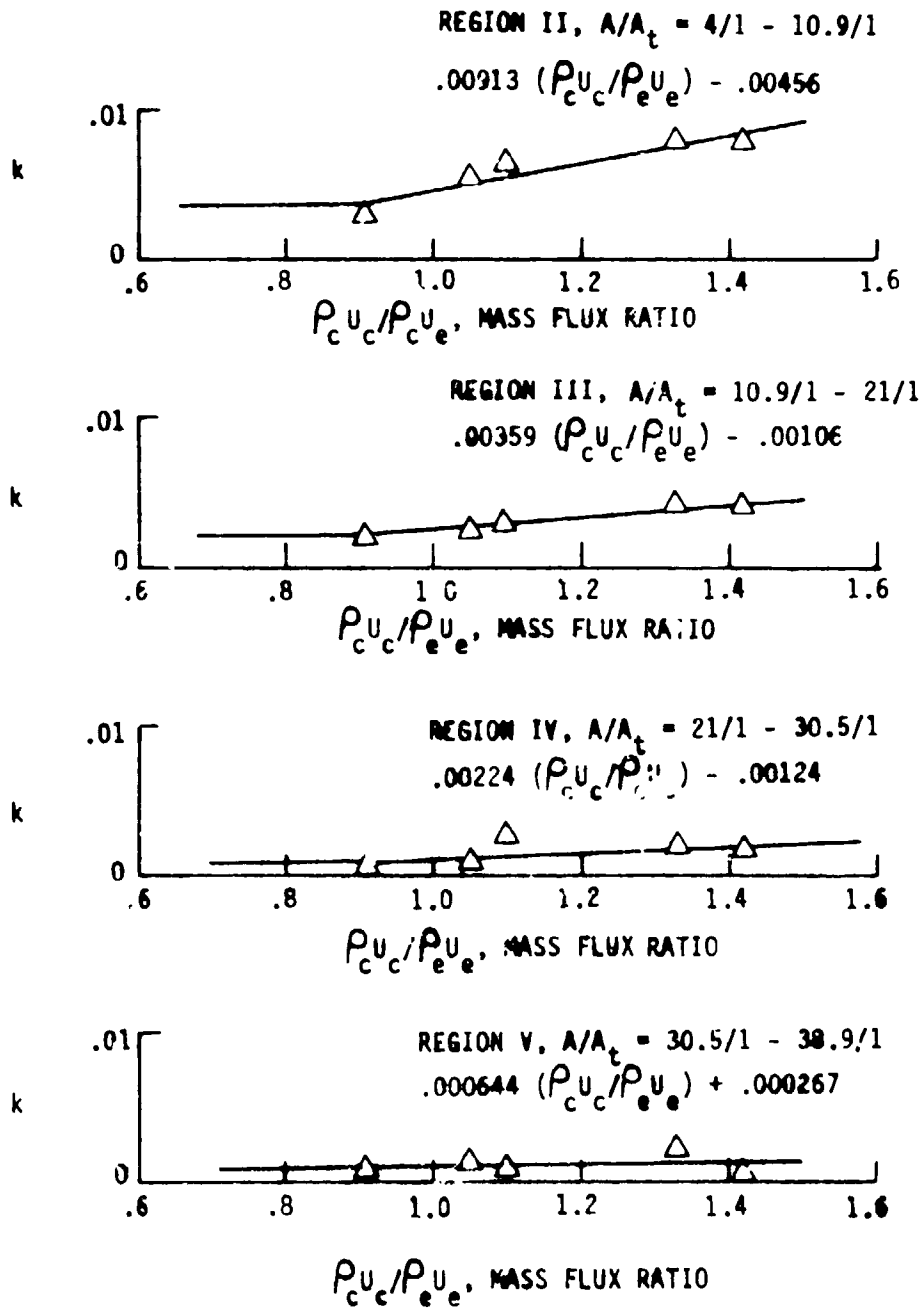

Figure 13. APS Supersonic Entrainment Fraction Data

V, D, Wall Temperature Data Correlations (cont.)

Equation 7 predicts that the entrainment fraction decreases as the core gas accelerates.

The rocket engine data obtained during the Combustion Effects Program indicated that the reduction in k caused by core gas accelerations may be greater than predicted with m = 0.65. The magnitude of the acceleration effects in the Combustion Effects data is difficult to determine because it is necessary to separate acceleration effects from turning effects. This is not the case with the APS and Plug Cluster Module data because the film coolant was injected through a conical injection sleeve and there was no wall turn until very near the nozzle throat.

Analysis of the data from this program and the APS program shows that core gas acceleration effects are indeed greater than predicted with m = 0.65 and that m = 1.6 provides a good correlation of the data. The m = 1.6 value was obtained by comparing the average entrainment fractions of the two subsonic regions which were instrumented as shown on the two upper graphs of Figure 44. The lower graph on Figure 44 shows that m = 1.6 also agrees with a parametric evaluation of the Plug Cluster Program data to determine the value of m which makes k_m, defined below (Equation 23 of Reference 3), equal in both subsonic regions.

$$k_m = \frac{k}{k_o \left[\frac{\rho_e U_e}{(\rho_e U_e)_i}\right]^{-m}} \qquad (8)$$

Equation 7 with m = 1.6 is therefore recommended for evaluating acceleration effects in film cooled rocket engines

VI. POST-TEST ANALYSIS

The objective of the post-test analysis was to evaluate the performance potential of an ITA type thruster operating with O_2/H_2 propellants at 5.5 overall mixture ratio and 20.4 atm (300 psia) chamber pressure. It was assumed that the engine must be capable of 1200 firings, and that the total operation life is 10 hours. Based on the findings of the pretest analytical work, the following "ground rules" were adopted for the post-test analysis:

1. APS injection sleeve design (lower entrainment fractions than with the ITA sleeve design).

2. Haynes 188 chamber with constant wall thickness.

3. Variable injection point location (current location is 3.18 cm upstream of the throat).

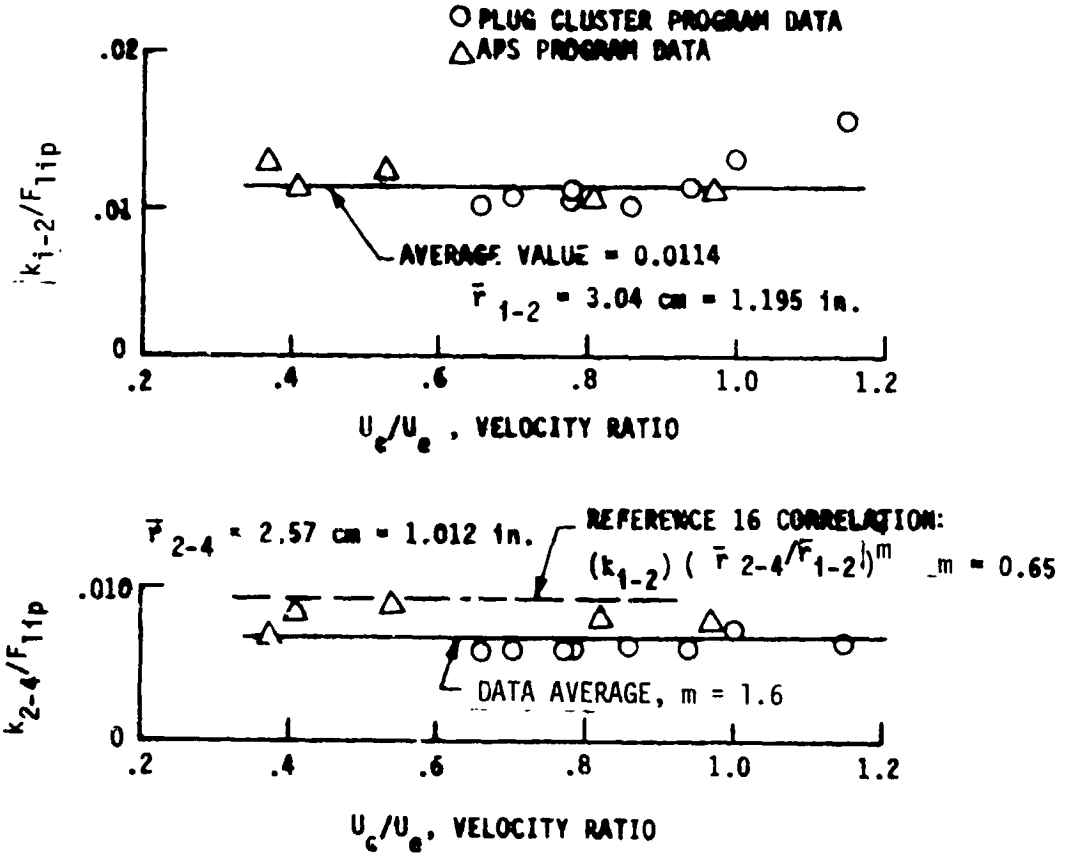

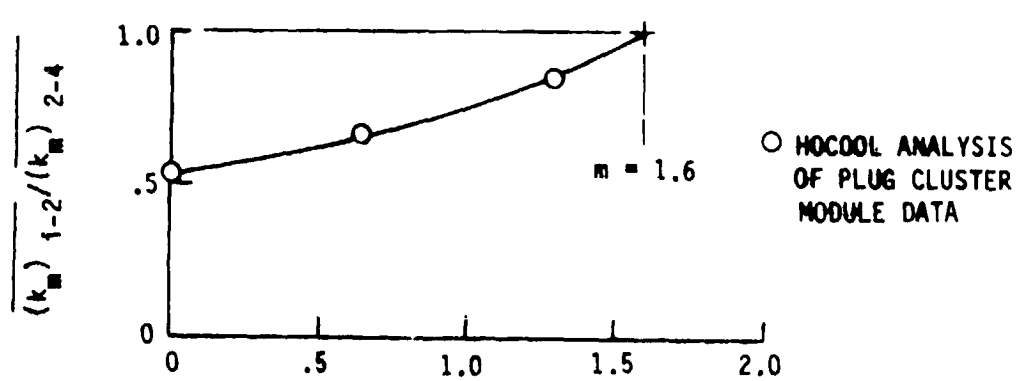

Figure 44. Correlation of Acceleration Effects in APS and PCMD Data

VI, Post-Test Analysis

Ambient temperature oxygen/hydrogen propellants were generally assumed; however, the effect of reduced film coolant temperature on coolant requirements was evaluated.

A. POST-TEST STRUCTURES ANALYSIS

1. Film Cooled Chamber

The cycle life capability and creep strength of the film cooled chamber were evaluated as a function of Haynes 188 wall thickness and wall temperature. The analytical procedures of the pretest analysis were used except that the cycle life analysis was modified slightly as explained in the following two paragraphs.

The pretest cycle life analysis was performed assuming that the maximum thermal stress occurs at the maximum wall temperature. This is a very conservative assumption for a film cooled adiabatic wall chamber. Figure 29 shows that the maximum ΔT through the chamber wall occurs early in the wall heating transient when the wall temperature is still relatively low. Using Figure 7.1 of Reference 5 it can be shown that the thermal stress is also a maximum at the same time that ΔT is a maximum. This effect was accounted for in the post-test analysis by evaluating certain analysis parameters at the surface temperature corresponding to maximum thermal stress rather than at the adiabatic wall temperature. The parameters so evaluated are: E and α in Equation 1; F_{tu} in Equation 2; E in Equation 3; and F_{tu}, E, and RA in Equation 4. The gas-side surface temperature at maximum thermal stress is shown as a function of wall thickness and recovery temperature in Figure 45. Cycle life vs strain curves for Haynes 188 calculated from Equation 4 and used in the post-test analysis are shown on Figure 46. These curves were adjusted during the post-test analysis using the properties data in Reference 12.

One additional modification to the cycle life analysis was made to account for creep damage effects. This was done using Miner's rule (Ref. 6) as indicated in Equation 9.

$$N_f = [N_f \text{ from Equation 4}] \left(1 - \frac{t}{SR}\right] \qquad (9)$$

where:

N_f = cycle life

t = total cumulative operating life, hours

SR = stress rupture time, hours (Figure 21)

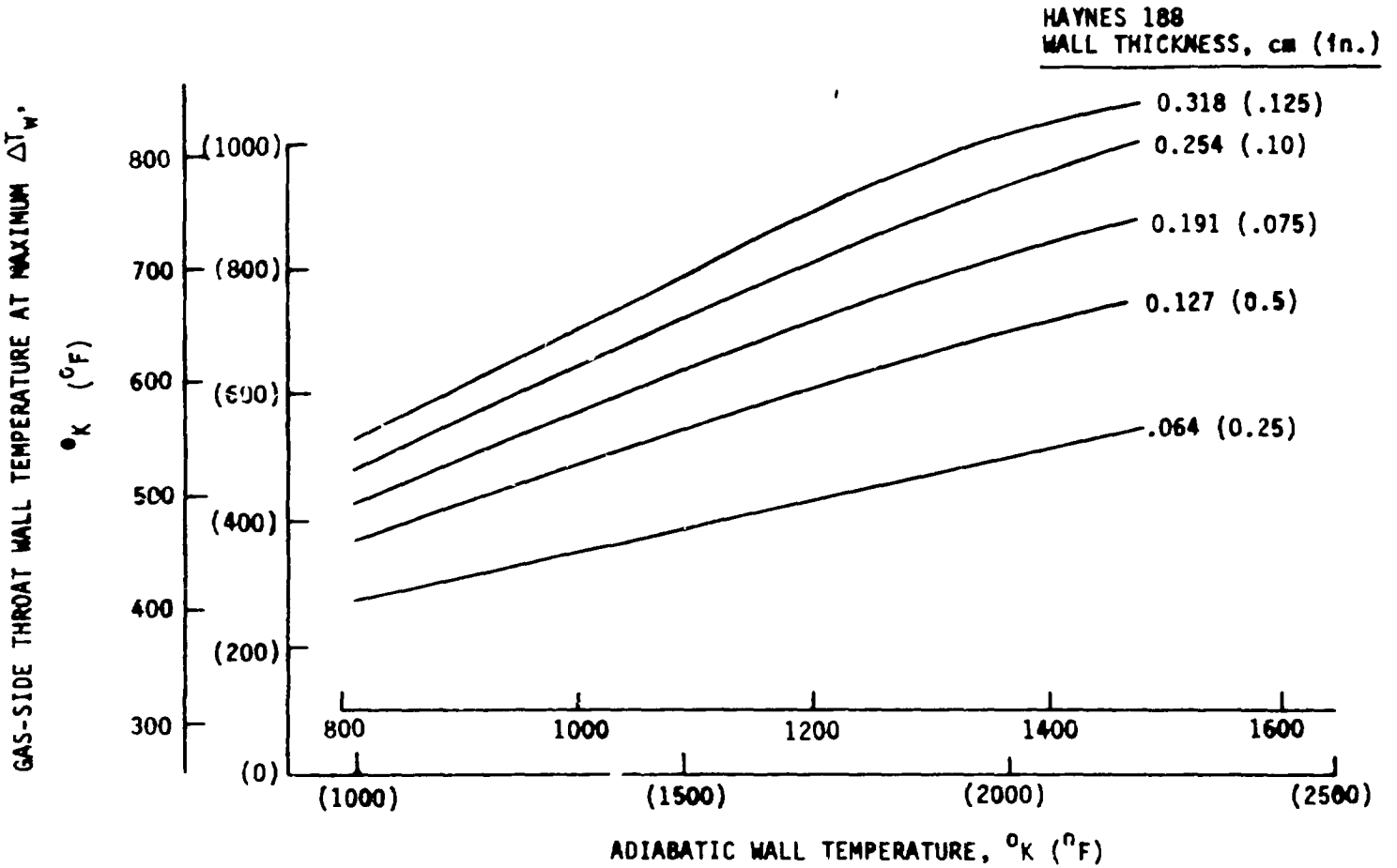

Figure 45. Gas-Side Wall Temperature at Maximum Thermal Stress

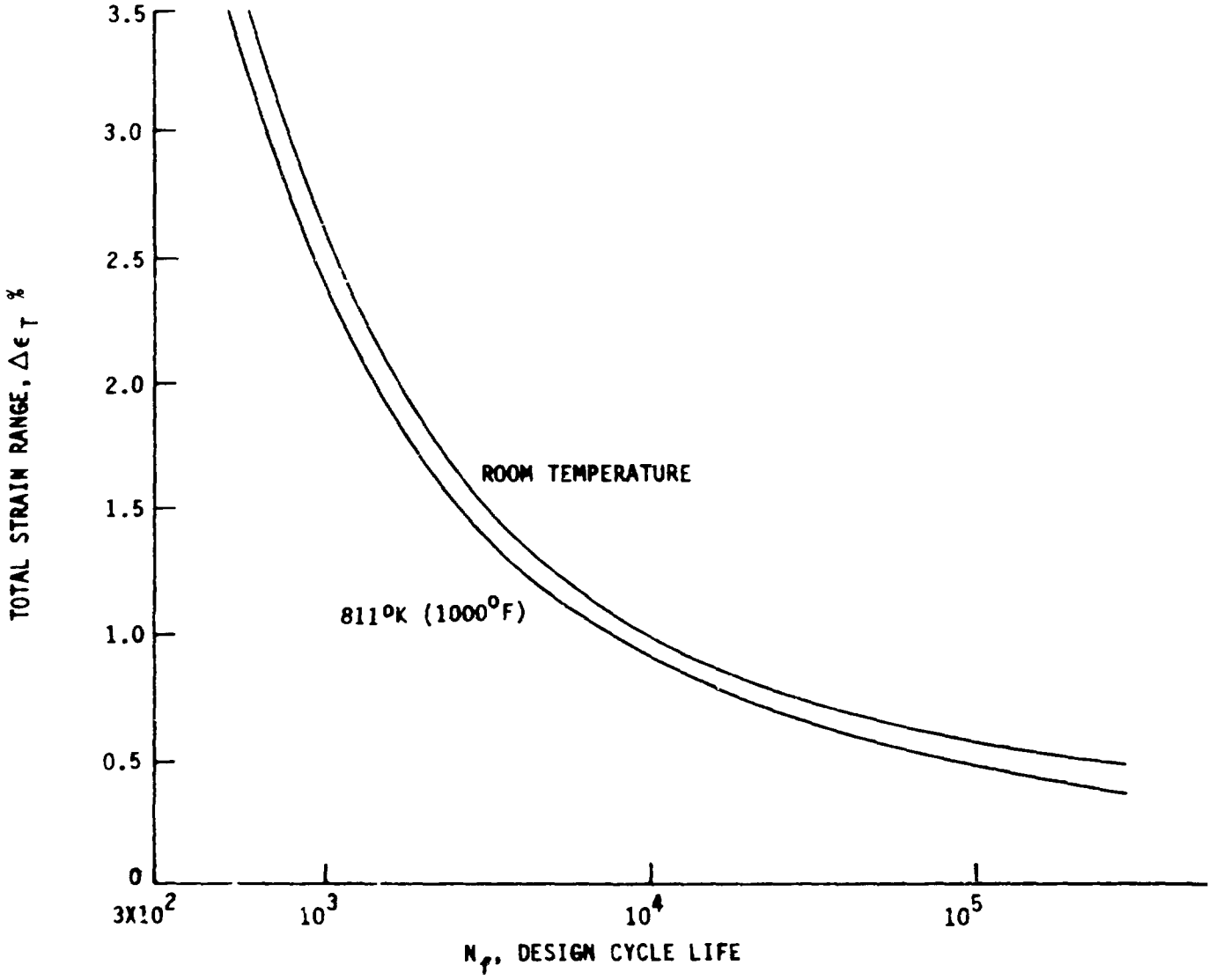

Figure 46. Design Cycle Life of Haynes 188 Calculated from Equation 4

VI, A, Post-Test Structures Analysis (cont.)

Creep damage effects were found to be significant only at temperatures greater than 1300°K. This is shown on Figure 47 where cycle life results from the pretest and post-test analysis are compared.

Creep limits were defined as described in Section IV.C. and by assuming that the stress levels due to internal pressure are inversely proportional to the chamber wall thickness. Stress levels for the ITA configuration (t_w = .081 cm) were previously evaluated and are tabulated below.

Chamber Location	Stress, MN/m^2 (psi)
Throat	48.3 (7000)
Nozzle (Maximum Temperature Region)	8.96 (1300)

The post-test structures analysis results are summarized on Figure 48 where the wall thickness requirements based on cycle life and creep requirements are plotted as a function of steady state wall temperature. Curve 1 shows maximum allowable throat wall thickness for a nominal cycle life of 4800 cycles. This is considered to be an appropriate design cycle life for an engine which must be fired 1200 times. Curve 1a is shown for comparison and indicates that a significantly thicker wall is allowable if the design cycle life is 1200 cycles.

Curve 2 of Figure 48 shows the minimum throat wall thickness dictated by the requirement of 1% creep during the desired 10 hour operating life. Slightly lower wall thicknesses are allowable for a 5 hour operating life as shown by Curve 2a.

Curves 1 and 2 define the optimum chamber throat wall thickness since by choosing a design point near their intersection the allowable throat wall temperature is a maximum. As a result, the throat film coolant requirements and the corresponding cooling performance loss are minimized. The following design point was chosen based on the Figure 48 results:

Wall thickness = 178 ± .025 cm (.070 ± .010 in.)

Throat Adiabatic Wall Temperature = 1340°K (1950°F)

Curve 3 on Figure 48 depicts the minimum nozzle wall thickness required to maintain 1% or less creep over a 10 hour operating life at the nozzle maximum temperature region (4 to 11 cm downstream of the throat). The effect of operating life is small as shown by the 5

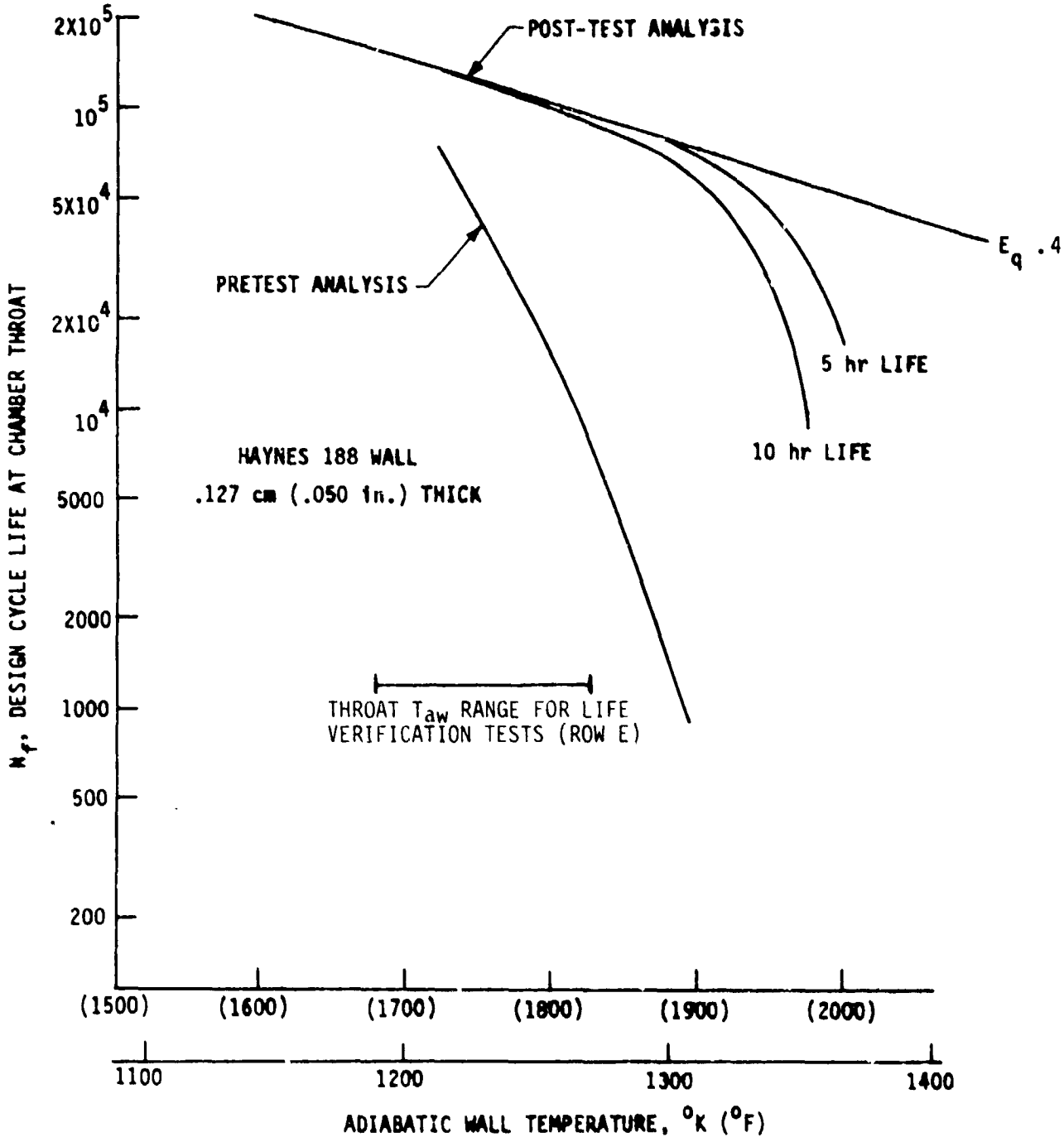

Figure 47. Chamber Wall Cycle Life Predictions

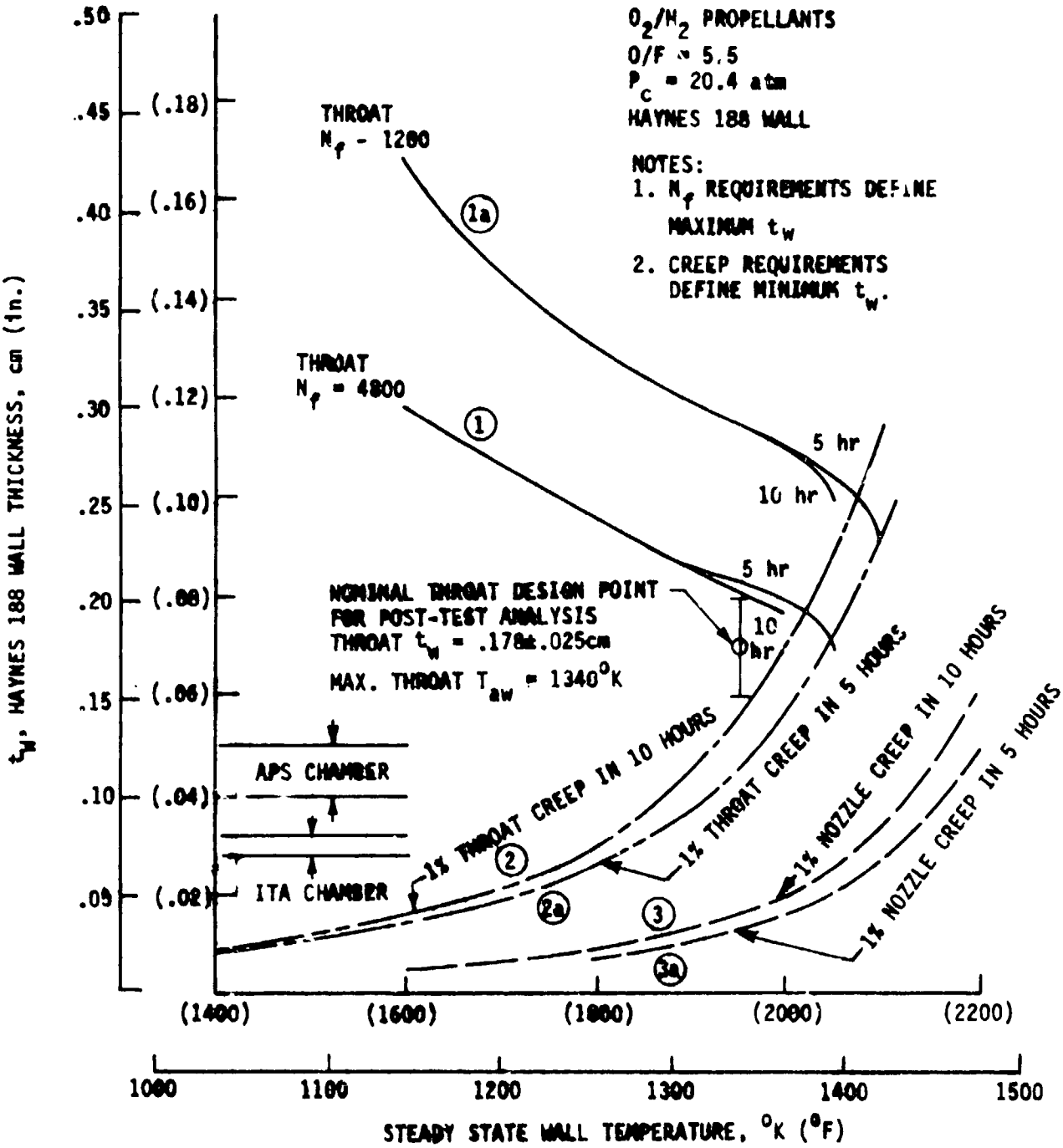

Figure 48. Chamber Wall Thickness-Temperature Requirements Based on Cycle Life and Creep Limits

hour results, Curve 3a. For the nominal design wall thickness range, the 1% creep limit is not achieved until the nozzle temperature approaches 1480°K (2200°F). This is considered to close to the 1575 - 1600°K (2375 - 2425°F) melting range of Haynes 188 for rocket engine applications where local circumferential variations in wall temperature generally occur. A design limit of 1420°K (2100°F) was chosen for the post-test design analysis summarized in Section VI.B.

Figure 48 does not provide the complete story in engine operating limits because the wall temperature in the nozzle is generally not equal to the wall temperature at the throat. For practical purposes, the throat wall temperature is equal to the throat adiabatic wall temperature. The adiabatic wall temperature in the critical nozzle region is generally higher than at the throat, but the nozzle is cooled by thermal radiation through the nozzle exit and consequently the nozzle wall temperature is less than the local adiabatic wall temperature. Therefore, in order to define the film cooled chamber cooling requirements, it is necessary to evaluate two film cooling requirements: one dictated by throat cycle life and creep, and the other dictated by maximum nozzle wall temperature. The cycle life of the injection sleeve must also be considered in order to fully evaluate engine cooling requirements. These three cooling requirements were evaluated in the performance potential evaluation discussed in Section VI.D.

2. Injection Sleeve

The cycle life of the injection sleeve was evaluated using the empirical equation listed below which has been found to approximate finite element model results reasonably well.

$$\Delta\varepsilon_T = K \alpha \Delta T + \varepsilon_p \qquad (10)$$

where:

ΔT = Max. temperature gradient across wall

$\Delta\varepsilon_T$ = Total strain

K = Empirical geometric constant = 2.0

α = Coefficient of thermal expansion

ε_p = Strain due to pressure stress

The calculated total strain was related to cycle life using the data plotted on Figure 49 for zirconium copper (Reference 14) and Nickel 200 (Reference 2). Nickel 200 was considered as an alternate sleeve material because it can operate at higher temperatures than copper.

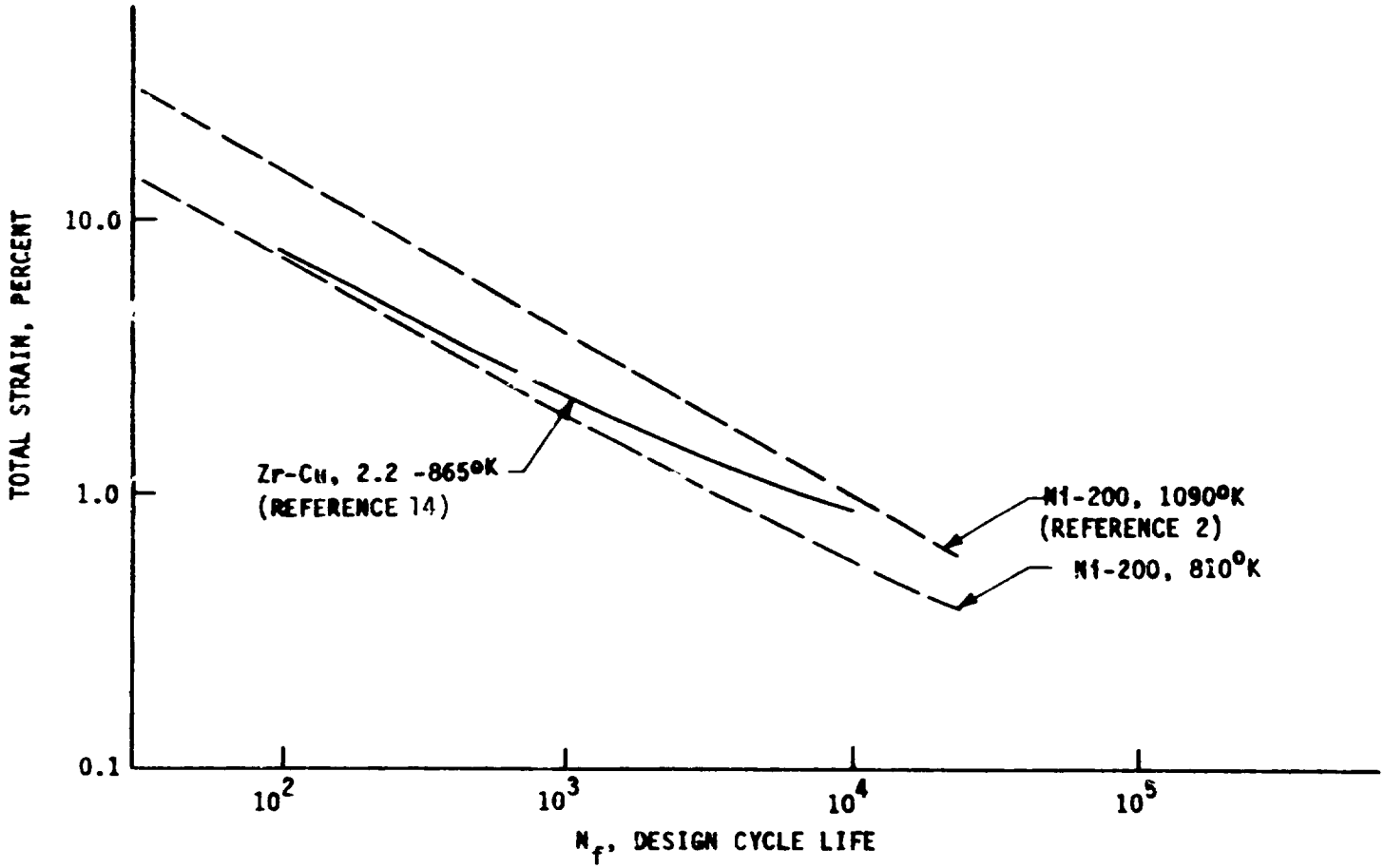

Figure 49. Design Cycle Life of Zirconium Copper and Ni-200

Temperature gradient values were determined using the 2-dimensional conduction network sketched on Figure 50. The cycle life results are summarized in Figure 51 as a function of film coolant flow rate and ΔZ the axial distance from the injection point to the throat (the existing ITA injection point is 3.18 cm upstream of the throat). These results show that the desirable safety factor of 4.0 on the required engine life of 1200 cycles (i.e., design cycle life of 4800 cycles) can be achieved at the existing injection point (Δz = 3.18 cm) but not at positions closer to the throat. The negative slope of the Nickel 200 curves are caused by the increase in cycle life with temperature indicated by the Reference 2 data.

B. POST-TEST HEAT TRANSFER ANALYSIS

The first step in the post-test heat transfer analysis consisted of thermal analyses to determine throat adiabatic wall temperature, film coolant injection sleeve temperature, and maximum nozzle wall temperature as a function of film coolant flow rate. The results of these thermal analyses are plotted on Figures 52, 53 and 54.

Figure 52 shows the sleeve, throat, and nozzle temperatures for the O/F = 5.5, P_c = 20.4 atm operating condition when the film coolant injection point varies from 3.18 to 1.91 cm upstream of the nozzle throat. Zirconium copper and Nickel-200 injection sleeves were considered. All wall temperatures decrease with increased coolant flowrate. Moving the injection point from the existing location (3.18 cm) toward the throat decreases the throat and nozzle temperatures due to the reduced coolant mixing, but the sleeve temperature increases due to the higher heat fluxes in the throat region. The nickel sleeve runs hotter than the Zr-Cu sleeve because of thermal conductivity effects.

The effect of engine mixture ratio on engine wall temperature is summarized on Figure 53. It was found that increasing mixture ratio increased the throat and nozzle temperature because of the reduced total fuel flowrate. The sleeve temperature decreases slightly as mixture ratio is increased because the sleeve heat flux decreased.

The effect of hydrogen film coolant temperature on engine temperatures was found to be relatively small. This is shown on Figure 54 which shows results obtained assuming film coolant hydrogen inlet temperatures ranging from 83 to 300°K. The temperature of the main injector propellants was assumed constant at 300°K in this analysis.

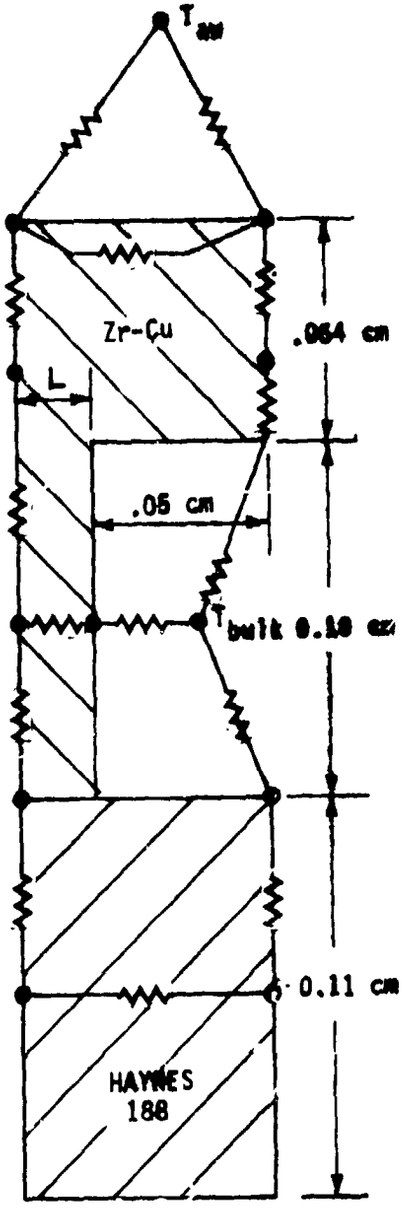

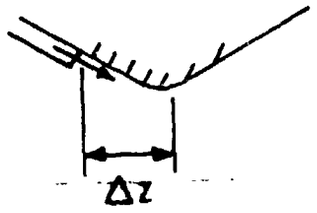

ΔZ, cm (in.)	L, cm (in.)
3.18 (1.25)	.034 (.0135)
2.54 (1.00)	.028 (.011)
1.90 (0.75)	.022 (.0085)

ORIGINAL PAGE IS
OF POOR QUALITY

Figure 50. Thermal Network for Sleeve Life Analysis

MTL.	ΔZ, cm	%FFC	MAX ΔT °F	T* °K	$\Delta\epsilon_t$	N_f, CYCLES
ZrCu	3,18	15%	297	611	.0113	5000
ZrCu	2.54	15%	344	795	.0135	3600
ZrCu	1.91	15%	392	856	.0155	2600
Ni-200	3.18	15%	500	961	.016	2600
Ni-200	2.54	15%	561	1033	.018	2800
Ni-200	1.91	15%	622	1111	.020	3000

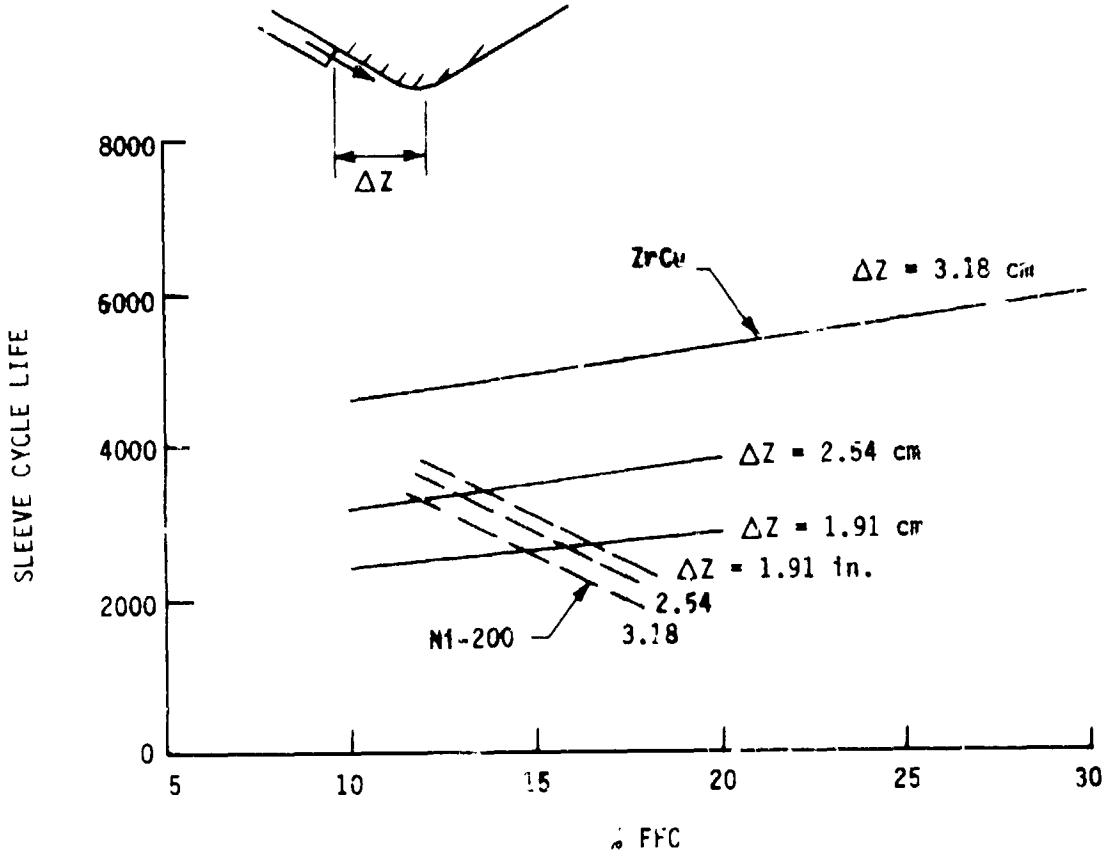

Figure 51 Sleeve Cycle Life Results

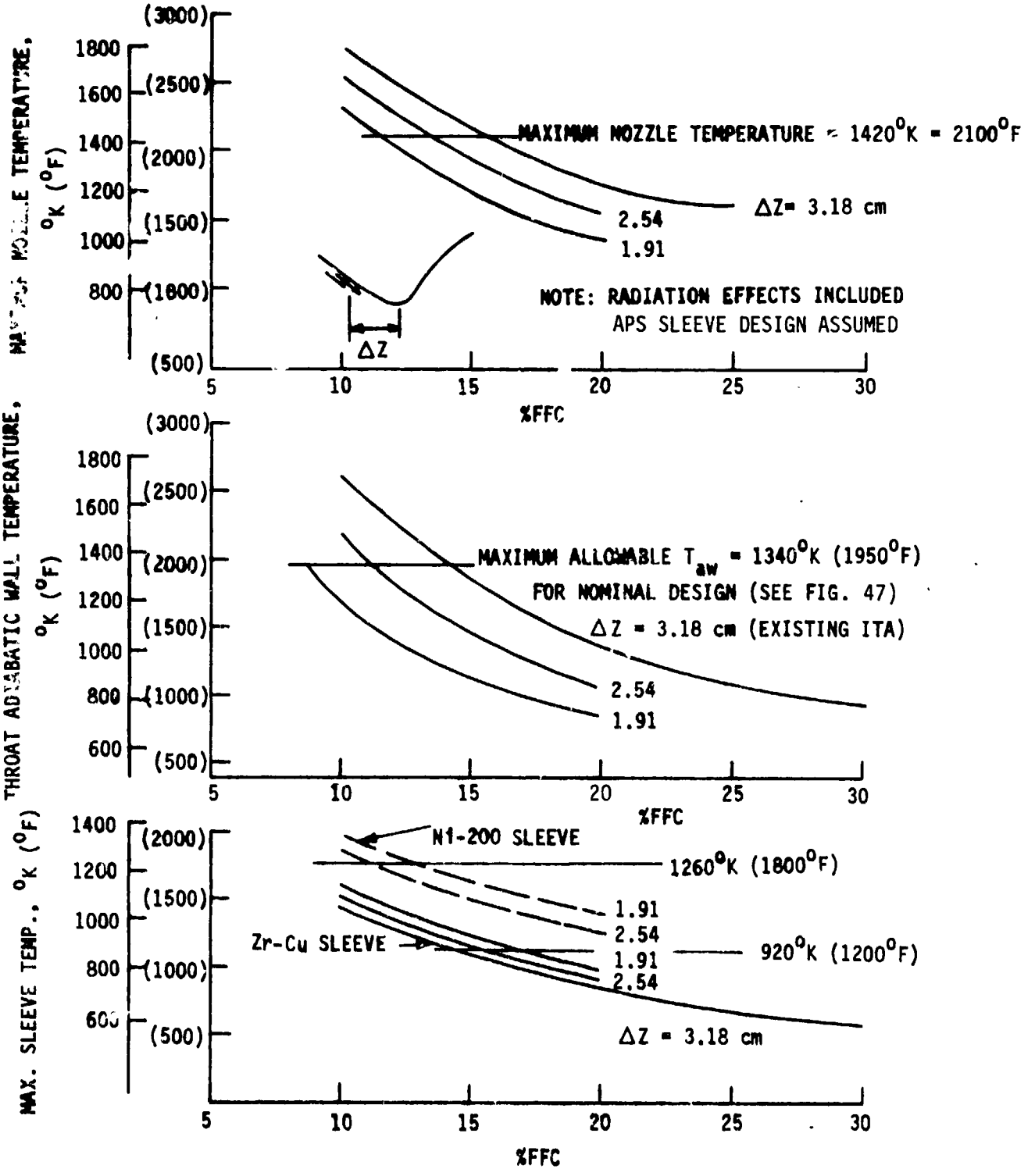

Figure 52. Post-Test Thermal Analysis Results, O/F = 5.5

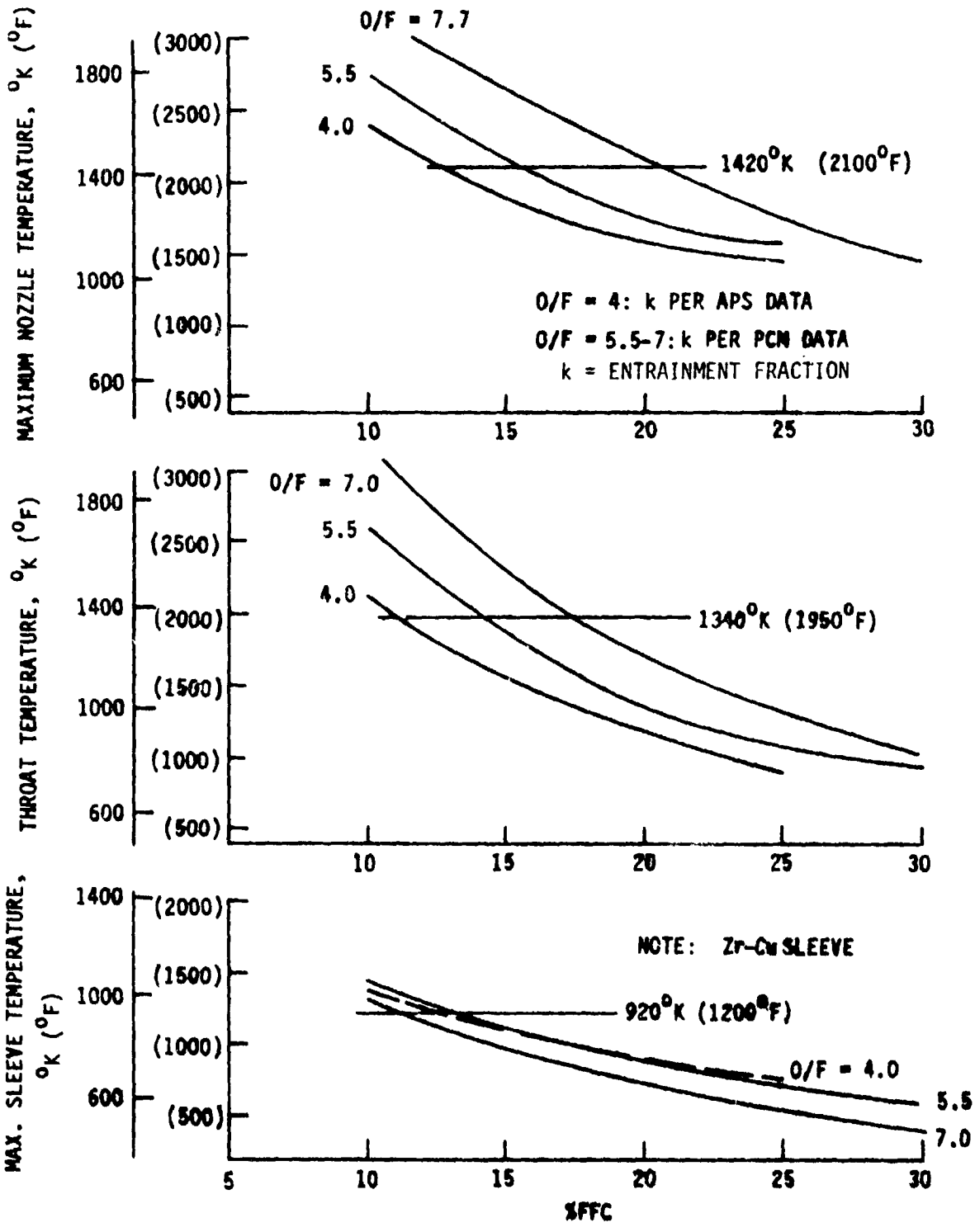

Figure 53. Post-Test Prediction of O/F Effect on Engine Temperature

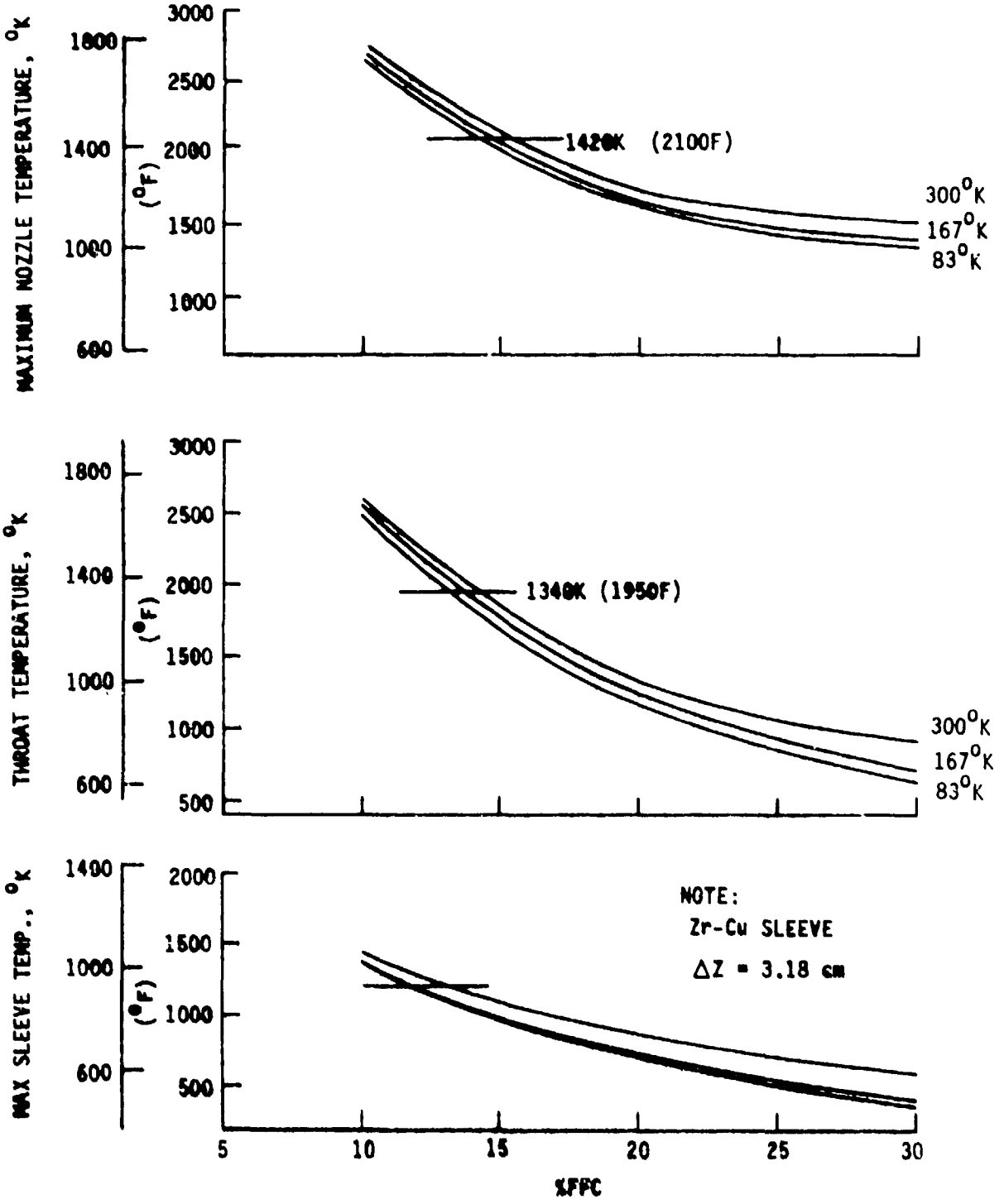

Figure 54. Post-Test Prediction of Hydrogen Film Coolant Temperature Effect on Engine Temperatures

VI, Post-Test Analysis (cont.)

C. FILM-COOLING-PERFORMANCE LOSS

An additional result obtained during the post-test film cooling analysis was the film cooling performance loss which is plotted on Figures 33 and 55. Figure 55 shows that the loss increases significantly as film coolant flow rate and mixture ratio are increased. The difference in performance potential at the overall and core mixture ratios increases as the overall mixture ratio is increased and this causes the predicted O/F effect. Performance decreases with increased cooling because the mixing layer performance is relatively low. It was also found that the loss increases slightly as the coolant injection point is moved toward the throat (less mixing in the subsonic region).

The predicted effect of nozzle area ratio on film-cooling-performance loss is illustrated on Figure 56. The HOCOOL film-cooling-loss model predicts that the film-cooling-loss can be decreased by utilizing a large area ratio nozzle. For example, the loss predicted for a 200/1 nozzle with 15% film cooling is 3 seconds less than the 40/1 nozzle loss. This effect is predicted because of the shape of the performance vs O/F curve as illustrated on Figure 57. As the area ratio increases, the performance at $(O/F)_{core}$ increases more than the performance at O/F. The variations in mixing layer performance with $(O/F)_{ML}$ is a second order effect because the mixing layer performance contribution is relatively small. Tests to experimentally evaluate this predicted area ratio effect are recommended.

D. LIFE VS PERFORMANCE RELATIONSHIP

The performance potential of the AFS/ITA engine as a plug cluster module engine operating with 40/1 nozzle area ratio and with ambient temperature propellants was evaluated using the post-test performance correlation (Figure 34); the post-test heat transfer analysis results of Figures 52, 53 and 54; and the post-test structures analysis results shown on Figures 48 and 51.

Figure 58 shows the life vs performance characteristic of the film cooled chamber region which was obtained by combining the heat transfer, performance, and structures results. Throat cycle life is plotted as a function of delivered performance for chamber wall thicknesses of .127 and .254 cm (.05 and .01 in.). Results are shown for three film coolant injection points: 3.18 cm (.125 in.), 2.54 cm (1.0 in.), and 1.91 cm (.75 in.) upstream of the throat.

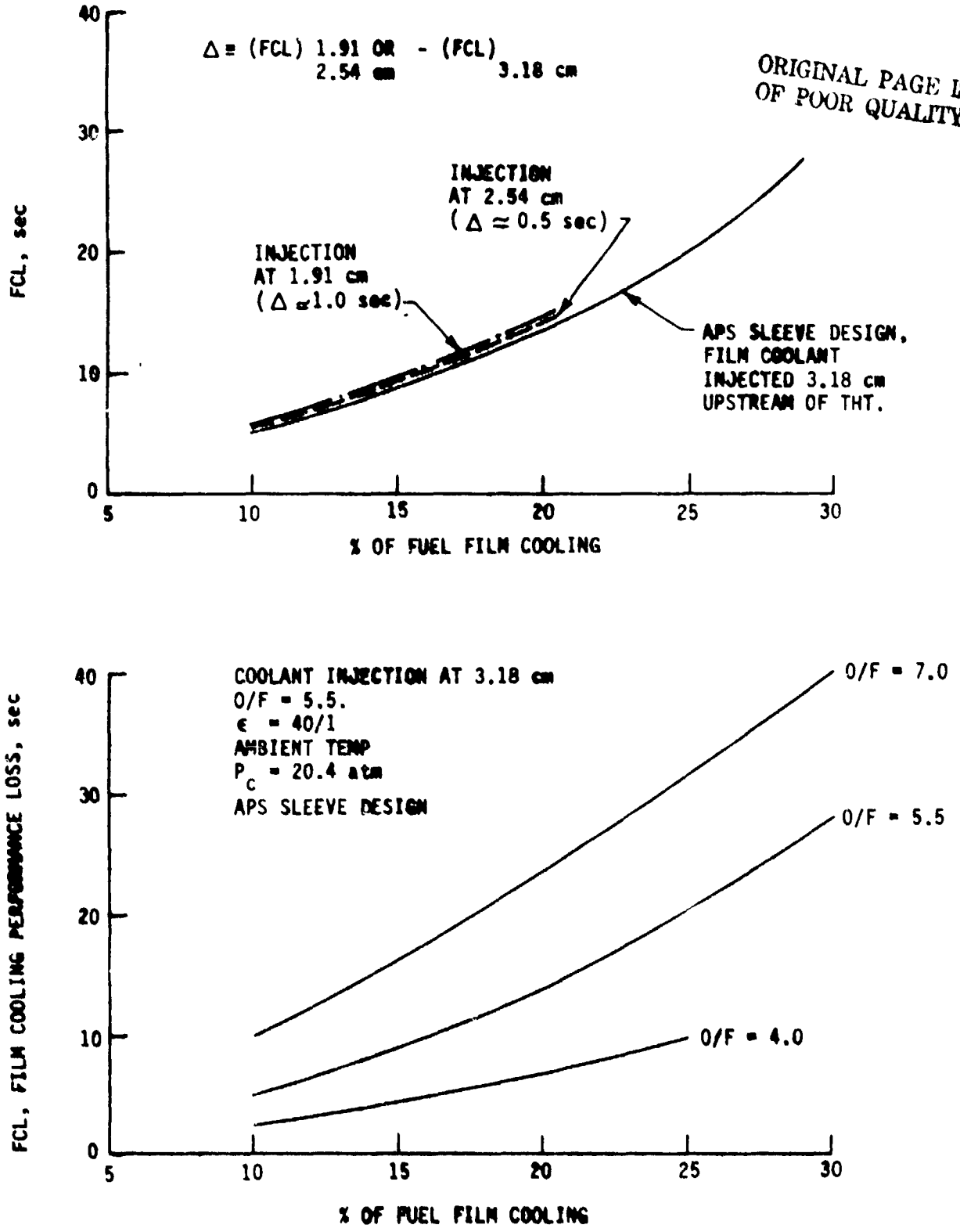

Figure 55. Post-Test Prediction of Film-Cooling-Performance Loss as a Function of O/F, Injection Point, and Coolant Quantity

% FFC	(O/F) CORE	$\dot{W}_{core}$	$(O/F)_{ml}$	$\dot{W}_{ml}$	$\dot{W}_{total}$	W_c
10	6.11	3.593	1.82	.237	3.830	.0589
15	6.47	3.608	1.31	.258	3.866	.0892
20	6.880	3.628	.99	.279	3.906	.1202

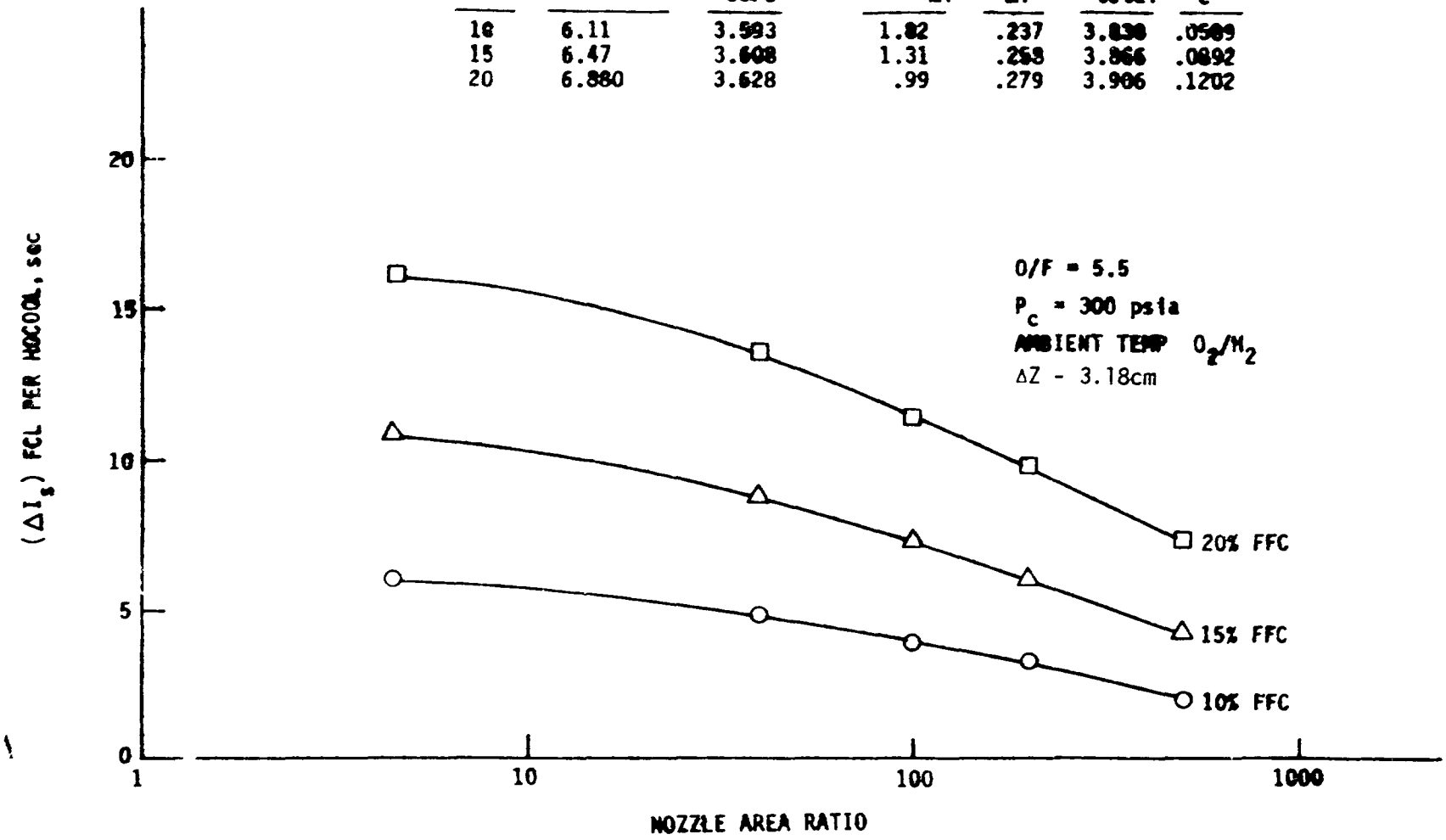

Figure 56. Effect of Nozzle Area Ratio on Film Cooling Loss

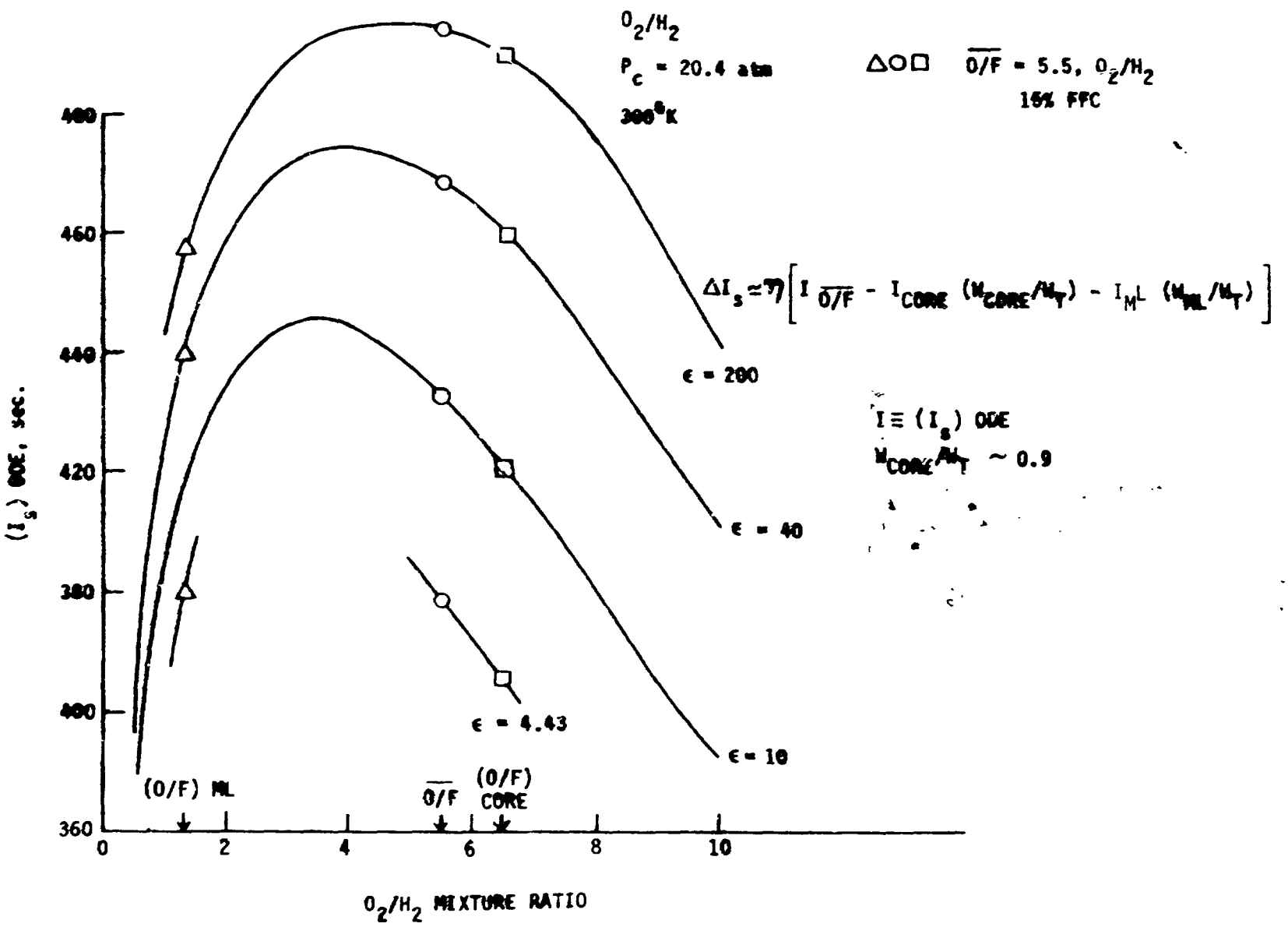

Figure 57. ODE Performance vs Mixture Ratio

VI, D, Life Vs Performance Relationship (cont.)

The general characteristic event in the curves plotted on Figure 58 is that the cycle life decreases as the performance increases. This results from the fact that the performance can be increased only by decreasing the film coolant flowrate and hence increasing the throat wall temperature. As the performance increases, the slope of N_f vs I_s eventually becomes very steep until the curve becomes almost vertical. This is a result of the creep damage effect predicted by Equation 9.

Moving the injection point toward the throat has the effect of increasing performance for a given throat cycle life. This is predicted, despite the fact that the film-cooling-loss for a given flow rate increases as the injection point is moved downstream, because a significantly lower coolant flow rate is required to produce a given throat wall temperature.

Performance limits imposed by maximum nozzle temperature and creep strength at the throat are also shown on Figure 58. The throat creep limit occurs at about the point where the N_f-I_s curves becomes very steep. This is an undesirable region from the standpoint of cycle life because it is difficult to predict, therefore the throat creep limit is generally satisfied by avoiding the steep region of the N_f-I_s curve.

The 1420K (2100°F) maximum nozzle temperature limits performance by about 1-2 seconds more than the throat creep limit. Increasing the allowable temperature to 1480K (2200°F) has a relatively small effect, 1/2 - 1 sec, and is not recommended. For the N_f = 4800 requirement of the plug cluster engine, the nozzle temperature is the limiting factor in almost all of the cases considered on Figure 58. Both nozzle temperature and throat cycle life are limiting factors in one of the cases (.254 cm wall, 3.18 cm injection point).

E. ENGINE DESIGN OPTIONS

Engine design options derived from the post-test thermal, structures, and performance analysis are listed on Table X. A total of ten different design and operating condition cases are listed. Design variables considered are: film coolant injection point location, and film coolant injection sleeve material. Operating condition variables considered are: engine mixture ratio and propellant film coolant temperature. Two film coolant flowrate requirements are listed, one based on the throat cycle life and creep and the other based on a maximum nozzle temperature of 1420°K (2100°F). The nozzle temperature was the limiting condition in each case. Temperature and cycle life of the injection sleeve are also shown because the sleeve operating limits must also be evaluated.

Case 1 of Table X is the existing ITA engine modified to include the APS injection sleeve and a .178 cm (.070 in.) chamber wall.

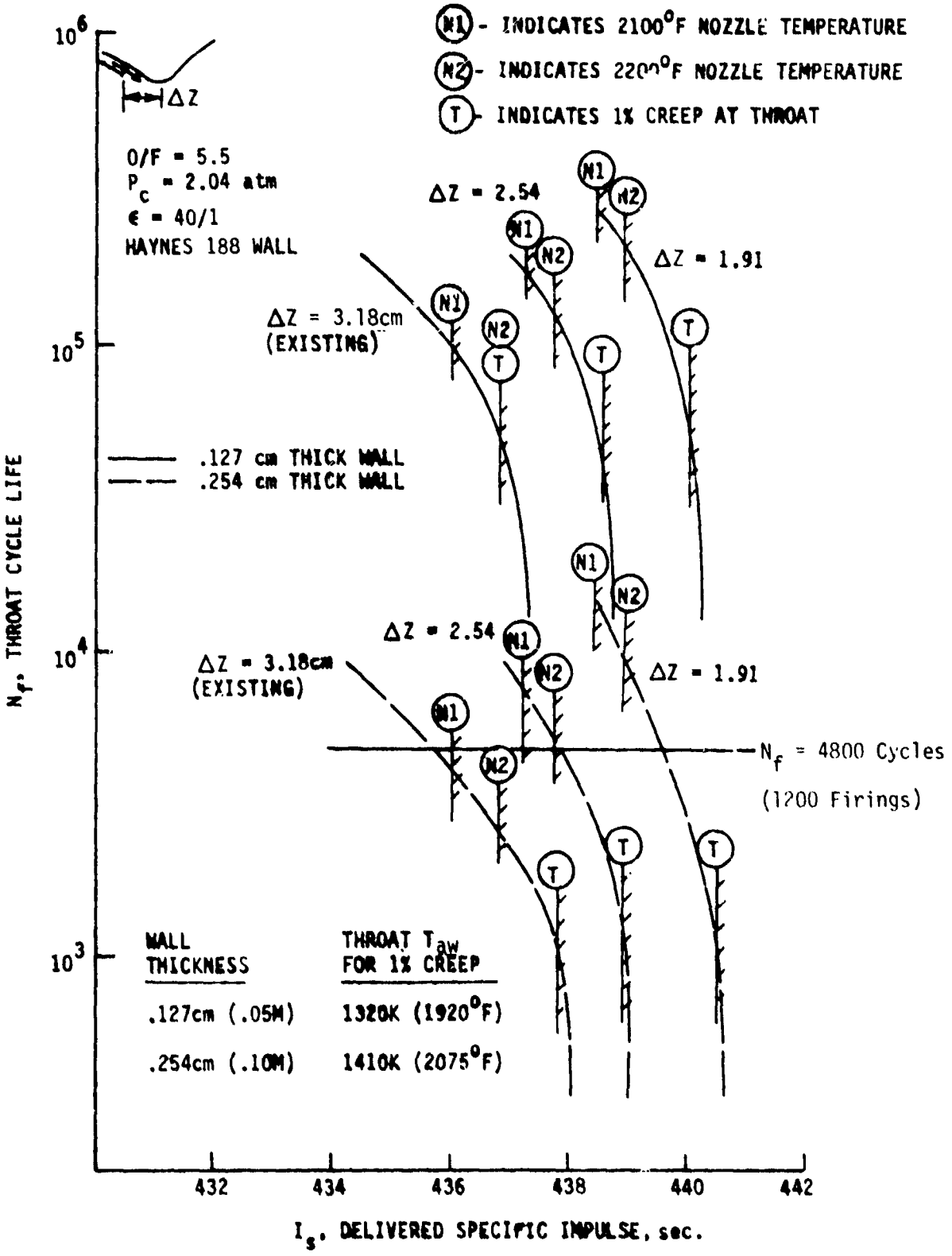

Figure 58. Throat Cycle Life vs Delivered Performance

TABLE 7

ENGINE DESIGN OPTIONS

Case	(1) ΔZ cm (in.)	O/F	O_2/H_2 Temp °K	Pc atm	(2) 1200 Firings Throat FFC Requirement	(3) 300 Firings Throat FFC Requirement	(4) Nozzle FFC Requirement	(5) Isp vac at %FFC, sec	Sleeve Analysis Results For %FFC: Material	Sleeve Analysis Results For %FFC: T_{max} °K (°F)	Sleeve Analysis Results For %FFC: N_f	Remarks
1	3.18 (1.25)	5.5	300	20.4	14.3	13.8	*15.0	436	ZrCu	845 (1060)	5000	Recommended For 1200 Firings
2	2.54 (1.0)	5.5	300	20.4	11.3	10.8	*13.3	437	ZrCu	960 (1270)	3500	Excessive Sleeve Temp
3	2.54 (1.0)	5.5	300	20.4	11.3	10.8	*13.3	437	Ni 200	45 (1650)	3200	Recommended For < 800 Firings
4	1.91 (.75)	5.5	300	20.4	8.8	8.3	*11.4	438	ZrCu	1090 (1500)	3300	Excessive Sleeve Temp
5	1.91 (.75)	5.5	300	20.4	8.8	8.3	*11.4	438	Ni 200	1290 (1870)	3800	Excessive Sleeve Temp
6	3.18 (1.25)	4.0	300	20.4	11.3	10.8	*13.7	449	ZrCu	920 (1200)	4900	1200 Firing Capability
7	3.18 (1.25)	7.0	300	20.4	17.7	17.1	*20.4	398	ZrCu	655 (720)	5700	Smaller ΔZ would Improve I_s vac
8	3.18 (1.25)	5.5	167(6)	20.4	13.7	13.2	*14.7	-	ZrCu	795 (970)	[illegible]	
9	3.18 (1.25)	5.5	83(6)	20.4	13.2	12.8	*14.2	-	ZrCu	800 (980)	5100	

Notes:
(1) Axial Distance Between Injection Point and Throat
(2) Nf = 4800 Cycles, t wall = .178 - .025 cm (Haynes 188), Creep ≤ 1%, Taw = 1340K (1950 F)
(3) Nf = 1200 Cycles, t wall = .24 - .025 cm (Haynes 188), Creep ≤ 1%, Taw = 1380 K (2020 F)
(4) Maximum Nozzle Temperature = 1420 °K (2100°F), Creep < 1%
(5) Specific Impulse with 40/1 Nozzle and 300°K Propellants
(6) Main Injector Propellant Temperature = 300°K.

ORIGINAL PAGE IS OF POOR QUALITY

VI, E, Engine Design Options (cont.)

The film coolant is injected 3.18 cm (1.25 in.) upstream of the throat and the injection sleeve material is zirconium copper. This configuration is recommended for a plug cluster engine which operates at O/F = 5.5 that must be capable of 1200 firings. A 15.5% fuel film cooling requirement is indicated. The predicted 40/1 specific impulse performance with ambient temperature propellants is 436 seconds.

The possibility of increasing the engine performance by extending the injection sleeve so that the film coolant is injected closer to the throat was evaluated and the results are summarized as Cases 2 through 5. The coolant injection point is 0.64 cm (1/4 in.) closer to the throat for the Case 2 and Case 3 design. A total of 13.3% of the fuel flowrate is required for film cooling. The specific impulse with a 40/1 nozzle and ambient temperature propellants is one second higher (437 sec) because the film cooling flowrate is lower. The Case 2 design has a zirconium copper sleeve. The 960°K (1270°F) sleeve temperature calculated for Case 2 is considered excessive and this design is not recommended. The Case 3 design has a Ni - 200 sleeve that operates at 1145°K (1600°F) which is acceptable. The estimated cycle life of the Ni - 200 sleeve is 3200 cycles. Case 3 is not recommended for a design which must be fired 1200 times because the safety factor on cycle life is less than 4. Case 3 does represent a higher performance design option if the number of required engine firings is reduced to 800.

In the Cases 4 and 5 designs, the coolant injection is another 0.64 cm (1/4 in.) closer to the throat. This reduces the film cooling requirement to 11.4% and the 40/1 ambient temperature performance is another second higher (438 sec). The injection sleeve temperatures calculated are also higher because of the reduced coolant flow rate and the higher heat flux. A 1090°K (1500°F) temperature was calculated for the Zr-Cu design and a 1290°K (1870°F) temperature was calculated for the Ni - 200 design. This configuration is not recommended because of excessive sleeve temperatures.

The effect of engine O/F is illustrated by Cases 6 and 7 which compare to Case 1. At O/F = 4 (Case 6), 12.7% of the fuel is required as a film coolant and the 40/1 ambient temperature performance increases to 449 sec. A maximum temperature of 1200°F and cycle life of 4900 cycles was calculated for the Zr-Cu injection sleeve. This is an adequate cycle life and a marginally acceptable sleeve temperature. A Ni-200 sleeve could also be used; however, this case was not analyzed. At an O/F of 7.0, the performance is much lower (398 sec) and the film coolant requirement is 20.4%. The sleeve temperature is very low due to the lower heat flux, therefore the performance at O/F = 7.0 can probably be improved by extending the sleeve closer to the throat. This case was not analyzed. The film

cooling flow rate and performance vs O/F characteristic obtained for the existing coolant injection point is shown on Figure 59. Performance analysis details are listed on Table XI.

In Cases 8 and 9 of Table IX, the effect of film coolant temperature on film cooling requirements was evaluated. It was found that reducing the film coolant temperature from 300°K to 167°K reduced the cooling requirement from 15.5% to 14.7%. A further reduction in coolant temperature to 83°K reduced the coolant requirement to 14.2%.

VII. CONCLUSIONS AND RECOMMENDATIONS

The low pressure, film cooled rocket engine design concept developed during two previous ALRC programs was re-evaluated for application as a module for a plug cluster engine capable of performing space shuttle OTV missions. The nominal engine mixture ratio was 5.5 and the engine life requirements were; 1200 thermal cycles, 10 hours total operating life. The program consisted of pretest analysis; engine tests, performed using residual components; and post-test analysis. The following conclusions and recommendations are based on the experimental and analytical results obtained.

1. The film cooled APS/ITA thruster concept can be utilized in a slightly modified configuration as a module for a plug cluster rocket engine which operates at a 5.5 oxygen/hydrogen mixture ratio and has the following engine life requirements: 1200 thermal cycles, 10 hours total operating time. The specific impulse performance predicted for this modified ITA engine is 436 seconds based on a 40/1 nozzle and 300°K propellants. The nominal film coolant flow requirement is 15.6% of the total fuel flowrate.

2. The modifications recommended for the ITA engines are: (1) increase the wall thickness of the film cooled chamber from .114 + .013 cm to 0.178 + .025 cm, and (2) change the injection sleeve design to the APS configuration. This recommended sleeve design change consists of reducing the number of injection channels from 160 to 120 and increasing the size of the square injection channels from .076 cm (.03 in.) to .10 cm (.04 in.).

3. The durability of the APS/ITA concept was demonstrated in a life verification test series in which a used APS engine was fired 1220 times at O/F = 5.5, P_c = 20.4 atm, and with 19.5% to 21.5% fuel film cooling. Each test comprised a maximum thermal strain cycle for the critical throat region. These testing conditions correspond to a nominal performance range of 430 -432 seconds (40/1 nozzle, 300°K propellants). Testing at lower coolant rates was not possible because of damage which had occurred during the previous 16,310 firings of this engine at a nominal O/F = 1.0.

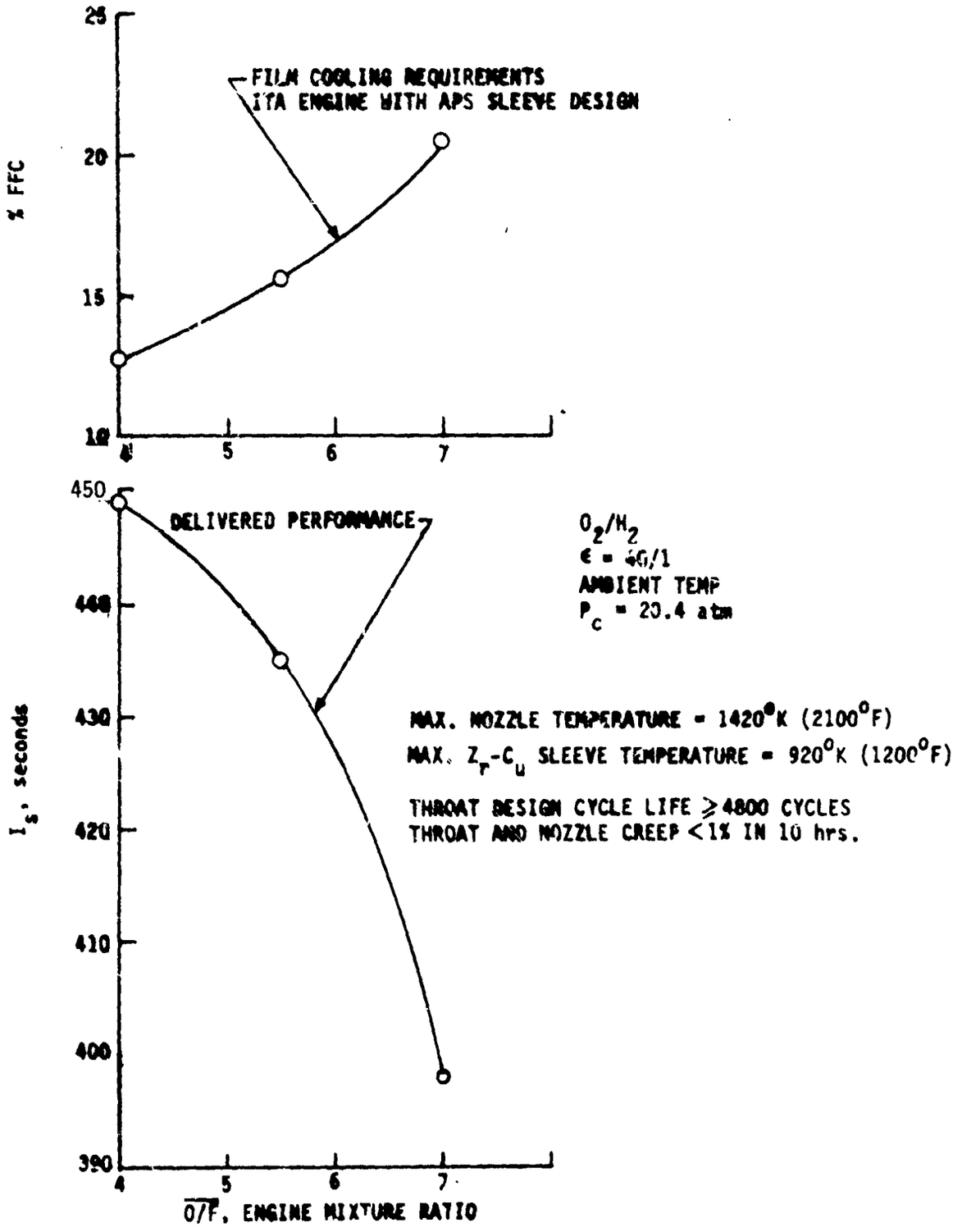

Figure 59. Film Cooling Requirements and Delivered Performance vs Engine O/F

TABLE XI

PLUG CLUSTER ENGINE PERFORMANCE EXTRAPOLATION

O/Feng	4.0	5.5	7.0
*Required % FFC	12.7	15.6	20.4
O/F_{core}	4.60	6.55	8.79
ϵ	40 →	→	→
T_{ox} ^{o}F	540 →	→	→
T_f ^{o}F	540 →	→	→
I_{sp}, ode	473.3	467.1	451.8
I_{sp}, odk	469.5	460.7	442.4
KL	3.8	6.4	9.4
BLL	6.1	6.5	6.6
DL	4.7	4.6	4.2
FCL	3.6	9.5	24.2
ERL	5.8	4.2	9.1
%ERE	98.8	99.1	98.0
E_m	0.8	.83	.76
I_{sp}, vac	449.3	435.9	398.3

*Film ccolant injected 3.18 cm upstream of nozzle throat

VII, Conclusions and Recommendations (cont.)

4. The energy release efficiency of the ITA injector did not decrease over the rangeof practical operating conditions with constant overall O/F = 5.5. Therefore, it is concluded that injector redesign is not necessary; however, this conclusion is based on operation with 300°K propellants and should be re-evaluated for other propellant temperatures.

5. The post-test performance and entrainment fraction correlations established from the performance verification tests can be used to evaluate design concepts for operation at O/F = 5.5.

6. Acceleration effects reduced the entrainment fraction significantly more than indicated by a correlation based on data obtained with heated nitrogen core gas. This means that there was less film coolant/core gas mixing than predicted with the previous correlation.

REFERENCES

1. Schoenman, L., "Hydrogen-Oxygen Auxiliary Propulsion for the Space Shuttle, Volume I, High Pressure Thrusters", Contract NAS 3-14354, NASA CR 120895, Aerojet Liquid Rocket Co. (ALRC), January 1973.

2. Blubaugh, A.L., "Integrated Thruster Assembly Program", Contract NAS 3-15850, ALRC, NASA CR 134509, November 1973.

3. Rousar, D.C. and Ewen, R.L., "Combustion Effects on Film Cooling", Final Report, NASA CR 135052, ALRC, Contract NAS 3-17813, 24 February 1977.

4. Calhoon, D.F., Ito, J.I. and Kors, D.L., "Investigation of Gaseous Propellant Combustion and Associated Injector/Chamber Design Guidelines", NASA CR 121234, ALRC, 31 July 1973.

5. Manson, S.S., "Thermal Stress and Low-Cycle Fatigue", McGraw-Hill Book Co., 1966.

6. Shigley, J.F., "Mechanical Engineering Design", 2nd Ed., McGraw-Hill (1972), p. 270 and p. 251.

7. ALRC Proposal LR 721213, "Integrated Thruster Assembly Investigation", Vol. I, 29 March 1972.

8. Manson, S.S., "Fatigue: A Complex Subject - Some Simple Approximations", Experimental Mechanics, Vol. 5, No. 7, p. 193 (1965).

9. Ewen, R.L., "Hydrogen Film/Conductive Cooling", NASA CR-120926, ALRC, Contract NAS 3-14343, November 1972.

10. Liess, C., "Experimental Investigation of Film Cooling With Ejection From a Row of Holes for the Application to Gas Turbine Blades", Trans. of ASME, Journal of Engineering For Power, January 1975.

11. Holdeman, J.D. and Walker, R.E., "Mixing of a Row of Jets With Confined Crossflow", AIAA Journal, Vol. 15, No. 2, p. 243-249 (1977).

12. "Haynes Alloy No. 188", Stellite Division, Cabot Corp., 1973.

13. Rousar, D.C. and Ewen, R. L., "Hydrogen Film Cooling Investigation", ALRC Final Report, Contract NAS 3-15844, NASA CR 121235.

REFERENCES (cont.)

14. Luscher, W.P. and Mellish, J.A., "Advanced High Pressure Engine Study for Mixed-Mode Vehicle Applications", NASA CR-135141, Contract NAS 3-19727, January 1977 (Figure 20).

15. Taylor, M.F., "Application of Variable Property Heat-Transfer and Friction Equations to Rocket Nozzle Coolant Passages and Comparison with Nuclear Rocket Test Results", AIAA Journal, 1970.

16. Nickerson, G.R., Coates, D.E. and Bartz, J.L., "Two-Dimensional Kinetic Reference Computer Program", Contract NAS 9-12652, December 1973.

17. Kushida, R., "Revision of CPIA 246, Section 6.2 Reaction Rate Data", JPL-Letter 383CR-76-311, 29 March 1976.

18. Pieper, J.L., "ICRPG Liquid Propellant Thrust Chamber Performance Evaluation Manual - Appendix B", CPIA No. 178, 30 September 1968.

APPENDIX A

NOMENCLATURE

ENGLISH LETTERS

BLL	=	Boundary layer performance loss
Cg	=	Heat transfer correlation coefficient
c*	=	Characteristic velocity
D	=	Diameter
DL = CDL	=	Performance loss due to nozzle divergence
E	=	Modulus of elasticity
ERE	=	Energy release efficiency
ERL	=	Performance loss due to imperfect energy release
E_m	=	Mixing efficiency
f(Uc/Ue)	=	Velocity ratio function (Figure 7 of Ref. 3)
FCL = FFCL=		$(\Delta I_s)_{FC}$ = Film-Cooling-Performance Loss
FFC = %FFC=		Percent of the total fuel flow rate injected as film coolant
F_{tu}	=	Ultimate tensile strength
H	=	Enthalpy
h_g	=	Gas-side heat transfer coefficient
I_{sp}	=	Specific Impulse
K	=	Empirical constant
k	=	Entrainment fraction and thermal conductivity
k_o	=	Reference entrainment fraction from Ref. 9 (defined on Figure B-4)
km	=	Entrainment fraction multiplier defined by Eq. 8
k_{sub}	=	Subsonic region entrainment fraction
k_{super}	=	Supersonic region entrainment fraction
KL	=	Performance loss due to Kinetics effects
m	=	Acceleration effect exponent (Eq. 7)
MW	=	Molecular weight
N_f	=	Design cycle life (safety factor not included)
O/F	=	Oxygen hydrogen mixture ratio
$\overline{O/F}$	=	Overall engine mixture ratio
Pc	=	Chamber pressure

ENGLISH LETTERS (cont.)

Pr	=	Prandtl Number
RA	=	Reduction in area
r	=	Radius
SR	=	Time required for stress rupture failure
t	=	Engine total operating life
t_w	=	Wall thickness
T_{aw}	=	Adiabatic wall temperature
T_i	=	Initial temperature
T_f	=	Fuel (H_2) temperature
T_{ox}	=	Oxidizer (O_2) temperature
T_{ref}	=	Reference temperature
T_∞	=	Core gas free stream temperature
$\overline{T}$	=	Equivalent temperature defined on Figure 24
T_{wg}	=	Gas-side wall temperature
ΔT	=	Temperature difference
Uc/Ue	=	Coolant-to-core gas velocity ratio at injection point
$\rho_c U_c/\rho_e U_e$	=	Coolant-to-core-gas mass flux ratio
$\rho_c U_c^2/\rho_e U_e^2$	=	Coolant-to-core-gas momentum flux ratio
Δz	=	Axial distance upstream from the nozzle throat to the film coolant injection point

GREEK LETTERS

α	=	Coefficient of thermal expansion
β	=	Biot Number = $h_g t_w/k_w$
ε	=	Nozzle area ratio
ε_p	=	Strain due to pressure stress
$\varepsilon_T = \Delta\varepsilon_T$	=	Total strain
η_{DL}	=	Nozzle efficiency
η_m	=	E_m = Mixing Efficiency
μ_g	=	Viscosity of combustion gas

GREEK LETTERS (cont.)

ν = Poisson's ratio

ρ_c = Density of injected coolant

ρ_e = Density of core gas at injection point

σ_a = Alternating stress component

σ_{eq} = Equivalent stress

σ_m = Mean stress

σ_{Press} = Pressure stress

ϕ = $(\rho u)2D/(\rho u)1D$ = 2 Dimensional flow factor

SUBSCRIPTS

ave : Average value

aw : Adiabatic wall

c : Coolant at injection point

e : Core gas at coolant injection point

i : Initial or injection point condition

ODE : One-dimensional-equilibrium

ODK : One-dimensional-Kinetic

vac : Vacuum back pressure condition

w : Wall condition

∞ : Core gas or free stream

APPENDIX B

HEAT TRANSFER ANALYSIS DETAILS

I. DUMP COOLED INJECTION SLEEVE

Gas-side heat transfer coefficients were calculated using the Bartz type equation listed on Figure B-1. The Cg factors were determined from two data sources: (1) the Cg vs axial position data shown on Figure VII-32 of Reference 1, and (2) the Cg vs O/F data reported for a premix type injector in Reference 4 (convergent nozzle region, tests 135, 136 and 137). The Cg vs O/F relationships used are indicated by the solid curves on Figure B-1. Coolant side heat transfer coefficients were calculated from the Taylor correlation (Ref. 15) except that the C_L correlation coefficients was increased 13% to correlate backside wall temperature predictions with APS test data as indicated on Figure B-2. This correction is considered to account for channel roughness effects which are difficult to predict and not accounted for in the Taylor correlation.

II. FILM COOLED CHAMBER

The film cooled chamber is defined as the region downstream of the film coolant injection point. The first step in establishing the film cooled region model was to utilize the entrainment fractions reported for a specific APS test to predict adiabatic wall temperatures for that test. The entrainment fraction, k, characterizes the rate of film coolant and core gas mixing in a mixing layer adjacent to the chamber wall. It has a strong influence on the wall temperature distribution downstream of the film coolant injection point (Ref. 3). The predicted Taw values are compared to Reference 1 data on Figure B-3. It was necessary to reduce the supersonic region entrainment fractions by 5% to account for minor changes incorporated into the supersonic model during the Reference 6 program.

Step two consisted of establishing a generalized correlation of all the entrainment fraction data reported in Reference 1 for the particular injector and chamber combination which was test fired on this program. These data are listed on Table B-I.

Axial distributions of the APS entrainment fraction data are shown on Figure B-4. The test velocity ratio, u_c/u_e, ranged from 0.37 to 0.97 and the hydrogen temperature ranged from 200 to 540°R. The distributions in the subsonic region are similar to the Combustion Effects data (Ref. 3) and are relatively constant (within $\pm$ 25%) with velocity ratio. Immediately downstream of the throat, a significant velocity ratio effect is evident. Higher entrainment fractions (higher mixing rates) are indicated for the higher velocity ratio tests. This indicates that a higher mixing layer momentum promoted penetration of the core gases by the mixing layer in the divergent throat turn. The u_c/u_e effect in the first supersonic region (0.69 cm downstream of the nozzle throat) was correlated by curve fitting the data. This curve fit was also used for the other supersonic regions because it yielded a sufficient approximation of the data.

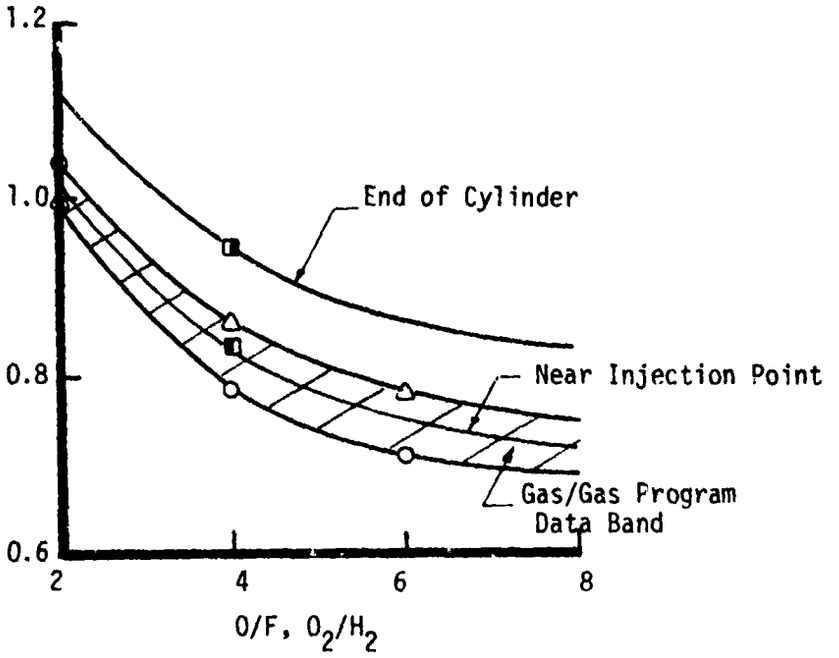

$$h_g = C_g \, DB_r \, \left(\frac{MW}{MW_\infty}\right)^{0.8} \left(\frac{H_{aw}-H_w}{T_{aw}-T_{wg}}\right) \left(\frac{\dot{(W)}}{D^{1.8}}\right)^{0.8} \left(\frac{T_\infty}{T_{ref}}\right)^{0.8}$$

$$DB_r = 0.026 \left(\frac{4}{\pi}\right)^{0.8} \left(\frac{\mu_g{}^{.2}}{P_r{}^{0.6}}\right)$$

$$T_{ref} = 1/2 \, (T_{WG} + T_{AW})$$

□ – Reference 1 Data

△○ – Referenc 4 Data

Figure B-1. Gas-Side Heat Transfer Coefficient Model

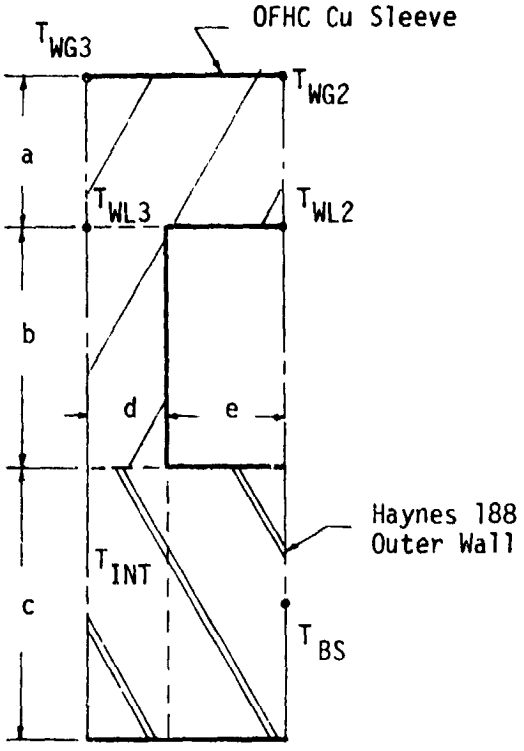

Parameter	Value
a	.064 cm (.025")
b	0.1 cm (.04")
c	0.11 cm (.045")
d	.034 cm (.0135")
e	.05 cm (.02")
T_{WG3}	672K (749F)
T_{WG2}	684K (771F)
T_{WL3}	639K (691F)
T_{WL2}	666K (739F)
T_{INT}	598K (616F)
T_{BS}	567K (560F)
h_L Factor	1.13

RESULTS FOR APS TEST 04-012

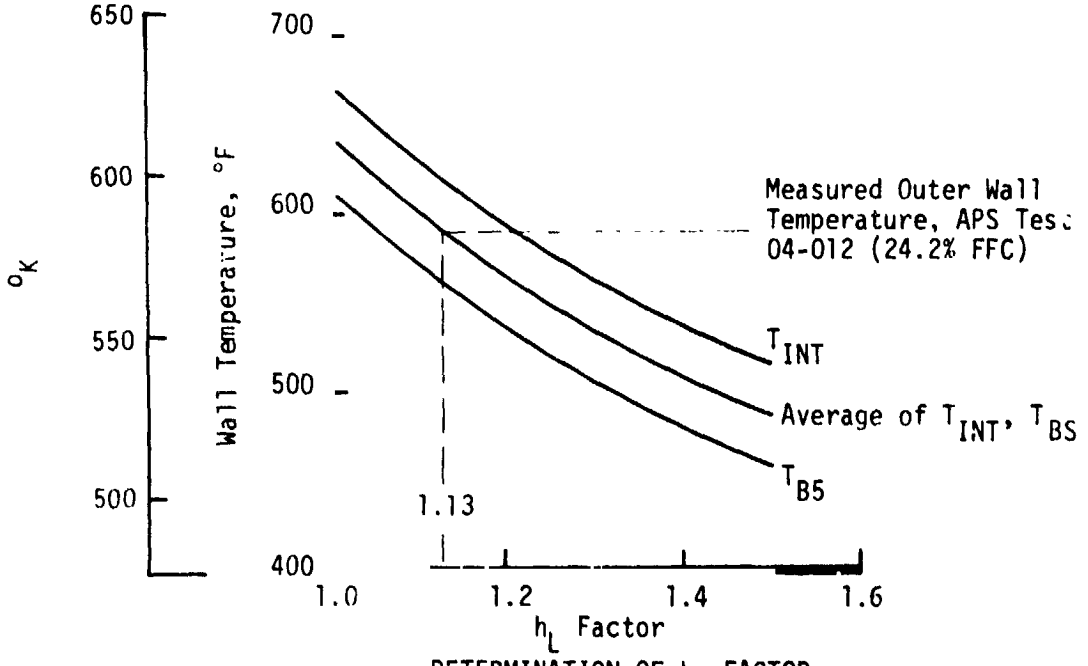

DETERMINATION OF h_L FACTOR

Figure B-2. Correlation of Regeneratively Cooled Injection Sleeve Model

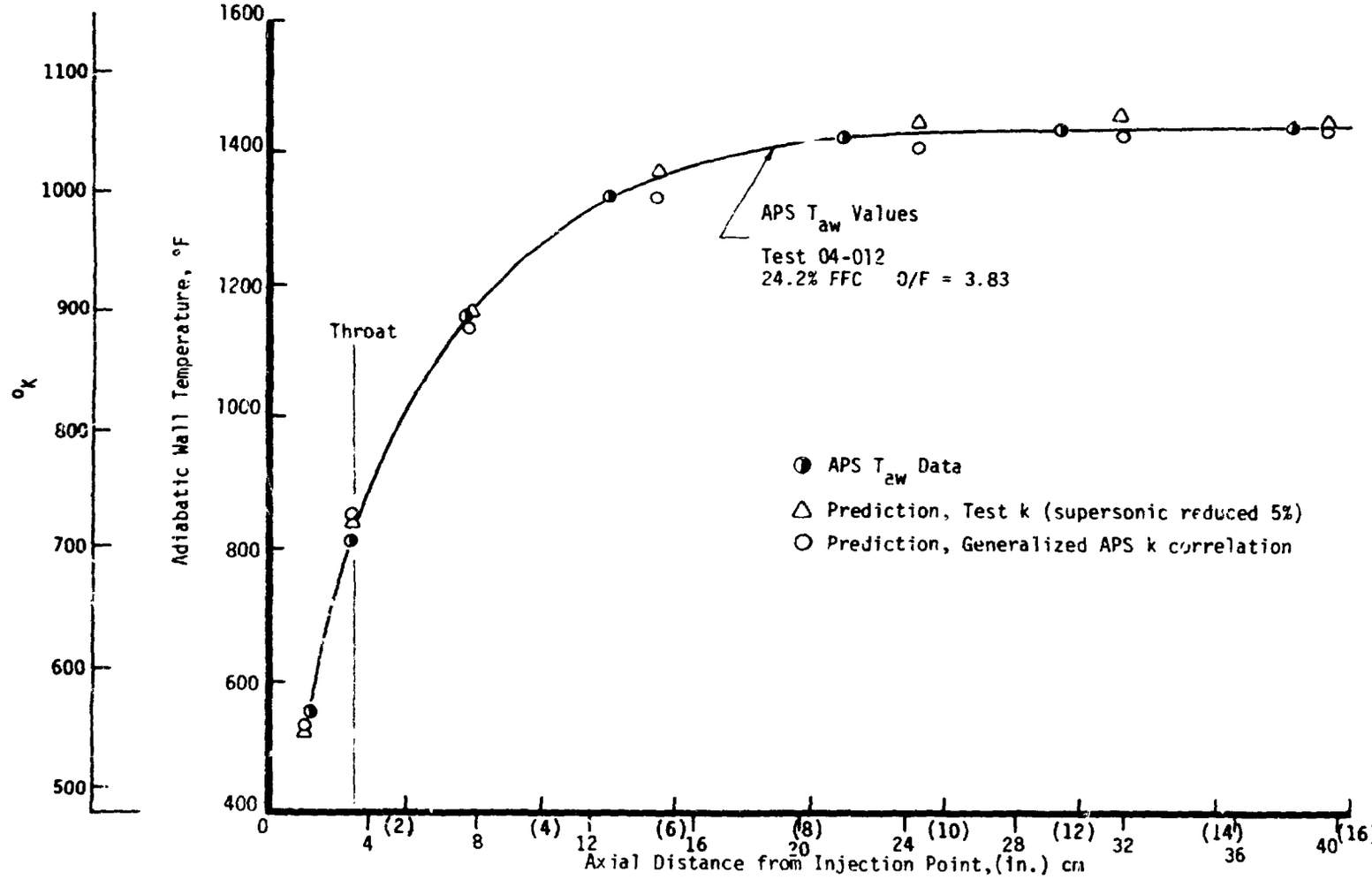

FIGURE 7. COMPARISON OF MEASURED AND PREDICTED ADIABATIC WALL TEMPERATURE

Figure B-3. Calibration of APS Pretest Analysis Model

TABLE BI

APS ENTRAINMENT FRACTION DATA

Injector: P/N 1161401, S/N 6

Chamber: P/N 1160334, S/N 2

Test:	04-012A	04-012B	04-018A	04-018B	04-018C
% FFC:	24.2	18.9	24.6	19.9	17.5
k_o:	.00694	.00816	.00795	.00975	.0108
u_c/u_e:	.97	.82	.54	.41	.37
O/F:	3.83	3.82	4.12	4.23	4.22
TH_2:	Amb.	Amb.	Cold	Cold	Cold

Region	Test 04-012A k/k_o	Test 04-012B k/k_o	Test 04-018A k/k_o	Test 04-108B k/k_o	Test 04-018C k/k_c	Average k/k_o	(1) Axial Position, cm	Nozzle Area Ratio	Reference Thermocouple Locations (Fig. 3)
Subsonic 1	2.74	2.94	3.34	2.68	2.79	2.9	0-15	-	i-2
Subsonic 2	1.99	1.94	2.40	2.04	1.45	1.97	1.5 - 3.18	-	2-4
Subsonic	2.33	2.39	2.82	2.32	2.06	-	0 - 3.18	-	i-4
I	2.23	1.37	1.63	1.15	1.04	1.48	3.18 - 7.6	1.0 - 4.4	4-6+ .64 cm
II	1.09	0.176	.97	.54	0.29	.73	7.6 - 12.9	4.4 - 10.9	/A
III	.54	.34	.50	24	0.16	.36	12.9 - 21.6	10.9 - 21.0	N/A
IV	0.21	0.28	.24	.06	0.04	.17	21.6 - 30.0	21.0 - 30.5	N/A
V	0.6	.10	.25	.11	.06	.12	30.0 - 38.5	30.5 - 38.9	N/A

(1) Axial distance from film coolant injection point
Throat Location = 3.18 cm (1.25 in.)

TEST	% FFC	u_c/u_e	°F	NOMINAL P_c, atm
04-012	24.2	.97	3.8	20.4
04-012	18.9	.82	3.8	20.4
04-018	24.6	.54	4.1	20.4
04-018	19.9	.41	4.2	20.4
04-018	17.5	.37	4.2	20.4

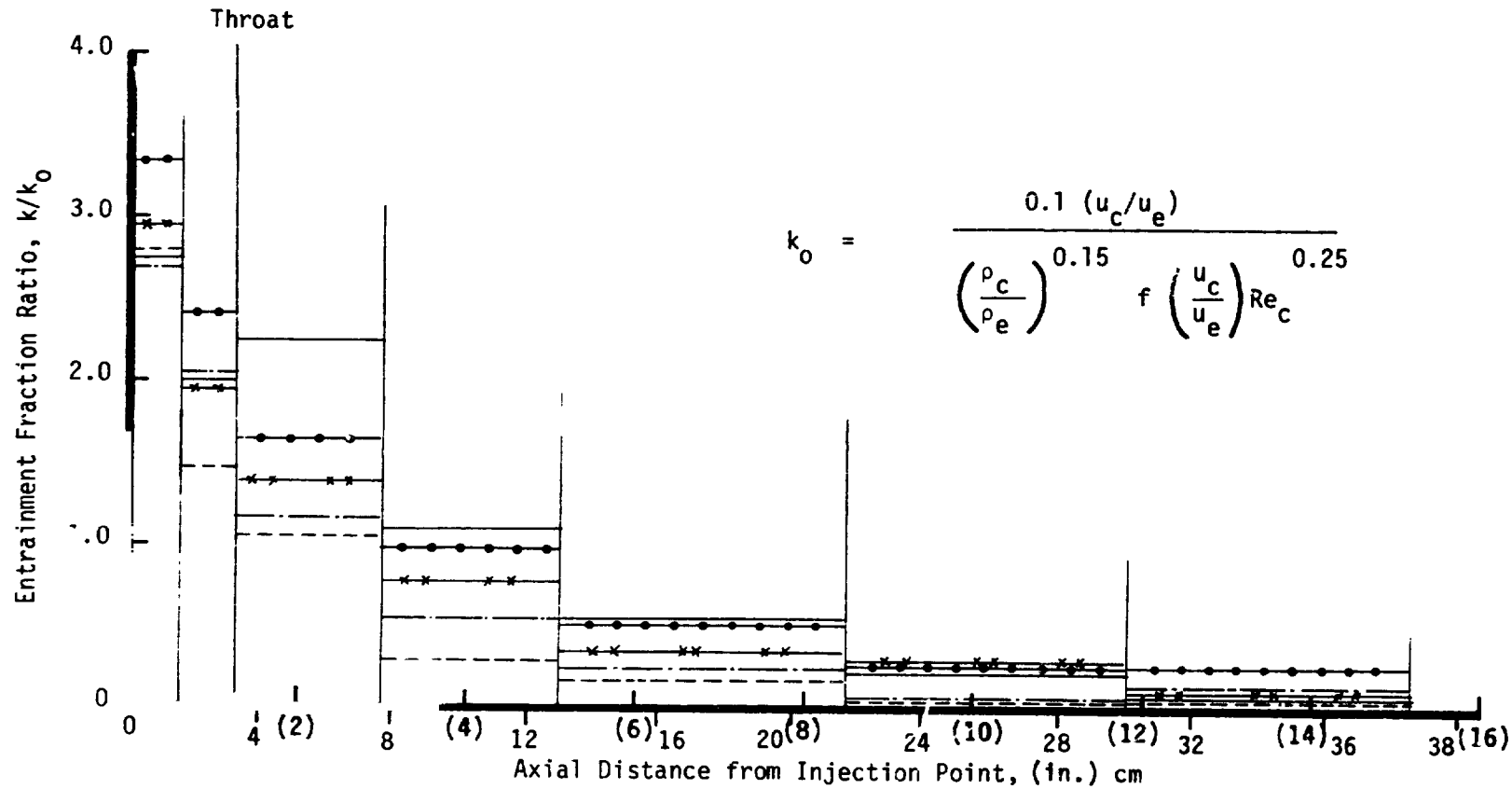

Figure B-4. APS Entra nment Fraction Distributions

II, Film Cooled Chamber (cont.)

The APS entrainment fraction data were generalized in the following manner:

$$\text{APS Subsonic Region:} \quad \frac{k}{k_o} = \left(\frac{k}{k_o}\right)_{ave} \tag{B-1}$$

$$\text{APS Supersonic Region:} \quad \frac{k/k_c}{(k/k_o)_{ave}} = 0.36 + 0.96\,\frac{u_c}{u_e} \tag{B-2}$$

where: $(k/k_o)_{ave}$ = a function of axial position per Table B-I

k_o = entrainment fraction for plane unaccelerated flow, defined on Figure B-4.

Agreement between APS test 04-012 wall temperature data and predictions obtained using the APS entrainment fraction correlation is good. This is shown on Figure B-3.

The film cooling sleeve design on the ITA chamber differs from the APS design in that: (1) the number of coolant channels was increased from 120 to 160, (2) the total film coolant injection flow area was decreased by 25%, (3) the size of the square individual coolant channels was decreased from .102 cm to .076 cm, and (4) the sleeve material was changed from OFHC copper to Zr-Cu. The smaller, higher velocity ITA film coolant streams apparently promoted mixing in the subsonic region because the measured ITA throat wall temperatures are significantly higher than predicted using the APS entrainment fraction correlation. This is demonstrated on Figure B-5 which compares the predictions to data from ITA Test -046. The APS supersonic mixing characteristic is not evident in these ITA wall temperature data. In order to obtain a satisfactory prediction of the ITA Test -046 subsonic wall temperature data, it was necessary to increase the subsonic APS k values by 50%. The average APS supersonic k values yielded a satisfactory prediction for the ITA nozzle wall temperatures. Consequently, for ITA chamber analyses the following entrainment fractions were used:

$$\text{ITA Subsonic Region:} \quad \frac{k}{k_o} = 1.5\left(\frac{k}{k_o}\right)_{ave} \tag{B-3}$$

$$\text{ITA Supersonic Region:} \quad \frac{k}{k_o} = \left(\frac{k}{k_o}\right)_{ave} \tag{B-4}$$

where: $(k/k_o)_{ave}$ = a function of axial position per Table B-I.

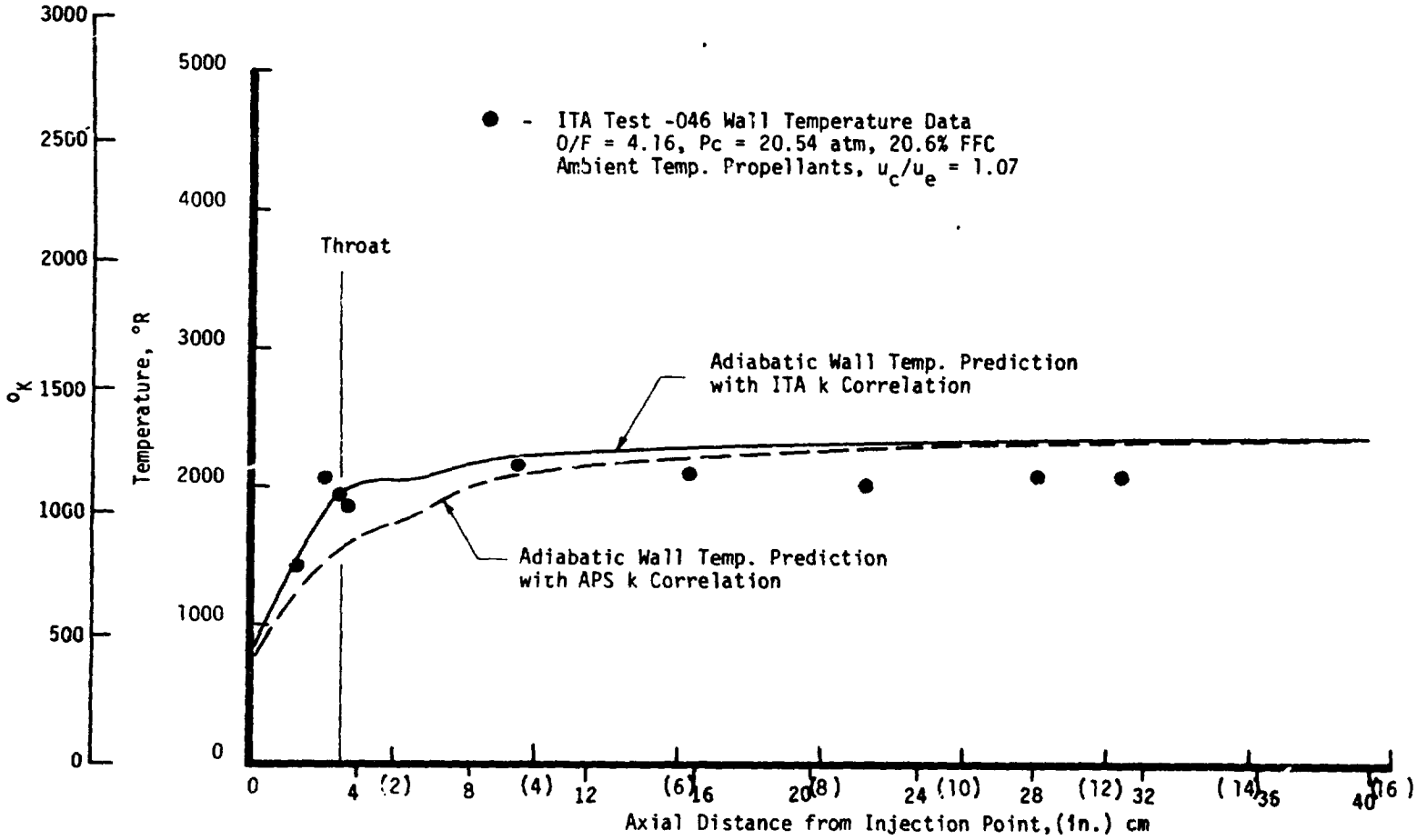

Figure B-5. ITA Wall Temperature Data and Pretest Model Correlation

APPENDIX C

PERFORMANCE ANALYSIS DETAILS

I. PRETEST PERFORMANCE ANALYSIS

A. THEORETICAL PERFORMANCE POTENTIAL

Theoretical One Dimensional Equilibrium (ODE) performance data for characteristic exhaust velocity (C*) and vacuum specific impulse (Isp) were calculated using the JANNAF-recommended TDK Computer Program described in Reference 16. Nozzle exit area ratios of 40/1 and 4.43/1 were considered and the results are shown on Figures C-1 through C-3. Ambient temperature propellants (300°K) were assumed. The hydrogen was assumed chemically pure but the oxygen was assumed to include trace quantities of argon and nitrogen diluents.

The effect of propellant inlet temperature on theoretical ODE specific impulse is shown on Figure C-4. Note that the temperature incluence at O/F = 5.5 is less than at O/F = 4. This occurs because the reactant enthalpy is primarily determined by the fuel rather than the oxidizer due to much higher hydrogen heat capacity. If the fuel and oxidizer inlet temperatures are unequal, Figure C-4 defines an equivalent enthalpy-weighted inlet temperature, $\overline{T}$. FigureC-4 only accounts for the difference in theoretical ODE performance and does not account for the energy release efficiency variations with inlet temperature which can occur with a specific injector design.

B. NOZZLE PERFORMANCE

Kinetic Loss (KL) - The influence of nozzle kinetics on performance is illustrated on Figures C-2 and C-3. The One Dimensional Kinetic (ODK) performances shown were obtained using the kinetic reaction rate recently recommended in Reference 17. The new reaction rates resulted in 0.7 to 0.9 sec higher ODK performance predictions than were assumed in References 1 and 2. These new reaction rates had no impact on ODE performance predictions and a negligible effect on theoretical C* performance.

Divergence Loss (DL) - The nozzle DL was evaluated by analyzing the ITA (ε = 40:1) Rao nozzle contour with the Ideal Gas expansion option of the Reference 16 TDK Computer Program. An altitude (ε = 40) divergence efficiency (η_{DL}) of .9896 was predicted.

The thrust chamber tested on this program has a similar Rao contour except that it is truncated at ε = 4.43 and has a local nozzle divergence half-angle of 30.8 degrees. Due to its highly non-optimum expansion angle, its divergence performance is reduced to .9067. This large divergence loss must be accounted for in interpreting the sea level performance and extrapolating to the altitude engine. The ratio of two dimensional exit pressure to ambient pressure predicted was 0.93.

For the pre-test analysis, a typical DL was calculated for the 20% FFC case and the DL absolute value was assumed constant with % FFC. The calculated loss was obtained from the following equation.

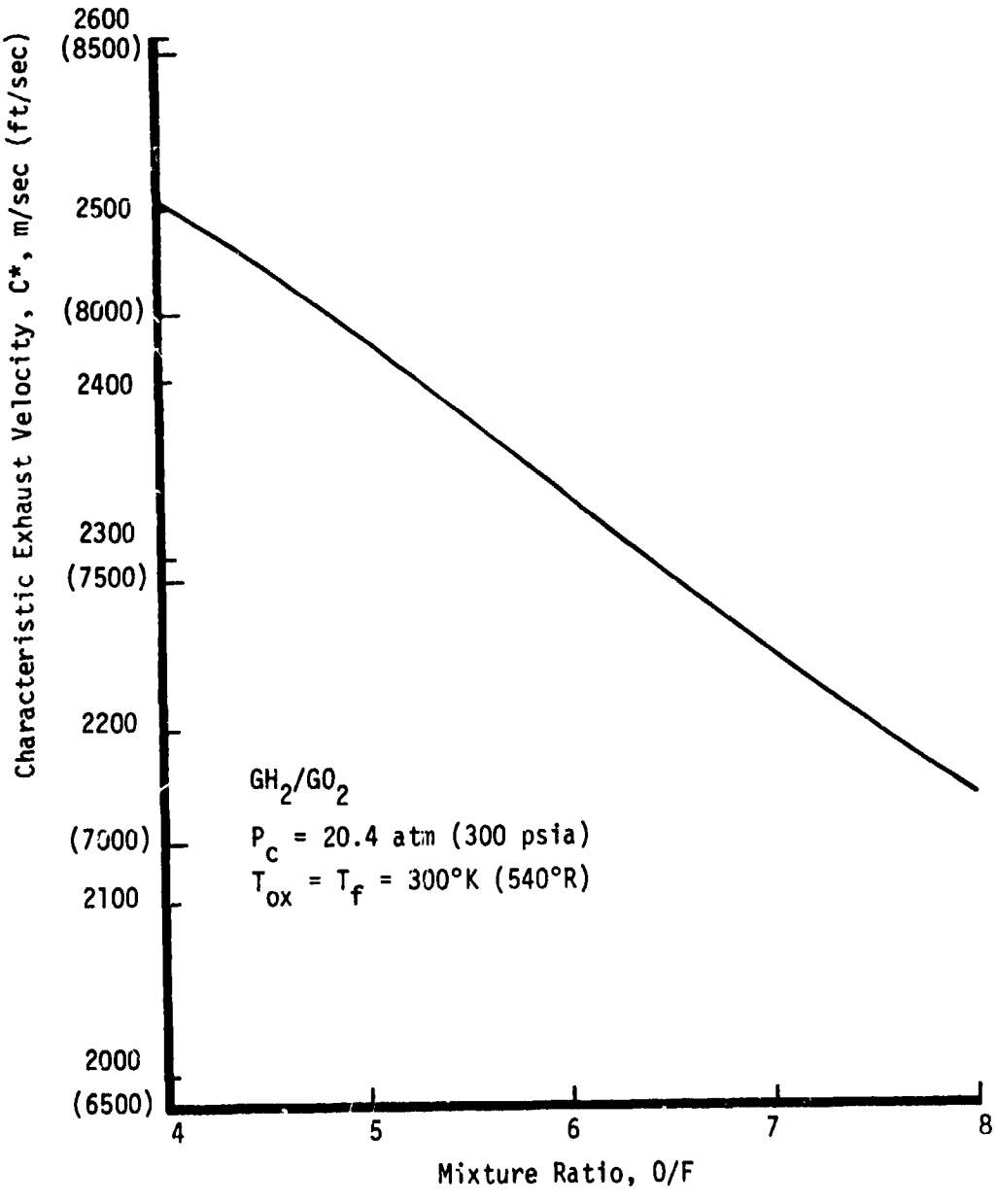

Figure C-1. Theoretical Characteristic Exhaust Velocity

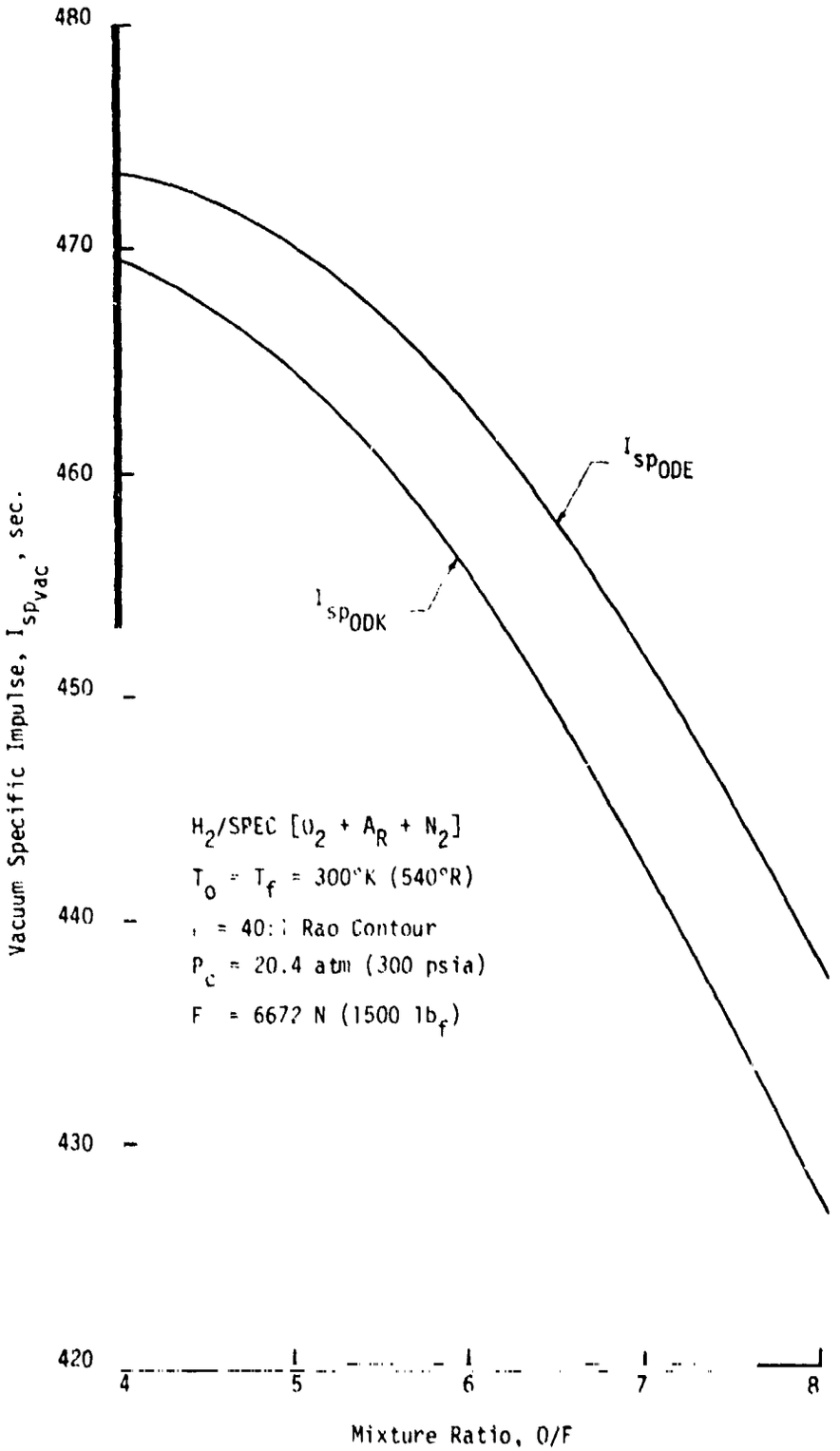

Figure C-2. Theoretical Vacuum Specific Impulse

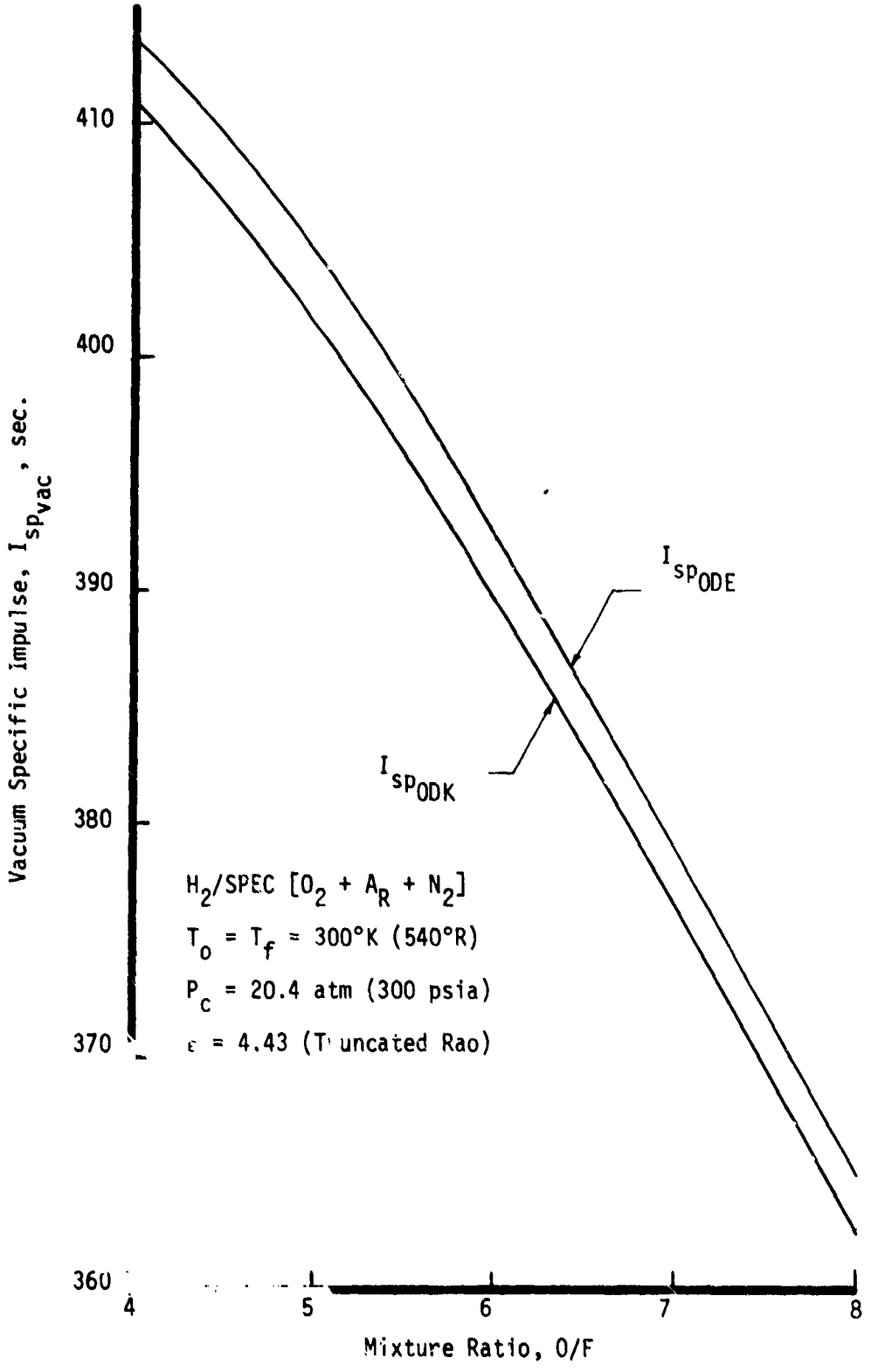

Figure C-3. Theoretical Sea Level Nozzle Vacuum Specific Impulse

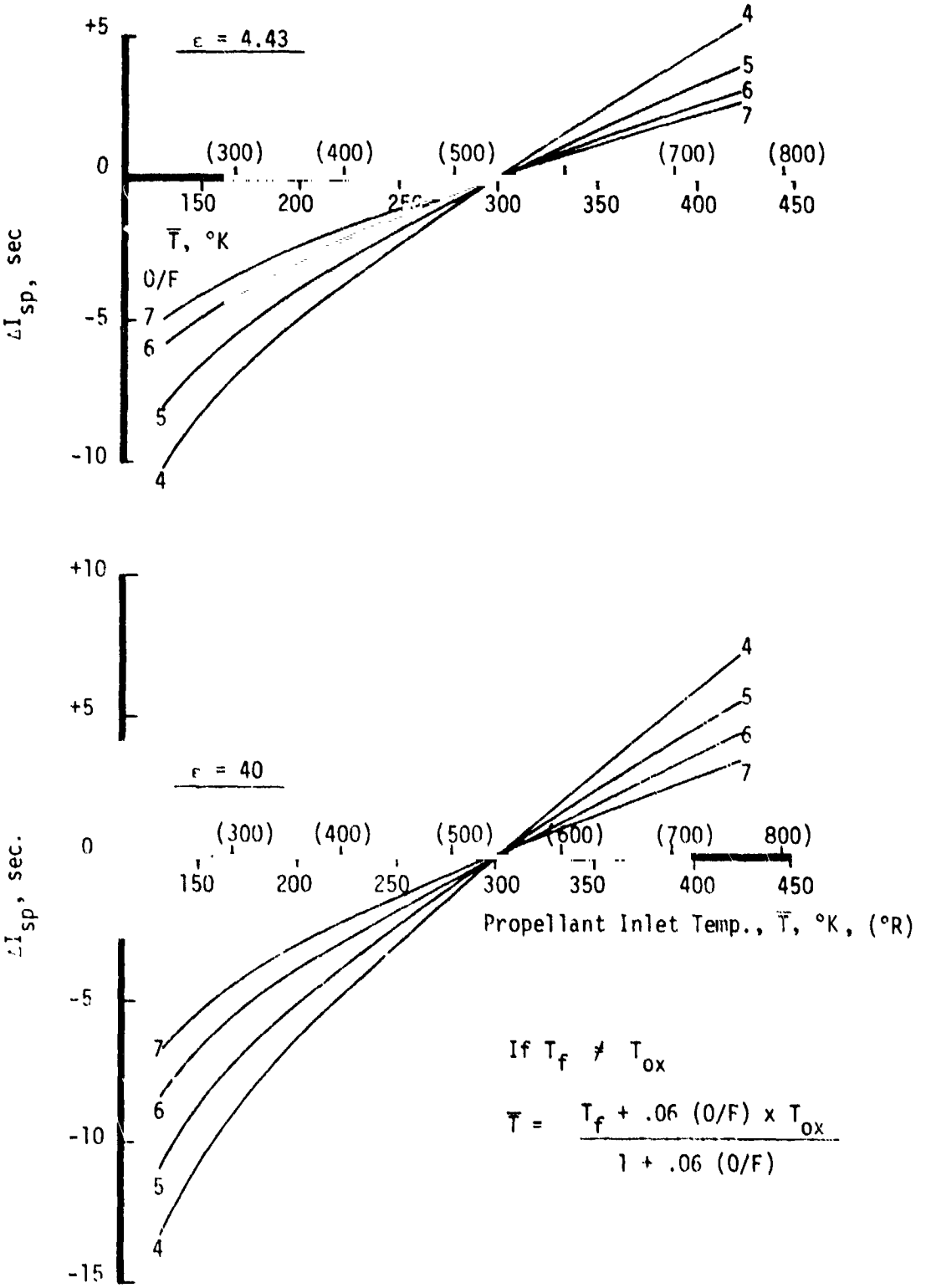

Figure C-4. Performance Variation with Propellant Inlet Enthalpy

I, B, Nozzle Performance (cont.)

$$DL = (1 - \eta_{DL}) [(I_{sp})_{ODE} - KL - BLL - FCL - ERL] \quad (C\text{-}1)$$

$$= \frac{1 - \eta_{DL}}{\eta_{DL}} (I_{sp\ Delivered}) \quad (C\text{-}2)$$

Boundary Layer Loss (BLL) - The nozzle BLL was evaluated using the simplified Boundary Layer Chart methodology described in Appendix B of Reference 18. Results of the parametric BLL analysis are summarized on Table C-I for both altitude (ε = 40) and sea level (ε = 4.43) nozzles and for O/F = 4.0, 5.5, and 6.0. A range of wall temperature to gas temperature (TWTS) ratio from 0.2 to 1.0 are included with an assumed nominal TWTS ratio of 0.8. The influence of both high and low chamber pressures of 500 psia and 100 psia respectively are included as well as the nominal P_C = 300 psia. The predicted BLL are 6.5 sec and 2.0 sec for the altitude and sea level nozzles, respectively. The BLL loss was assumed constant with film coolant flow rate.

C. FUEL FILM COOLING PERFORMANCE LOSS (FCL)

The fuel film cooling loss was evaluated with the HOCOOL computer program and is shown on Figure C-5. The loss values calculated are based on the APS and ITA entrainment fraction correlations described in Appendix B.

D. CORE INJECTOR PERFORMANCE

The injector utilized on this program is the Modified I Premix-Triplet type design developed on the Reference 1 and 2 programs. The performance of the Modified I design was experimentally evaluated in both the APS and ITA programs.

The APS performance data (Ref. 1) is generally good, i.e., it is self-consistent, it appears reasonable in comparison with analytical predictions, and is considered to be generally accurate. Its limitation is that its primary objective was to screen a multitude of injector types and chamber cooling techniques and thus has insuffficient data to statistically characterize the Modified "I" Triplet injector at O/F = 5.5.

The main objective of the ITA Program (Ref. 2) was to demonstrate engine durability rather than performance. Although much statistical data is available, wide data scatter exists and absolute performance accuracy is questionable.

TABLE CI

PREDICTED NOZZLE BOUNDARY LAYER PERFORMANCE LOSS SUMMARY

Parameter:	Symbol	Units																			
Chamber Pressure	PC	psia	300	→	100	500	300	→	100	500	300	→	100	500	300	→					
Nozzle Exit Area Ratio	EPS	-	4.43	→																	
Nozzle Exit Angle	THE	degree	30.8	→																	
Nozzle Length, X/RT	LGTH	-	1.72	→																	
Mixture Ratio (Ref.)	O/F	-	6	→					5.5	→					4	→					
Wall Temp. Ratio	TWTS	-	1.0	.8	→	.6	.4	.2	1.0	.8	→	.6	.4	.2	1.0	.8	→	.6	.4	.2	
Char. Exhaust Velocity	CSTAR	fps	7150	→					7350	→					7950	→					
Gas Viscosity	VIS	$\frac{lbm}{ft\text{-}sec}$	6.1E-5	→					5.97E-5	→					5.2E-5	→					
Specific Heat Ratio	GAMMA	-	1.136	→					1.144	→					1.22	→					
Exit Mach No.	XACH	-	2.572	→					2.584	→					2.703	→					
ΔI_{sp}	BLL	$\frac{lbf\text{-}sec}{lbm}$	1.60	2.03	2.52	1.83	2.45	2.87	3.26	1.61	2.05	2.55	1.85	2.48	2.92	3.32	1.39	1.81	2.26	1.64	2.26	2.72	3.17
	PC		300	→	100	500	300	→	100	500	300	→	100	500	300						
	EPS		40	→																	
	THE		10	→																	
	LGTH		15.0	→																	
	O/F		6	→					5.5	→					4	→					
	TWTS		1.0	.8	→	.6	.4	.2	1.0	.8	→	.6	.4	.2	1.0	.8	→	.6	.4	.2	
	CSTAR		7150	→					7350	→					7950	→					
	VIS		6.1E-5	→					5.97E-5	→					5.2E-5	→					
	GAMMA		1.170	→					1.18	→					1.22	→					
	XACH		3.863	→					3.910	→					4.108	→					
	BLL		5.60	6.52	8.12	5.8	[illegible]	8.52	9.04	5.53	6.49	8.09	5.86	7.51	8.56	9.62	5.04	6.08	7.57	5.49	7.18	8.31	9.44

Common Input (All Cases)

NOZ = 0, (Rao Nozzle Contour)

RSTAR = 0.960

RTHETA = 1.00

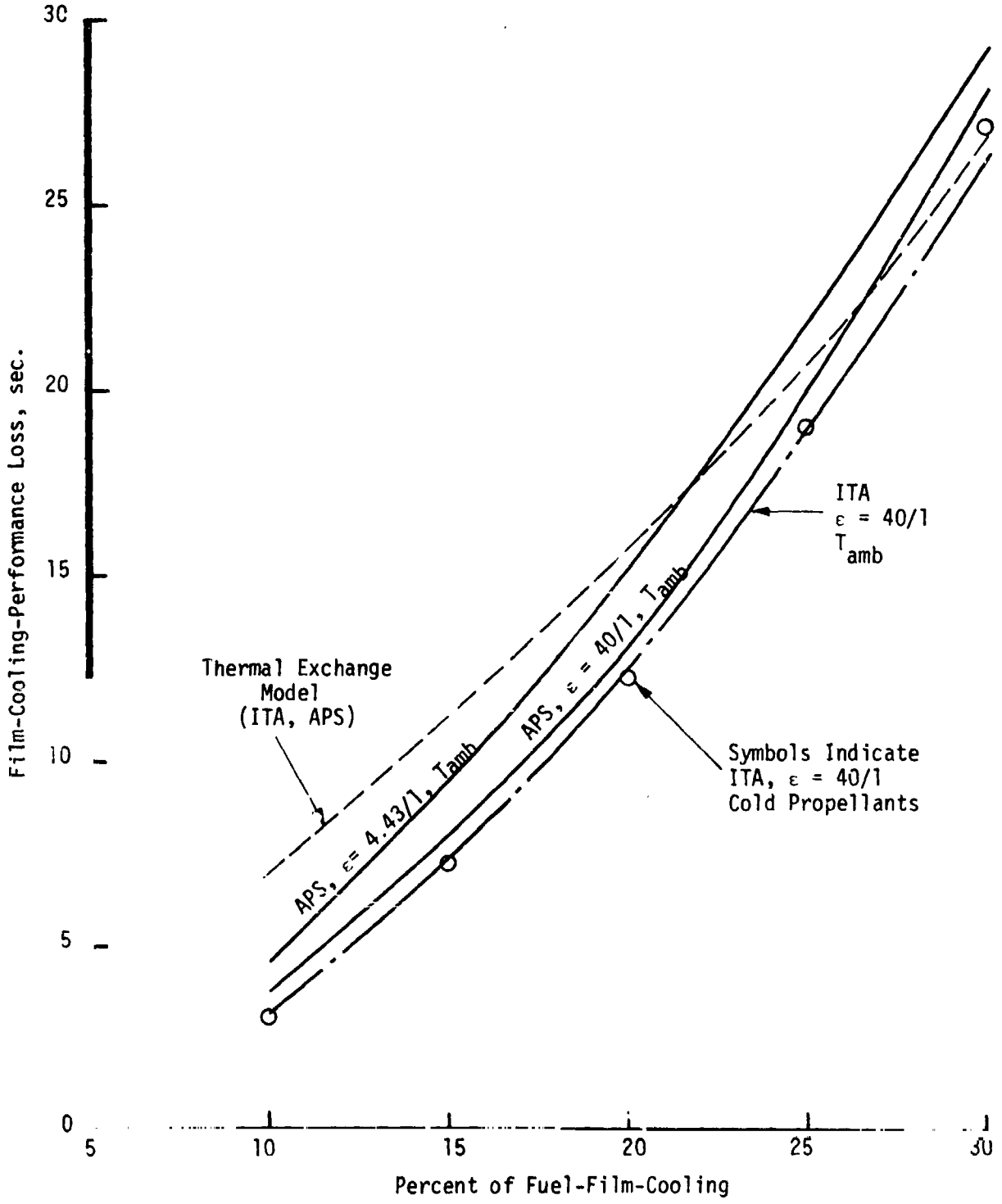

Figure C-5. Pretest Film-Cooling-Performance Loss Predictions

I, D, Core Injector Performance (cont.)

Subsequent to the design of the Modified "I" Triplet Injector, References 3 and 4 established empirically calibrated analytical models which provided valuable physical insight into gas/gas combustion performance and mixing/cooling processes. Thus the approach taken to extrapolate the existing engine operating characteristics at O/F = 4.0 to O/F = 5.5 was to use analytical models to identify important engine design parameters and their characteristic effects, and to use the statistical data (recognizing its possible inaccuracies) to calibrate the model results.

1. Analytical Gas/Gas Mixing Performance Model

Gaseous injector energy release efficiency was evaluated with the analytical mixing model contained in the Design Handbook portion of Reference 4. The Modified "I" (Pre-Mix) Triplet was parametrically analyzed to evaluate the effects of core mixture ratio variation, chamber pressure variation, and propellant inlet temperature variation upon the mixing efficiency E_m which can be used to predict ERE. The primary results are summarized on Table C-II. This model would have been used to evaluate injector element design changes if the test data had shown that the ERE of the premix injector at O/F = 5.5 was low. The data showed that ERE was very satisfactory at O/F = 5.5, being on the order of 99%.

2. Mixture Ratio Influence Upon ERE

The Modified "I" Triplet was design optimized at 4.0 engine mixture ratio because this was the nominal design point on both the APS and ITA programs. Operating this injector at 5.5 O/F increases the oxidizer to fuel injection momentum ratio, thus reducing the penetration of the radially inward fuel jet into the axially oriented oxidizer jet. This in turn can possibly reduce ERE at higher mixture ratios as indicated by the empirical data shown in Figure C-6 which was obtained from Reference 1. Part of the wide data scatter shown on Figure C-6 is attributable to uncertainties in the fuel film cooling loss computed with the now obsolete Thermal Exchange Model. These data might be more consistent if the FCL had been evaluated with the HCCOOL film cooling performance loss model.

3. Propellant Inlet Temperature Effect Upon ERE

In Reference 4 it was shown that experimental ERE for a given premix injector element design is reduced at colder propellant injection temperatures and the physical mechanism was explained. Although the data is scant, Figure C-7 appears to corroborate this analytical prediction. Furthermore, its influence appears greater at higher O/F.

TABLE CII

ANALYTICAL MIXING MODEL PREDICTIONS

Case No.		1	2	3	4	5	6	7	8	9	10	11	12	13	14	15	16	17	18	19	20
T_f	°R	540	→													250	250	250	375	375	540
T_{ox}	°R	540	→													250	375	540	375	540	375
Pc	psia	100	→		300	→							500	→		300	→				
O/F	-	2	4	6	2	3	4	5	6	7	8	10	2	4	6	6	→				
Isp*	sec	381	375	355	381	382	375	368	352	345	332	300	381	375	355	352	→				
$\dot{W}_T$	lbm/sec	.01833	.01875	.01944	.05458	.05444	.05555	.05667	.05930	.06000	.06250	.06875	.09125	.09306	.09222	.05930	→				
$\dot{W}_{ox}$	lbm/sec	.01222	.01250	.01667	.03639	.04983	.04444	.04722	.05083	.05250	.05555	.06250	.00083	.07444	.08333	.05083	→				
$\dot{W}_f$	lbm/sec	.00611	.00375	.00278	.01819	.01361	.01111	.00995	.00847	.00750	.00604	.00625	.03042	.01861	.01389	.00847	→				
P_{ox}	lbm/ft^3	.55232	→		1.6570	→							2.7616	→		3.5790	2.3860	1.6570	2.3860	1.6570	2.386
ΔP_{ox}	psid	26.0	39.1	48.3	76.8	96.6	114	129	150	160	175	226	129	193	242	69.3	104	150	104	150	104
Cd_{ox}	-	.80	→																		
P_f	lbm/ft^3	.034796	→		.10439	→							.17398	→		.22548	→		.15032	→	.10439
ΔP_f	psid	146	54.9	30.2	431	241	161	116	93.4	73.2	62.7	50.9	723	271	151	43.2	→		64.9	→	93.4
Cd_f	-	.47	→																		
Cd_{cup}	-	.887	→																		
η_m	%	86.3	83.2	82.4	80.0	77.0	75.8	75.6	76.0	76.8	77.7	79.2	76.6	71.6	71.8	52.6	58.5	65.0	66.2	70.5	73.3
% C*	-	99.76	99.09	99.38	99.74	98.52	98.06	98.17	98.62	98.90	99.38	99.60	98.74	97.16	98.12	93.69	95.59	96.8	97.26	97.95	98.20
% Isp ε=40		99.89	99.45	98.94	99.64	99.21	98.53	97.92	97.63	97.91	96.53	99.46	99.40	97.56	96.73	90.57	93.44	95.44	95.39	96.72	96.75
η_t	%	92.3	90.6	90.8	88.8	86.9	86.0	86.0	86.3	86.7	87.2	88.3	86.5	83.4	83.7	70.5	75.1	79.2	80.2	82.8	84.7
% C*	-	99.95	99.73	99.82	99.86	99.68	99.38	99.48	99.58	99.63	99.77	99.93	99.77	99.10	99.40	97.95	98.64	99.04	99.11	99.4	99.39
% Isp ε=40		99.98	99.85	99.68	99.94	99.85	99.6-	99.27	99.36	99.41	99.94	99.89	99.45	98.97	96.48	97.83	99.58	98.50	98.99	98.99	98.95

Isp* Based on Figure 4[illegible] of Reference (d)

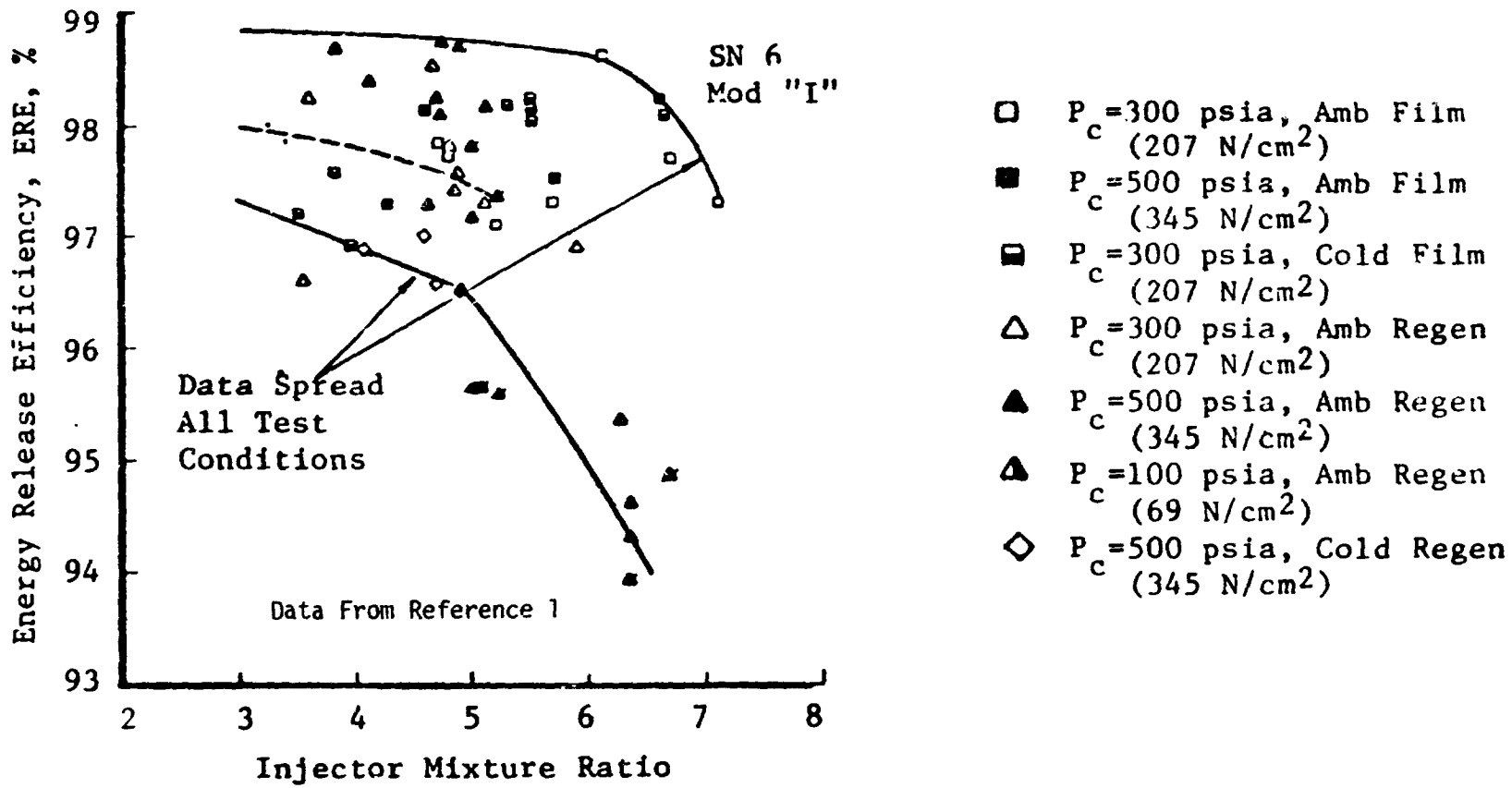

Figure C-6. Effect of Mixture Ratio on Energy Release Efficiency, 40/1 Area Ratio

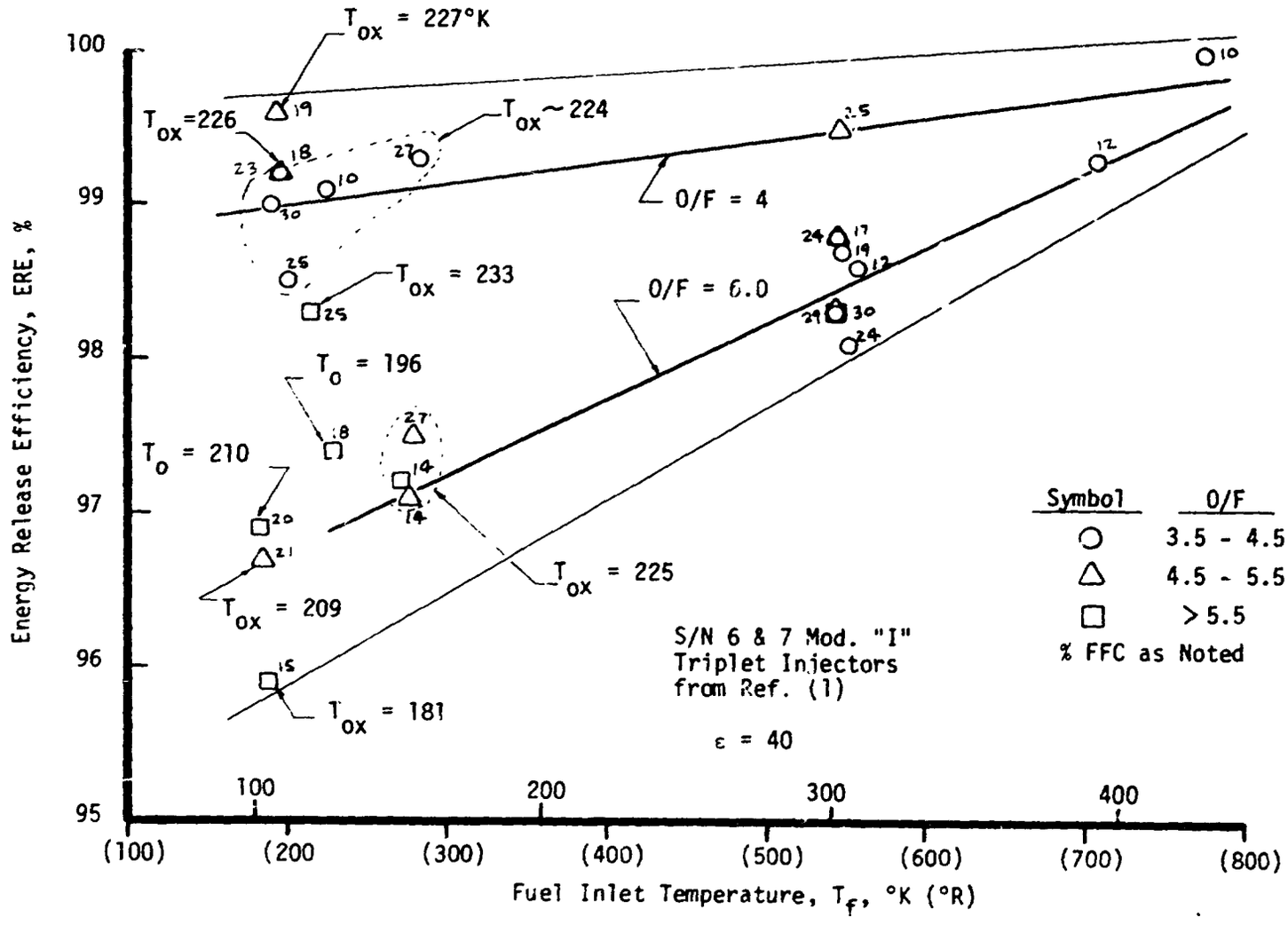

Figure C-7. Effect of Propellant Temperature on Energy Release Efficiency

I, D, Core Injector Performance (cont.)

In Figure C-8, the relative effects of temperature and O/F on ERE of the premix injector are illustrated. The trend lines and ranges of uncertainty shown are based on the test data and predictions from the Reference 4 mixing model.

4. Chamber Pressure Influence

The primary influence of P_c on predicted performance is due to reduced Kinetic Loss (KL) at high P_c. The effect of P_c on ERE is expected to be second order.

5. Selected Premix Injector ERE Values

Based on the available pre-test data for Modified "I" Injector, the following ERE values were chosen for the pretest analysis at O/F = 5.5 and Pc = 300 psia operating conditions. These values were used for both the 40/1 and 4.43/1 nozzle predictions

% FFC	ERE for Ambient O_2 and H_2 (300°K)	ERE for Cold Propellants (139°K H_2, 208°K O_2)
0	99.6	99.4
10	99.3	98.7
15	99.1	98.2
20	98.9	97.7
25	98.6	97.2
30	98.2	96.5

E. PRE-TEST ENGINE PERFORMANCE PREDICTION

The delivered engine performance was estimated by subtracting losses due to kinetics (KL), nozzle divergence (DL), boundary layer effects (BLL), imperfect energy release (ERL), and film cooling (FCL) from the theoretical ODE performance at the overall O_2/H_2 mixture ratio of 5.5. The calculations performed for 20% FFC are summarized on Table C-III. Predicted effects of film coolant flow rate and temperature are shown on Figures 16 and 17.

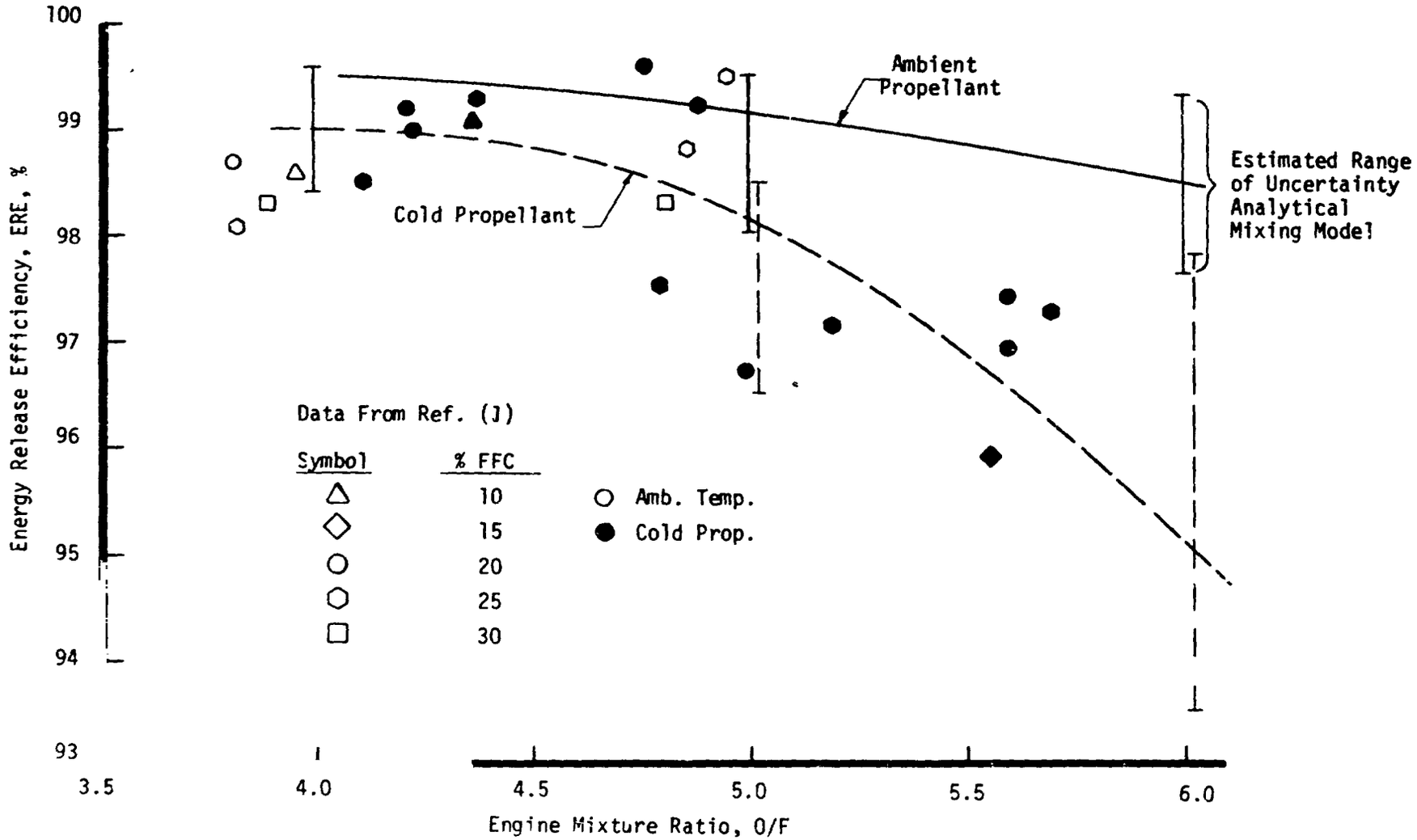

Figure C-8. Extrapolated ERE Correlation for the Modified I Triplet

TABLE CIII

PREDICTED PERFORMANCE SUMMARY (PRETEST)

Parameter	Units								
O/F	-	6 →				5.5 →			
Pc	psia	300 →							
T_f	°R	540	250	540	250	540	250	540	250
T_{ox}	°R	540	375	540	375	540	375	540	375
ε	-	40	40	4.43	4.43	40	40	4.43	4.43
$I_{sp,ODE}$	sec	463.2	455.5	392.1	386.7	467.1	459.9	398.8	393.4
ΔKL	sec	7.7	7.7	2.5	2.5	6.4	6.4	3.0	3.0
$I_{sp,ODK}$	sec	455.5	447.8	389.6	384.2	460.7	453.5	395.8	390.4
BLL	sec	6.5	6.5	2.0	2.0	6.5	6.5	2.0	2.0
CDL	sec	4.4	4.3	34.1	33.2	4.5	4.4	34.8	33.9
% FFC	-	20	20	20	20	20	20	20	20
FFCL	sec	*17.4	*17.4	*17.4	*17.4	**12.5	**12.3	**14.5	**14.3
ERL	sec	7.0	13.7	4.7	9.3	5.1	10.6	4.4	9.1
% ERE	-	98.5	97.0	98.8	97.6	98.9	97.7	98.9	97.7
$I_{sp,pred.}$	sec	*420.2	*405.9	*331.4	*322.3	**432.1	**419.7	**339.9	**330.7

* Preliminary - Based on Thermal Exchange FFCL

**Based on HOCOOL Predictions for ITA

II. INJECTOR ENERGY RELEASE EFFICIENCY (POST-TEST ANALYSIS)

Experimental energy release loss (ERL) was determined by subtracting the kinetic loss, divergence loss, boundary layer loss, and film cooling loss from the difference between theoretical $I_{SP_{ODE}}$ and delivered performance. It was determined that this combustion loss attributable to incomplete energy release corresponded to about a 1% Isp loss or a 99% ERE over the entire range of operating conditions tested. This measured ERE, however, was obtained with the truncated (ϵ = 4.43) sea level nozzle and is not necessarily indicative of a 40/1 area ratio nozzle ERE. The method and analytical rationale for extrapolating this ERE to ϵ = 40/1 is described in the following paragraphs.

In gas/gas rocket engines, such as the APS and ITA engines, the propellants are completely gassified prior to injection into the combustion chamber. The only physical mechanism by which gaseous propellant engines can incur an ERL is due to incomplete combustion enthalpy release which results from imperfect microscale mixing efficiency.

In order to extrapolate sea level ERE to vacuum nozzle conditions, it is assumed that primary fuel/oxidizer mixing occurs within the subsonic chamber and that supersonic mixing effects are negligible. Consistent with this assumption, a two stream tube distribution is inferred with one being fuel rich and the other oxidizer rich. An overall mixing efficiency parameter (E_m) is defined by assuming that the fuel rich stream tube has an effective mixture ratio of:

$$(O/F)_i = E_m \times (O/F)_c \qquad \text{(C-3)}$$

where:

$(O/F)_i$ = Fuel rich stream tube mixture ratio,

$(O/F)_c$ = Injector core mixture ratio,

E_m = Mixing efficiency (≤ 1.00).

Similarly, it is assumed that the oxidizer rich stream tube mixture ratio can be characterized by:

$$(O/F)_j = (O/F)_c / E_m \qquad \text{(C-4)}$$

To satisfy mass continuity, it can be shown that the mass fraction of the fuel rich stream tube (X_i) and the oxidizer rich stream tube (X_j) can be calculated from the following equations.

II, Injector Energy Release Efficiency (Post-Test Analysis) (cont.)

$$(O/F)_i/(O/F)_j = E_m^2 \tag{C-5}$$

$$X_i = \frac{W_{fi}}{W_{f\ total}} \frac{[1 + (O/F)_i]}{[1 + (O/F)_c]} = \frac{[1 + (O/F)_i]}{[1 + E_m][1 + (O/F)_c]} \tag{C-6}$$

$$X_j = 1.0 - X_i \tag{C-7}$$

The gaseous injector ERL and ERE are then given, by the following equations.

$$ERL = (Isp)_{core} - [X_i\ (Isp)_i + X_j\ (Isp)_j] \tag{C-8}$$

$$ERE = \frac{X_i\ (Isp)_i + X_j\ (Isp)_j}{(Isp)_{core}} \tag{C-9}$$

where:

Isp = ODK performance

Subscript i refers to the fuel rich stream tube

Subscript j refers to the oxidizer rich stream tube

Subscript core refers to the core injector mixture ratio.

Even when given fixed values for $(O/F)_c$ and E_m, which in turn uniquely determine the assumed two stream tube mass and mixture ratio distribution, the ERL and % ERE will vary as a function of nozzle expansion ratio because the nozzle recombination chemistry alters the relative relationships between the fuel rich, uniform core, and oxidizer rich mixture ratio Isp's. That is, a concave downward region of Isp vs O/F will result in lower ERE with the same distribution than another nozzle exit area ratio which has a more linear slope wherein the low performance stream tube is more nearly offset by the opposite high performance stream tube.